**Title**
Vascular Endothelial Growth Factor (VEGF) Presentation Modulates Endothelial Cell Signaling and Vascular Branching in engineered matrices in vitro and in vivo



**Author**
Gojgini, Shiva

**Publication Date**
2014

Peer reviewed|Thesis/dissertation

UNIVERSITY OF CALIFORNIA

Los Angeles

# Vascular Endothelial Growth Factor (VEGF) Presentation Modulates Endothelial Cell Signaling and Vascular Branching in engineered matrices *in vitro* and *in vivo*

A dissertation submitted in partial satisfaction of the requirements for the degree Doctor of Philosophy in Chemical Engineering

By

Shiva Gojgini

2015

ABSTRACT OF THE DISSERTATION

Vascular Endothelial Growth Factor (VEGF) Presentation

Modulates Endothelial Cell Signaling and Vascular Branching

in engineered matrices *in vitro* and *in vivo*

by

Shiva Gojgini

Doctor of Philosophy in Chemical Engineering

University of California, Los Angeles, 2015

Professor Tatiana Segura, Chair

The process of angiogenesis, defined by the development of new blood vessels from pre-existing vessels, is essential in tissue remodeling and regeneration. This complex process involves extensive interplay between cells, soluble factors and extra-cellular matrix (ECM) components. Insufficient angiogenesis, implicated in many disease processes such as heart failure and stroke, results in inadequate nutrient and oxygen delivery. Thus, therapeutic strategies to promote revascularization have been extensively investigated. Although several angiogenic growth factors have been identified and delivery investigated to induce revascularization, no clinical product

exists to date to promote revascularization. This thesis investigates the delivery of Vascular Endothelial Growth Factor (VEGF) from bioengineered matrices to promote revascularization in the brain. Two approaches will be described, non-viral gene delivery and protein delivery, both from matrix metalloproteinase degradable hyaluronic acid based hydrogels. Non-viral gene delivery has the potential to overcome limitations with protein degradation and inactivation by delivering plasmid DNA (more chemically stable then proteins). Non-viral gene delivery to cells seeded within hyaluronic acid matrices was investigated to begin to understand the process of gene transfer within hydrogel matrices. However, due to the low protein expression achieved, protein delivery was investigated. To directly deliver VEGF from our hydrogel biomaterials we first investigated how the presentation of VEGF affected endothelial cell activation. We showed that through controlling the discrete distribution of VEGF and integrin co-ligands in engineered matrices, ECs phenotype can be modulated to favor the tip cell phenotype when VEGF is bound and clustered, leading to controlled vessel branching. In addition, we found that controlled vessel branching leads to enhanced blood vessels with pericyte coverage after stroke. Further studies should be done to further improve the efficiency of our delivery strategy and their effect on tissue regeneration through a controlled vessel formation.

The dissertation of Shiva Gojgini is approved.

S. Thomas Carmichael

Harold Monbouquette

Tatiana Segura, Committee Chair

University of California, Los Angeles

2015

I dedicate this to my family

# Table of Contents

# List of Figures and tables

**Scheme 4.1**. Schematic of HA Modification and Hydrogel Formationa(A) HA-acrylate synthesis is a two-step process, first reacting HA with ADH and then using the pendant hydrazide to react with NHS-acrylate. (B) Schematic of DNA-loaded hydrogel formation. Liquid HA-AC is first modified with RGDpeptides using Michael type addition. HA-RGD is then crosslinked using an MMP degradable peptide in the presence of DNA/PEI polyplexes.

**Fig. 4.1.** Hydrogel mechanical properties. The mechanical properties of the hydrogels were determined using plate-to-plate rheometry storage (A) and average (B) modulus over a frequency range of 0.1_10 rad/s at a constant strain of 0.03 and are shown for increasingly stiff hydrogels (Gel ID 1 < 2 < 3 < 4 < 5).

**Fig.4.2.** Polyplex activity, distribution inside hydrogel scaffolds, and release. (A) Activity of the entrapped polyplexes was determined through the release of the polyplexes post-hydrogel formation using trypsin and a subsequent bolus transfection with the released polyplexes. The gene transfer of the released polyplexes was compared to fresh polyplexes with trypsin added and fresh polyplexes with gel degradation products added. (B) DNA/PEI polyplexes were stained with ethidium bromide post-hydrogel formation and imaged with a fluorescence microscope equipped with a z-stack capability. Scale bar = 100 μm.C) DNA release was determined using radiolabeled DNA. DNA/PEI loaded hydrogels were incubated in different release solutions, and at predetermined time points samples were gathered and analyzed for radioactivity using a scintillation counter. At the final day of the release assay the hydrogel was fully degraded with trypsin and the final activity measured. Data are plotted as the percentage of cumulative release.

**Fig.4.3.** Gene transfer as a function of the N/P ratio. The effect of the N/P ratio on transgene expression was studied for cells cultured inside MMP degradable HA hydrogels. For these studies a 3% hydrogel with an r ratio of 0.3 was used. The cell viability, ability of the cells to spread, and the metabolic activity of the cells were studied using the LIVE/DEAD assay, phalloidin staining (A), and MTT assay (B). Gene expression was determined over time using a reporter plasmid, pGluc, which is secreted by the cell when expressed (C). The cumulative expression at days 2 and 8 is plotted for ease of comparison (D). The statistical significance was determined using multiple comparisons and either the Dunnett or the Tukey multiple comparison's tests. The symbol ** indicates statistical significance at the level of 0.01 between the indicated condition and the corresponding noDNAcontrol in B or between the indicated conditions in D. The symbols *, **, and ***

indicate statistical significance at the level of 0.05, 0.01, and 0.001 between the indicated conditions in B. N/P= 0 represents the condition with no DNA polyplexes added to the hydrogel. Scale bar = 100 μm.

**Fig.4.4.** Gene transfer as a function of hydrogel stiffness. The effect of hydrogel stiffness on the ability of cells seeded inside the hydrogel to become transfected was studied for hydrogels with storage modulus ranging from 100 to 1730 Pa. The cell viability, ability of the cells to spread, and the metabolic activity of the cells were studied using the LIVE/DEAD assay, phalloidin staining (A), and MTT assay (B). None of the cell stiffness resulted in lower cellular viability. However, cell spreading was inhibited for stiffer hydrogels. Gene expression was determined over time using a reporter plasmid, pGluc, which is secreted by the cell when expressed (C). The cumulative expression at days 2 and 8 is plotted for ease of comparison (D). Matrix stiffness influenced transgene expression. The numbers 1_5 represent different hydrogel stiffness: 1 = 100 Pa, 2 = 260 Pa, 3 = 839 Pa, 4 = 1360 Pa, 5 = 1730 Pa. The statistical significance was determined using multiple comparisons and either the Dunnett or the Tukey multiple comparison's tests. The symbols ** and *** indicate statistical significance at the level of 0.05, 0.01, and 0.001 between the indicated condition and the corresponding noDNAcontrol in B or between the indicated conditions in D. The symbols *, **, and *** indicate statistical significance at the level of 0.05, 0.01, and 0.001 between the indicated conditions in B. Gel ID 0 represents the condition with no DNA polyplexes added to the hydrogel. Scale bar = 100 μm.

**Fig.4.5.** Hydrogel mechanical properties for hydrogels with different RGD concentrations and presentations. The mechanical properties of the hydrogels were determined using plate-to-plate rheometry storage (A, B) modulus over a frequency range of 0.1_10 rad/s at a constant strain of 0.03 are shown for hydrogels with variousRGDconcentrations and presentations, respectively. RGD presentation is displayed as the number of RGD/HA molecules with 4.7 RGD/HA being the most clustered condition and 0.2 RGD/HA being the least clustered/homogeneously distributed condition.

**Fig. 4.6**. Gene transfer as a function of RGD concentration. The effect of RGD concentration on the ability of cells seeded inside the hydrogel to become transfected was studied for hydrogels with RGD ranging from 10 μMto 400 μM. The cell viability, ability of the cells to spread, and the metabolic activity of the cells were studied using the LIVE/DEAD assay, phalloidin staining (A), and MTT assay (B). Gene expression was determined over time using a reporter plasmid, pGluc, which is secreted by the cell when expressed (C). The cumulative expression at days 2 and 8 is plotted for ease of comparison (D). Different RGD concentration

influenced transgene expression. The statistical significance was determined using multiple comparisons and either the Dunnett or the Tukey multiple comparison's tests. The symbol *** indicates statistical significance at the level of 0.001 between the indicated condition and the no DNA control in B or between the indicated conditions in D. The symbols *, **, and*** indicate statistical significance at the level of 0.05, 0.01, and 0.001 between the indicated conditions in B. 100* represents the condition with no DNA polyplexes added to the hydrogel. Scale bar = 100 μm.

**Fig.4.7. Gene transfer as a function of RGD presentation.** The effect of RGD presentation on the ability of cells seeded inside the hydrogel to become transfected was studied for hydrogels with 100 μM RGD displayed either homogeneously (100% HA-RGD, 0.2 RGD/HA molecule) or as RGD clusters (52% to 4.3% HA-RGD, 0.4 and 4.7 HA/RGD molecule, respectively). RGD clustering is achieved by reacting different amounts of HA-AC with the same amount of RGD and then mixing the resulting HA-RGD with unmodified HA. The cell viability, ability of the cells to spread, and the metabolic activity of the cells were studied using the LIVE/DEAD assay, phalloidin staining (A), and MTT assay (B). Gene expression was determined over time using a reporter plasmid, pGluc, which is secreted by the cell when expressed (C).The cumulative expression at days 2 and 8 is plotted for ease of comparison (D). RGD presentation influenced transgene expression. The statistical significance was determined using multiple comparisons and either the Dunnett or the Tukey multiple comparison's tests. The symbols ** and *** indicates statistical significance at the level of 0.01 and 0.001 between the indicated condition and the corresponding no DNA control in B and between the indicated conditions in D. The symbols * and ** indicate statistical significance at the level of 0.05 and 0.01 between the indicated conditions in B. 4.7* represents the condition with no DNA polyplexes added to the hydrogel. Scale bar = 100 μm.

**Fig. 5.1.** Heparin nanoparticle formation and VEGF binding and characterization.(A) After modification of heparin, it is combined with surfactants into a hexane solution for sonication. During the inverse emulsion sonication process, radical initiators (APS) are added to the solution to generate radical polymerization. The purification of heparin nanoparticles is perfomred through a liquid-liquid extraction process and then move to the next step for binding to VEGF (B) VEGF is incubated with heparin at 4°C overnight so that VEGF interact with heparin and forms its specific electrostatic interaction. Then, UV light activates the crosslinker, which covalently binds to VEGF. The heparin-binding domain of VEGF has many available amines on the lysine groups that interact with the sulfate groups on heparin. To form different VEGF presentation, the same amount of VEGF is mixed with different amount of heparin particles. After washes and purification, Dot Blot and ELISA is used to quantify the amount of VGEF that is bound to heparin. (C) TEM is used to measure the

size of the particles. TEM shows homogenously distributed of heparin nanoparticles which is consistent with the result from DLS. (B) DLS characterization of heparin nanoparticles shows a size of about 100 nm with the PDI of 0.2. Also, measurement of these particles after each step and also after binding to VEGF with different densities has been collected.

**Fig. 5.2.** VEGF binding and activity characterization. VEGF binding to different amount of particle was characterized using ELISA on the successive washes as well as ELISA and Dot Blot on the samples. Also, for the activity of VEGF bound to particles, proliferation assay and western blot were performed. (A) In direct ELISA was performed on all the washes to quantify the amount of VEGF that is bound to mg of heparin. Also the plot confirms the high cluster formation of VEGF to heparin by having the most unbound VEGF amount in the washes to show that heparin reached to its saturation binding to VEGF. (B) Proliferation assay for different concentration of VEGF is confirmed the activity of VEGF bound to different densities of heparin. (C) VEGFR-2 phosphorylation assay also confirms the activity of the bound VEGF. Binding of VEGF to particles enriches Y1175 signaling for the medium cluster formation at different dilutions of the VEGF as well as for the soluble VEGF as a positive control.

**Fig. 5.3.** VEGFR-2 phosphorylation assay. Plot quantifies phosphorylated VEGFR-2 band intensities and is normalized to total VEGFR-2 for each condition (n = 3 blots). Top band shows pVEGFR-2 and bottom band shows total VEGFR-2.Western blot data is shown for phospho-VEGFR-2 at Y1175 at 5min (A), for Y1214 at 5 min (B), phospho Erk ½ at 5 min (C) and phospho p-38 at 5 min (D). Western blot data for all has been shown for different time points (5, 15, 30 min)(E) and the quantification of those data has been plotted in (F). Data show increased activation of phospho Y1175 and Y1214 for hcV over the other two conditions. Also, hcV show sustained activation of pY1175 at 15 min compared to mcV and lcV.

**Fig. 5.4.**Tube formation assay with different VEGF clusters. (A)Different VEGF clusters are introduced to a fibrin gel with endothelial cell-coated cytodex beads, while fibroblast are cultured on top of the gel. Sprouting was analyzed over the course of 7 days for number of branching, number of sprouts and total network. (B) in all the analysis, hcV leads to a significant increase in branching points for endothelial cells as well as number of sprouts and total network over mcV and lcV. (C) Flourescent images of different sproutinf from cytodex beads. Endothelial cells are stained with pholloidain actin and DAPI and images are representing of different

shows the size of 78 nm with the PDI of 0.21. low PDI inditae the homogenously distribution of heparin nanoparticles.(B) TEM image of heparin nanoparticle.

**Table 6.1.** Characterization of VEGF loading. ELISA and Dot blot has been performed for both VEGF and Fn fragment to confirm and quantify the amount of VEGF and Fn binding.

**Fig. 6.2.** Proliferation assay. To test the activity of VEGF bound cell proliferation of HUVECs exposed to different VEGF/Fn cluster formation was performed.(A) cells were exposed to low concentration of VEGFand it show an increase in number of cells after 2 days for all the conditions that has cluster VEGF/Fn over just cluster VEGF and soluble VEGF. (B) High concentration of VEGF didn't show that much effect on the proliferation of cells.

**Fig. 6.3.**VEGFR-2 phosphorylation assay. Western blot data for two different concentration of VEGF(20, 100 ng/ml) for phosphorylation of Y1175 is shown in (A) and (B) respectively. Plot quantifies phosphorylated VEGFR-2 band intensities and is normalized to Beta actin each condition. Top band shows pVEGFR-2 and bottom band shows Beta actin. (C) and (D) Western blot data for downstream signaling of activation of Erk ½ for two different concentration of VEGF. Data indicate the activity of VEGF after binding to heparin nanoparticles.

**Fig. 6.4.** Western Blot data for phosphor focal adhesion kinase and integrin linked kinase. (A) Western blot data and plot for integrin linked kinase for different conditions indicate the activity of Fn fragments after clustering with VEGF on the heparin. There is no significantly difference between different conditions. (B) Western blots data for phosphorylation of focal adhesion kinase for different conditions. All the data is normalized to Beta actin.

**Fig. 6.5.** Tube formation assay with different VEGF clusters. Different conditions are introduced to a fibrin gel and analyzed the data for different branching formation. (A) there is no significant differences between different conditions. The reason could be the presence of the fibronectin in the fibrinogen that blocks the effect of the cluster Fn/VEGF on branching formation. (B) Flourescent images of different sproutinf from cytodex beads. Endothelial cells are stained with pholloidain actin and DAPI and images are representing of different cluster VEGF branching inside fibrin gel. The soluble condition was replenished with 5 ng/ml of soluble VEGF in the media every other day.

# VITA

**Education**

- M.S. in Chemical Engineering, University of Sharif Technology, Iran 2007
- B.S. in Chemical Engineering and Minor in Petroleum,Amir Kabir Univesity of Technology 2005

**Honors and Awards**

- MCTP bridge intern, University of California Los Angeles 2009
- Nationwide University Master Exam, Ranked 16th among 2000 students, Iran 2000
- High School Diploma, Ranked 1st among 250 students, Iran 1999

**Experience**

- Segura Lab, Ph.D. Candidate, Bioengineering at UCLA 2009-2014
- Vosoughi Lab, graduate Research assistant, Sharif University of Technology, Iran 2006-2007
- Prof. Modaress Lab, Undergraduate research assistant, Amir Kabir Universiy, Iran 2005

**Peer-reviewed Publications** (*- authors contributed equally)

1. **Gojgini, S**, Tokatlian, T., Segura, T. Utilizing Cell-matrix Interactions to Modulate Gene Transfer to Stem Cells inside Hyaluronic Acid Hydrogels. 2011 Molecular Pharmaceutics. 8,1582-91.*)*
2. Lei, Y., **Gojgini, S.**, Lam, J., Segura, T. The spreading, migration and proliferation of mouse mesenchymal stem cells cultured inside hyaluronic acid hydrogels. 2011 Biomaterials. 32, 39-47.

**Podium Presentations** (* - presenting author)

1. **Gojgini, S.**, Segura, T., "Engineering clustered VEGF to promote angiogenesis *in vitro"* 2013 AIChE Annual Meeting, San Francisco, CA, USA, Nov. 2013.
2. **Gojgini, S.**, Segura, T. "Utilizing Cell-matrix Interactions to Modulate Gene Transfer to Stem Cells inside Hyaluronic Acid Hydrogels." Nagoya-UCLA International Symposium, Los Angeles, CA, USA, Aug. 2011.

**Poster Presentations (* - presenting author)**

1. **Gojgini, S.***, Segura, T. "Engineering clustered VEGF to promote angiogenesis *in vitro",* Nanotechnology & Nanomedicine Symposium, CNSI, Los Angeles, CA, USA, Oct. 2013.
2. **Gojgini, S.***, Segura, T. "Engineering clustered VEGF to promote angiogenesis *in vitro"* Gordon Research Conference 2013, Holderness School, NH. Aug. 2013.
3. **Gojgini, S.***, Segura, T "Design of hydrogel scaffolds for non-viral gene delivery", Vascular Biology Conference, Hyannis, MA, USA, Oct. 2012.
4. Lam, J.*, **Gojgini, S.**, Lei, Y., Segura, T. "Effect of various hyaluronic acid hydrogel formulations on stem cell survival, proliferation and migration." Vascular Biology Conference, Los Angeles, CA, USA, June 2010.

5. **Gojgini, S.***, Lei, Y., Rahim, M., Segura, T. "Design of hydrogel scaffolds for non-viral gene delivery" IVBM Conference, Los Angeles, CA, USA, 2010.
6. **Gojgini, S.***, Lei, Y., Rahim, M., Segura, T "Non-viral Gene Delivery in Fibrin and HA Gels", Materials Creation Training Program 8th Annual Symposium, Los Angeles, CA, USA, Nov. 2009.
7. **Gojgini, S.***, Vosooughi, M. "Protein Immobilization on Carbon Nanotubes as a Template for Drug Delivery Applications", the 5th International Chemical Engineering Congress & Exhibition, Kish Island, I.R. Iran, Jan.2008.
8. **Gojgini, S.***, Vosooughi, M. " Two Different Approaches of Functionalisation of Carbon Nanotubes and Binding of Amphotericin B to these f-CNTs for Drug Delivery Applications", the 2nd Conference on Nanostructures, Kish University, kish Island, I.R. Iran, March 2008

# Chapter 1

## *Overview of thesis and specific aims*

### 1.1 Motivation and objectives

The limited ability of the human body to regenerate tissue or whole organs after severe injuries has made tissue engineering and regenerative medicine one of the most extensively researched topics over the past years. Some success has been achieved with systems that are not dependent on complex formation of blood vessels such as skin and cartilage replacement therapy[1]. Blood vessels are essential for the delivery of oxygen and nutrients to all tissues in the human body[2]. A number of diseases, such as stroke, heart failure are caused by a restriction in blood supply to tissues which results in a shortage of oxygen and nutrient delivery and can lead to tissue death[3, 4]. To induce the formation of a normal vasculature in ischemic tissue sites, biomaterials can be used to facilitate the regeneration and revascularization of the newly formed tissue by providing physical and chemical cues to the surrounding tissue[2, 5]. Current tissue regeneration approaches involved in developing scaffolds aim to mimic the extracellular matrix (ECM). Then in order for cells to grow, attach,

migrate, differentiate and finally remodel the scaffold/ECM, several biochemical molecules and bioactive signals must be loaded inside the scaffold. This scaffold can then be implanted along with stem cells in the area of injury to promote healing and regenerate the tissue. Hydrogels, a three-dimensional scaffold fabricated from different backbone polymer chains, have served as a scaffold to deliver drugs, cells or both to the site of injury. To design a biocompatible bioactive scaffold to promote tissue regeneration through of stem cell transplantation, one must first select the optimal polymer backbone and then incorporate the necessary biochemical cues. To improve tissue regeneration, it is also crucial to consider and direct how the biochemical cue is presented to the cell. Thus, the objective in this thesis is to develop a scaffold which will then be used as a delivery vehicle for cells to promote vascularization. The focus is to understand the role of growth factor incorporation in biomaterials from both the molecular and cellular point of view. We aim to promote angiogenesis to re-vascularize the ischemic tissue. The focus is on the vascular endothelial growth factor (VEGF), previously shown to regulate the process of angiogenesis. The regulation of cellular functions through VEGF signaling pathway is poorly understood. One of the main questions is how VEGF initiates and then modulates the proliferation, migration and differentiation of endothelial during the angiogenesis and more specifically during the branching process. Here, we aimed at designing biomaterials that can promote guided vascular sprouting, in order to developing a method to answer this question.

### 1.2 Specific aims

VEGF regulates migration and proliferation of endothelial cells (ECs) in pre-existing blood vessels[6, 7]. Several types of specialized ECs are required to build a functional blood vessel branch[8]. The presence of VEGF at the site of an ischemic damage enables ECs to undergo a phenotypic switch to tip cells, which lead the way in a branching vessel[8, 9]. In order to engineer materials capable of restoring the vascular network of a damaged or diseased tissue, the material must be able

to induce the tip cell phenotype switch. Genetic studies have already evidenced that the presence of both VEGF gradient and the overall concentrations of VEGF are important in the process of selection and induction of the tip cell phenotype[10]. In addition, the activation of integrins has been shown to promote angiogenesis[11], possibly through synergistic signaling between VEGF receptor-2 and integrin receptors, leading to the induction of the tip cell phenotype. Fibronection (Fn) is an ubiquitous extra-cellular matrix (ECM) ligand for several integrins[12]. Our overarching hypothesis is that modulating VEGF presentation to its receptor by displaying the growth factor in a cluster conformation activates the VEGFR-2 signaling pathway and enhances the tip cell phenotype switch and thus controls vessel branching in a more efficient and controlled way than the VEGF in its soluble form. In addition, we hypothesize than the addition of Fn fragments to VEGF clusters further increases this effect.

### 1.2.1 Specific aim 1 (chapter 2, 4)

In this first section, we aim at engineering a hydrogel material by crosslinking hyaluronic acid (HA) with matrix metalloproteinase (MMP) degradable peptide using a Michael addition chemistry that can be used as a vehicle for gene transfer. Stem cells will be encapsulated inside this hydrogel after being studied its matrix stiffness, RGD concentration, RGD presentation and ratio of polyplex nitrogen to phosphate (N/P ratio).

> *Hypothesis (Chapter 4)*: Design of hydrogel scaffolds is crucial for an effective delivery of DNA to stem cells. Parameters such as higher N/P ratios, softer hydrogels and higher RGD concentration is associated to higher gene transfer efficacy.

### 1.2.2 Specific aim 2 (chapter 2, 3, 5)

In this aim, we will first synthesize and characterize heparin nanoparticles. Heparin has been identified to have electrostatic binding sites for VEGF, later used to covalently attach the growth factor to heparin. We will also use a protein immunoblot assay to test the activity of bound VEGF to nanoparticles, and to further characterize the different presentations of VEGF depending on the clustering density on nanoparticles. We will also evaluate the tip cell phenotype switch of ECs exposed to both clustered and soluble VEGF in 2D and 3D. Then, we will test the effects of VEGF presentation on re-vascularization of the infarct core in a mouse model of cerebral ischemia. We will analyze vascular density and vessel maturity in this model.

*Hypothesis (chapter 5):* VEGF displayed in a clustered conformation results in enhanced level of phosphorylated VEGF receptor-2 and tip cell phenotype switch compared to soluble VEGF and the transplantation of HA-based hydrogel containing VEGF clusters in cerebral ischemia will enhance vessel formation and maturation.

### 1.2.3 Specific aim 3 (Chapter 3, 6)

Fn is a physiological co-factor for VEGF-A clusters and is known to enhance VEGF receptor-2 phosphorylation. We will introduce Fn fragments that have affinity for the main integrins $\alpha_5\beta_1$ to our VEGF clusters and will repeat the cellular and molecular experiments in Aim 2 to determine the role of Fn fragments in the migration, proliferation and phenotype switch of ECs. The overall goal of this project is to design a transplantable biomaterial that can promote the formation and maturation of newly formed vessels at sites of injury.

*Hypothesis (Chapter 6):* The addition of Fn fragments to heparin nanoparticles of VEGF enhances the effect of VEGF clusters on the activation of VEGFR-2 signaling pathway and vessel branching through synergistic signaling between VEGFR-2 and integrins on ECs surface.

## 1.3 Thesis outline

After this introductory Chapter, Chapter 2 and 3 provide a relevant background to the thesis topic. First, in chapter 2, the importance of designing scaffolds for vascularization will be reviewed. Hydrogel design parameters will be discussed as well as recent approaches to promote angiogenesis using biomaterials. Then, the different systems of growth factors delivery as well as non-viral gene delivery will be introduced. The following chapter will be more specifically focused on VEGF and its signaling cascade. The rest of the Chapters will be about the conducted research, methods and discussion. The flow of the thesis is illustrated in Figure 1.1.

In chapter 4, the design of scaffolds for DNA delivery will be described. Different parameters such as different ratios of polyplex to phosphate (N/P), stiffness of hydrogel scaffolds, concentration and presentation of adhesive ECM molecule (RGD) have been studied in terms of gene transfer efficiency to stem cell. The obtained results clearly demonstrate that cell-matrix interaction is an important factor to consider directing stem cell fate. Chapter 5 will be focused on the importance of VEGF in the initiation and control of the angiogenesis process. In this chapter, the distribution of VEGF in the form of clusters will be reviewed. The effect of growth factors distribution on neovessels tube formation at the cellular level and the mechanism by which this specific distribution promotes the tip cell phenotype switch was investigated. The aims and

hypotheses of this chapter detail the effect of VEGF presentation on HUVEC signaling and vessel tube formation *in vitro* and *in vivo*. Indeed, the results obtained in the previous chapters in the *in vitro* studies were translated *in vivo* to a mouse model of stroke, where the optimal VEGF cluster condition was transplanted within a hydrogel, in mice previously submitted to a cortical stroke and analyzed in terms of re-vascularization of the infarct core. In chapter 6, we incorporated another component to our system described in chapter 5, Fn, known to be a ligand for integrin receptors. In order to investigate the effect of cross talk between receptors. The results have been summarized in chapter 6. We aim to demonstrate the importance of considering growth factor presentation in a biomaterial when designing scaffolds for the regenerative medicine.

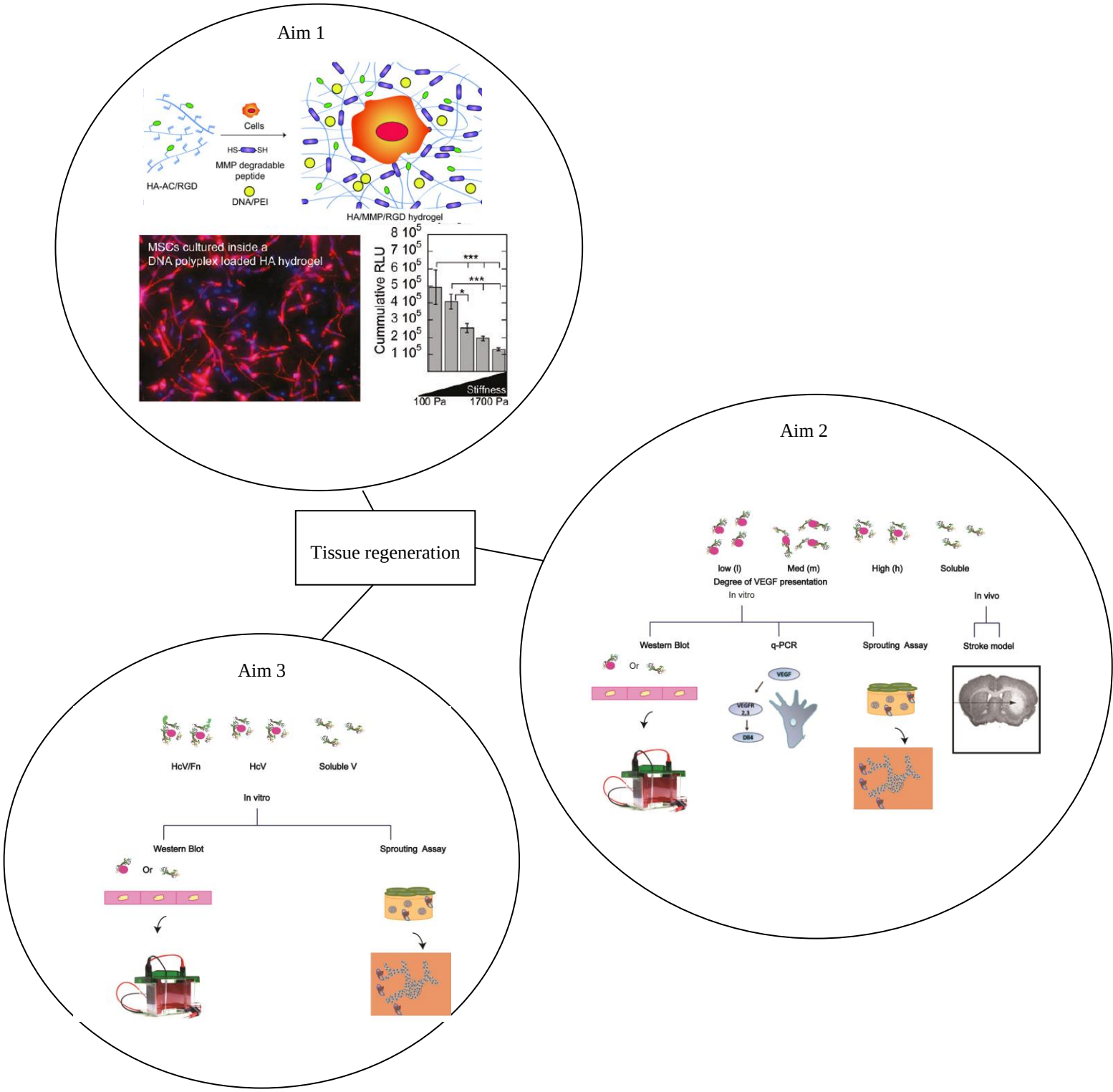


**Scheme 1.1.Overall Thesis review.** Aim1: Design of HA hydrogel for an optimal gene transfer efficiency to stem cells using cell-matrix interaction. Aim 2: *in vitro* study of VEGF presentation on vessel formation and tip cell phenotype at a molecular/cellular level and translation *in vivo* into a mouse model of cerebreal schemia. Aim 3: Incorporation of Fn fragments to VEGF nanoparticles to study *in vitro* the synergy effect of integrins and VEGFR-2.

# Chapter 2

# *Design of Scaffold for Vascularization*

## 2.1 Role of Vascularization in tissue regeneration

Tissue remodeling and regeneration of a damaged tissue requires a vascular supply to support survival of growing cells into the scaffold[13, 14].This complex process involves extensive interplay between cells, soluble factors and extra-cellular matrix (ECM) components. However, infiltration of blood vessel into a scaffold is not sufficient and the perfusion of branched capillaries is needed to provide a feasible mature tissue construct[1]. Thus, the promotion of angiogenesis, defined by the development of new blood vessels from pre-existing vessels, is essential in the success of formation of a new tissue. There are two approaches in this process; the first one is the general promotion of vascularizing scaffolds upon implantation *in vivo,* while the other one aim to pre-vascularize scaffolds *in vitro* or in vivo before implantation[13, 15]. The former approach is called inosculation and it offers the possibility of drastically accelerating vascularization of large three-dimensional (3D) tissue-engineered constructs and enhanced scaffold survival[15, 16]. However, the latter approach is more recent and challenging, since the cell source for future clinical application is still not clear.

Several attempts were made to promote angiogenesis through bio-engineered scaffolds with incorporated pro-angiogenic growth factors and genes. Here, we will discuss the key parameters and factors involved in the design of these biomaterials. Later, we will discuss the signal delivery from these biomaterials, focusing on hyaluronic acid (HA) hydrogel, the polymer used in the first part of this research.

### 2.1.1 Biomaterials

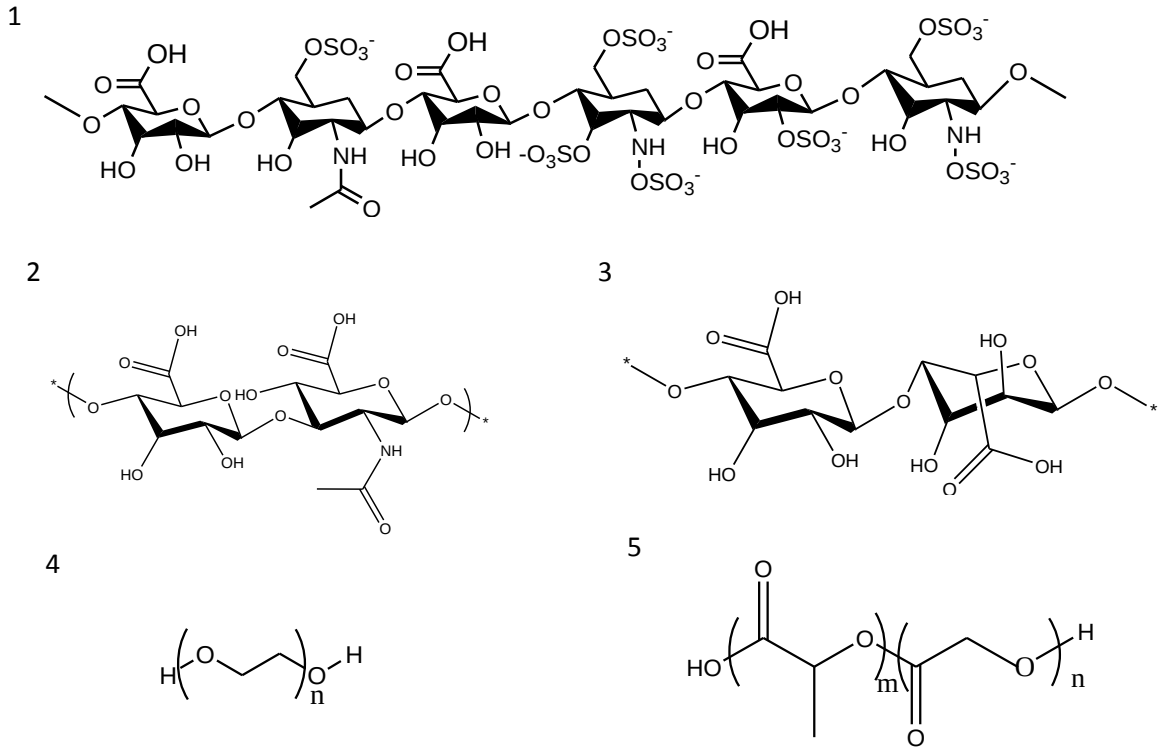


**Figure 2-1.** Chemical structures of synthetic and natural polymers. Natural: (1) Heparin, (2) Hyaluronic acid (HA), (3) Alginate. Synthetic: (4) Poly(ethylene) glycol, (5) Poly(glycosidic-co-lactic acid

Biomaterials can be originated from synthetic or natural or both polymers. Some common synthetic polymers have been used widely in tissue regeneration: Polyethylene Glycol (PEG), Polylactic-co-glycolic acid (PLGA) and Poly vinyl alcohol[17]. These polymers are favorable, because their physical properties are tunable during synthesis. PEG and PLGA are both part of the biocompatible polymers approved by the Food and Drug Administration (FDA)[17-20]. Another

biodegradable polymer scaffold that has been used as a supportive 3D environment for human embryonic stem cells (hESCs) growth is a mixture of pol(L-lactic acid)/poly(DL-lactic-co-glycolic acid) (PLLA/PLGA). In vivo studies with this mixed hydrogel showed significant effect on enhanced vascular colonization after transplantation[20]. Natural polymers such as collagen, alginate, chitosan, hyaluronic acid, fibrin, matrigel and heparin are another alternative that possess intrinsic properties that can play a role in signaling to surrounding cells[17, 21]. The first natural polymer that used as a 3D network reconstructed in vitro within a 3D tissue-engineered skin substitute was chitosan-linked collagen-glycosaminoglycon sponge in 1998[22]. Fibrin is a natural hydrogel that has been studied in stem cell delivery *in vitro* [23]and *in vivo*[24]. Fibrin has been used in various medical applications such as wound healing model and also in surgical applications to prevent bleeding. Because of its high biocompatibility and biodegrability, this last polymer was used widely as a cell delivery matrix for tissue engineering[25-27]. Hyaluronic acid (HA), an anionic, non-sulfated glycoaminoglycan and major component of the ECM, is widely distributed in connective, epithelial and neural tissue[28]. Recently, HA has gained popularity as a biomaterial for tissue engineering and tissue regeneration due to its high biocompatibility and low immunogenicity[29-32]. Several studies have demonstrated that HA-based hydrogels are good candidates for culturing stem cells[33-37]. Indeed, it has been shown that HA specifically interacts with cell surface receptors, such as CD44, RHAMM (receptor for HA mediated motility) and ICAM-1 (intercellular adhesion molecule 1), and contributes to tissue hydrodynamics, cell proliferation and migration[38, 39]. Semi-synthetic hyaluronic acid (HA) hydrogels which are also degradable by matrix metalloproteinases (MMPs) have previously been developed for culturing mouse mesenchymal stem cells in 3-dimensions[40]. While peptides and growth factors can be easily incorporated within these hydrogels, rapid degradation by proteases generally limits their effectiveness in long-term cell culture.

### 2.1.2 Mechanical

Elasticity (*E)* is different for different tissues: it can be as stiff as striated muscle (about 10 kPa) or as soft as brain tissue (ranges between 300 and 1000 Pa)[25]. It is now known that ECM changes of the mechanical properties or its elasticity affect protein expression, organization and differentiation of cells. For mesenchymal stem cell differentiation, the stiffness of the substrate determines the fate of these cells, thus leading toward a hard tissue fate such as bone or a soft tissue fate like the skin[26, 27,41].The effect of stiffness on stem cell differentiation has been studied on various materials including collagen and hyaluronic acid hydrogels[42, 43]. It has been shown for instance that a stiff hyaluronic acid (HA)-based hydrogel could be used as a conducive substrate for the differentiation of human mesenchymal stem cells (MSCs) into pre-osteoblasts without the addition of osteogenic supplements. This HA hydrogel system, referred as the doubly crosslinked networks (DXNs), is composed of densely crosslinked HA hydrogel particles (HGPs) covalently connected to a loosely crosslinked secondary HA-based network (with an average compressive modulus of 21kPa). After 28 days of culture of MSCs on the resultant composite gels, a production of Type I collagen as well as mineral deposition of the MSC could be detected[42].

Mechanical properties of the biomaterial also affect cell spreading, proliferation as well as migration. Cells behave differently in a two dimensional (2D) space than three dimensional (3D) one. For instance, cells seeded in stiff 2D matrices show enhanced transgene expression[44]. In a 3D space, it has been shown that MSCs behavior such as proliferation, spreading and migration is a function of HA hydrogels stiffness. Our group has previously shown that controlling the stiffness of HA through the concentration of HA polymer in the gel precursor solution or through the degree of crosslinking modulates cell proliferation. Indeed, a stiff HA gel leads to a lack of all these, and cells remain constrained to a spherical shape. In softer gels, however, they are nicely spread, proliferate and migrate[45].

Putman's research group demonstrated that matrix density effects capillary morphogenesis in 3D tissues *in vitro* by using a fibrin-based hydrogel where micro-carrier beads previously coated with human umbilical vein endothelial cells (HUVECs) were encapsulated. In this study, mesenchymal cells were cultured on top of the gel. They showed that an increased gel density was associated with inhibited vessel sprouting and branching, due to the inability of cells to secrete MMPs in order to remodel the gel and impeded diffusive transport[46]. Translated *in vivo*, their study showed the same results with the subcutaneous transplantation of encapsulated MSCs within fibrin gels of different stiffnesses into a wound model in SCID mice[47].

Gene transfer efficiency is also dictated by mechanical properties of the substrate. Mooney's research group investigated the influence of the rigidity of the substrate on gene transfer. Their 2D study showed that an increase in the stiffness of different substrate such as collagen, and alginate matrigels enhances gene transfer of cells seeded on top of these substrates[48]. However, in 3D spaces, cells intend to behave differently, as an increase in gel stiffness is associated with decreased gene transfer efficiency. Chapter 4 will discuss the differences between 2D and 3D for gene transfer.

### 2.1.3 ECM

The natural extracellular matrix (ECM) is a dynamic network consisting of protein fibers and polysaccharides that support cell fate and provide biophysical and biochemical cues to cells through cell surface receptors, such as integrins[49, 50]. Naturally cells degrade the ECM through proteases during their migration and tissue remodeling. Synthetic ECM hydrogels that aim to provide an environment in which to direct stem cell fate should recapitulate key features of the natural ECM such as integrin mediated cell binding and growth factor mediated signaling, while

also allowing for cell migration and proliferation. Our lab has previously tested the effect of ECM molecules on gene transfer using MSCs cultured on surfaces coated with different extracellular matrix proteins such as vitronectin, fibronectin, collagen type I, collagen type IV and laminin. We found that the overall gene expression was enhanced only on the surfaces coated with collagen type IV and fibronectin. This study suggested that the identity of the ECM proteins as well as their density play a crucial role in the gene transfer efficiency. This could be explained by the fact that different ECM proteins employ different pathways for internalization, leading to different intracellular trafficking and gene transfer effect[51]. Besides different ECM protein, matrix design also influences gene transfer. Another publication from our laboratory, Talar Tokatlian et al., showed that porous hydrogel scaffolds could represent a promising approach to deliver nucleotides to damages tissues. For this, microporous HA gels were engineered to incorporate DNA polyplexes with a high loading technique, leading to long-term sustained transfection and transgene expression of encapsulated MSCs. The system consisted in a two-phase hydrogel, in which the polyplexes were incorporated within a stiffer HA microporous gel, while MSCs were encapsulated in a softer nano-porous. They hypothesize that as the inner gel was degraded through cell-secreted proteases, cells were able to spread and proliferate faster, degrade the softer gel to reach the polyplexes and express the transfected genes[52]. Based on these findings, we will discuss in chapter 4 the role of these 2 phase matrices on gene transfer efficiency.

### 2.1.4 Peptide (RGD)

Cell-matrix interactions play an important role in cellular response such as differentiation, proliferation and migration, thus have a crucial role in regenerative processes such as wound healing, inflammation and angiogenesis. The interaction happens through integrin family of cell adhesion molecules that initiate signaling events leading to different cellular behavior and thus remodeling of the matrix[53, 54]. Several published studies showed the effect of RGD, a cell adhesive

peptide from fibronectin, on cell spreading and differentiation[45, 55]. RGD presentations in 2D spaces were shown to influence transgene expression. Indeed, clustered RGD results in enhanced gene transfer compared to when homogeneously distributed[56]. Studies in 3D spaces showed that the migration rates as well as the matrix degradation are important parameters that influence transgene expression[57, 58].

We showed that MSCs spreading from HA hydrogels only happens when both RGD and MMP degradation sites are present in the scaffold. Migration and cell spreading within the hydrogel requires the cells to displace the polymer chain and degrade them in order to make space for their movements. We also showed that RGD at a higher concentration can result in a higher spreading and faster migration of these cells[45]. Furthermore, another publication from my research group showed that not only the concentration of RGD affects cell behavior, but its presentation modulates MSCs integrin expression. We found that the degree of RGD clustering affects cell behavior. In addition, we found that an optimal RGD concentration associated with the optimal RGD clustering within the gel resulted in a better cell spreading and integrin expression[54]. Based on these results, we decided to use the RGD as a clustered conformation in our study (chapter 4).

## 2.2 Non-Viral gene delivery from scaffold

### 2.2.1 Bioactive signal /growth factor delivery

Promoting angiogenesis through the efficient delivery of proteins such as growth factors represents a challenge. Many proteins have a short half-life and their delivery routes are limited. This limitation motivates the study of a more controlled delivery system of growth factor. Some of the most promising systems for the controlled release of growth factors involve encapsulation or entrapment of proteins in biocompatible device[59].

#### 2.2.1.1Particle delivery

Delivering VEGF through particles can represent an efficient way to control the total dose

and the delivery efficiency. Steven et al. has previsouly developed a new method to release VEGF from small alginate microparticles using different ionic crosslinkers. They showed that the cytotoxicity and bioactivity of encapsulated VEGF in these particles were unaffected using crosslinking with $Zn^{2+}$ or $Ca^{2+}$. They then suggested that this approach could be used for the sustained VEGF delivery in association with ECs transplantation for the treatment of ischemic diseases[60]. Another work published by Justin et al. used PLGA nanoparticles for sustained VEGF release to promote blood vessel growth *in vivo*[61]. They found that 89% of the encapsulated VEGF was released gradually from the 200-600 nm PLGA nanoparticles within 4 days. An aortic ring angiogenesis assay was used to verify the bioactivity of encapsulated VEGF. In a mouse femoral artery ischemia model, VEGF-NP-treated limbs showed a significant increase in total vessel volume and thickness compared with soluble VEGF and saline conditions while no significant difference was found for vessel density or spacing. Interestingly, the unchanged anisotropy indicated that VEGF-NP treatment did not change the degree to which vessel were oriented in a specific direction[61]. Another example is the injection of PLGA microparticles releasing VEGF in the brain to recruit endothelial cells (ECs) from the host and to promote neovascularization in the lesion cavity. Treatment with VEGF-MP induced not only an increase in capillaries, but also in vessels of greater caliber (arterioles), suggesting that prolonged release of VEGF indirectly promotes arteriogenesis by stabilizing the vessels through pericyte and/ or smooth muscles recruitment and proliferation. They have evidenced that the release of VEGF from PLGA particles could provide a structural support for human neural stem cells (hNSCs), as well as promote a neo-vascularization of the cavity for in situ tissue engineering in the brain[62].

Another polymer that has widely been used is heparin, described later in the chapter. The *in vitro* data obtained with VEGF nanoparticles on ECs were then translated to an *in vivo* level. We will discuss in chapter 5 the use of heparin as a nanoparticle-based system to deliver VEGF to the

stroke cavity in a mouse model of cerebral ischemia.

#### 2.2.1.2 Co-delivery of growth factors

Besides delivering VEGF by itself, all kinds of other growth factors were used a co-administration delivery with VEGF. Some examples are: VEGF and PDGF through membrane[63], VEGF and FGF-2 from allografts[64]. Mooney's research group developed a polymeric system for dual growth factor delivery in which PDGF and VEGF, two pro-angiogenic growth factors, were incorporated into a polymer scaffold. Their system resulted in a rapid release of VEGF, while PDGF release was regulated by the degradation of the polymer, thus resulting in a significantly slower release. This sequential dual growth factor release system showed a significantly enhanced blood vessel formation compared to the delivery of either growth factor alone[65]. The Hammond's research group developed a technique in which they achieved a tunable release of dual growth factor BMP-2 and VEGF from a polyelectrolyte multilayer films fabricated using the layer by layer assembly. They used their system in a macroporous polycaprolactone/b-tricalcium phosphate (PCL) scaffold for both *in vitro* and *in vivo* model to test the enhancement of bone tissue regeneration after transplantation. Their *in vitro* study showed a release of 1/3 of the BMP-2 and 2/3 of VEGF after 3 days. The important element of their system is its ability to load independently two different growth factors and control their release. In addition, the electrostatic interactions between growth factor and the surrounding polymer chains in the film prevent the growth factors from leaching or diffusing out. The *in vivo* results of this study showed that the transplantation of this dual GFs system in the bone was associated with an increased mineral density within the transplanted scaffold, suggesting the presence of bone tissue formation, compared to the delivery of BMP-2 alone[66].

#### 2.2.1.3 Hydrogel/scaffold delivery

Another approach for non-viral delivery is hydrogel-based growth factor delivery. There are several methods that can be used: direct loading, electrostatic interaction or covalent binding of the growth factor to the hydrogels[67]. For instance, the subcutaneous transplantation of covalently bound basic fibroblast growth factor (GFG-2) to an HA hydrogel through heparin, into a mouse model of wound healing in Balb/c mice, showed an increased vessel growth within the gel over the course of 28-35 days, compared to a group where the growth factor was soluble within the gel[68].

One of the challenges of non-viral delivery is the 3D instability of growth factors. One of the strategies can rely on the electrostatic interaction between growth factors and polymers, ECM proteins or heparin. That protects growth factor conformation, and thus function, as well as increase during the delivery process. Heparin is a linear sulfated glycosaminoglycans (GAG) with a molecular weights of 10000~ 100000. Heparin is a highly negatively charge polymer that binds to a range of growth factor families such as VEGF and PDGF-BB. It has been showed that the electrostatic interaction between heparin and GFs through sulfation motifs leads to a better resistance to proteolysis and thermal denaturation[67, 69, 70]. Many studies have used heparin to deliver GFs either as a crosslinker or as a nanoparticle conformation[71, 72]. Lonnie Shea's research group has developed a heparin-chitosan nanoparticle system that binds GFs to porous PEG hydrogels to locally retain vectors and enhance lentivirus delivery efficiency. Using this method, they successfully over-expressed the angiogenic factors (sonic hedgehog (Shh) and VEGF) to promote blood vessel formation[71]. Another group has immobilized a sub-micron layer of heparin to a porous polycaprolactone (PCL) scaffolds including VEGF and subcutaneously implanted their system in a mouse model of wound healing. They observed that heparin-PCL scaffold loaded with VEGF leads to a significantly higher infiltration of blood vessels within the hydrogel and an enhanced formation of stable and functional vessels[72].

An alternative approach in protein delivery is to deliver the encapsulated gene encoded for the growth factor to promote the expression of those factors for the desired cell fate. Gene delivery as well as protein delivery is dependent on the development of an efficient delivery vector. Gene delivery has fallen in two categories: viral and non-viral. Viral vectors which are mostly viruses have higher efficiency for gene delivery. However, due to safety concern, immunogenicity, non-viral vectors are more preferred. The widely used non-viral vectors are cationic lipids or polymers that can complex with the nucleic acid through the negative-positive electrostatic charges to form particles. These nanoparticles are in the order of 100 nm which protects DNA from degradation[73].

### 2.2.2 Non-viral gene delivery

Local gene delivery using hydrogel scaffolds has been studied for over a decade primarily through the encapsulation of naked DNA during hydrogel formation. Naked DNA has been successfully incorporated inside collagen [74], pluronic-hyaluronic acid [75], PEG-poly(lactic acid)-PEG[76], alginate [48], oligo(polyethylene glycol) fumarate[77] and engineered silk elastin[78]. Although naked DNA has been evidenced to be capable of gene expression and to guide tissue regeneration *in vivo*[74, 79], limitations with low gene transfer efficiency and rapid diffusion of the DNA from the hydrogel scaffold has motivated the use of DNA nanoparticles instead of naked DNA. DNA condensed either with cationic peptides, lipids, or polymers was introduced into fibrin hydrogels[80-84], enzymatically degradable PEG hydrogels[80] and PEG-hyaluronic acid hydrogels[81]. PEI is a cationic polymer that has been widely utilized for non-viral gene delivery. PEI is able to condense DNA through electrostatic interactions between the positively charged amines on the PEI and the negatively charged phosphates on the DNA, forming nanoparticles (polyplexes) in the range of 50 to 200 nm[85]. PEI has been successfully used *in vivo* delivering DNA or siRNA to the brain[86, 87], lungs[88-91], abdomen[92], and tumors[93-95].

### 2.2.3 Non- viral DNA/PEI delivery

DNA/PEI has been delivered in natural polymer scaffold such as alginate and fibrin[82, 96]. In addition, many published studies have delivered DNA from synthetic polymer such as PEG that can be manipulated so the release of the DNA is controlled through the enzymatic degradation of the scaffold[58, 97]. Our group has developed a technique called caged nanoparticle encapsulation (CnE), which is a freeze dry process of DNA/PEI complex in order to overcome the problem of aggregation. With this method, we can load up to 5 μg of DNA polyplexes per microliter of HA hydrogel without a significant aggregation and maintain significant gene transfer efficiency. As we will discuss in chapter 4, the preparation of these CnE includes the use of agarose and sucrose during the lyophilization process. Agarose prevents the complex from aggregading during the gelation process while sucrose preserves the activity of the DNA during the lyophilization process. Our group has achieved efficient gene transfer by loading 5 μg of DNA polyplexes *in vivo* and *in vitro* using this method[45]. Chapter 4will discuss the use of this method to study gene transfer to stem cells as the effects of cell-matrix interactions on non-viral gene transfer are not well-established and required to further progress in hydrogel-mediated transfection.

## 2.3 Summary

Hydrogels are biomaterials that can be used for non-viral gene delivery to areas of damaged tissue to promote regeneration. Furthermore, because hydrogels are mimicking extracellular matrix, a variety of signal cues as well as proteins such as growth factors can be incorporated to this matrix to control encapsulated or attracted cell behavior. There are important design parameters to consider when developing a hydrogel system. The mechanical properties of the hydrogel as well as the distribution of the different cues such can change the fate of the encapsulated cells such as proliferation, spreading as well as gene transfer efficiency. Chapter 4 develops the appropriate design of hydrogel to achieve an efficient gene transfer utilizing ECM-cell interactions.

# Chapter 3

# *VEGF Signaling*

### 3.1 Introduction

Vascular endothelial growth factor (VEGF) is one of the most widely studied and applied growth factors that regulate vascular development. Since a major obstacle in tissue regeneration is the lack of stable blood vessel infiltration into engineered tissue implants, VEGF has been extensively utilized as a means to induce vascularization[98, 99] . It is now known that growth factors, particularly VEGF, send different signals to endothelial cells when presented to their receptors with different degrees of matrix affinity[100, 101]. By changing the growth factor affinity for the matrix, cells will receive different signals and behave accordingly. Incorporation of the heparin-binding (i.e. ECM binding) domain in exon 7 increases matrix affinity[102] and leads to induction of migration signaling over proliferative signaling[101]. Developmental biology studies in mouse embryos have shown that the physical presentation of VEGF is critical to the development of a normal vasculature. The over-expression of VEGF with high matrix affinity results in aberrant vessels with reduced vessel

thickness enhanced vascular branching and increased capillary density[103]. In contrast, embryos expressing VEGF with no matrix affinity displayed poor branching and enlarged vessel diameter.[103] Further, embryos expressing both VEGF with high and no matrix affinity contained a normal vasculature[103], indicating normal vasculature results in a combination of soluble and bound VEGF. In the adult, VEGF physical presentation is also critical for angiogenesis; VEGF lacking the protease sensitive region but containing the matrix binding domain (resembles high matrix affinity VEGF) results in highly branched vessels, while VEGF lacking the matrix binding domain (resembles no matrix affinity VEGF) results in vascular hyperplasia and increased permeability[104]. In a therapeutic setting, neither extreme in blood vessel morphology is desirable. Vessels should not be excessively branched (thin diameter) or large (thick diameter) and should remain impermeable to maintain blood within the blood compartment.

**3.2 VEGF discovery**

The VEGF family, in mammals, consists of five members: VEGF-A, B, C, D and Placenta growth factor (PLGF)[105-107]. VEGF-A was initially discovered as a vascular permeability factor (VPF) associated with tumor growth in 1983[105, 108]. In 1989, a few years after, Ferrara and Henzel, isolated a protein that induced the proliferation of endothelial cells and called it VEGF. Further studies showed that actually VEGF and VPF was the same molecule[105, 106].

Naturally, splicing of VEGF transcripts results in generation of different protein isoforms which regulates affinity for the ECM In particular, the gene encoding VEGF-A consists of eight exons that are separated by seven introns, resulting in the generation of 206, 189, 183, 165, 148, 145 and 121 amino acids. VEGF-A 165 is the most abundant isoform followed by 121 and 189 isoforms. VEGF-A 165 and 121 differs from each other only by lack of exon 7 in 121; as a consequence, 165 isoform binds heparan sulfate proteoglycans in the extracellular matrix, whereas the 121 does not. Another splice variant of VEGF-A, known as VEGF-A 165b, an inhibitory

isoform, has been proposed to negatively regulate VEGFR activity. In mice, VEGF-A isoforms are one amino acid shorter than their corresponding human isoforms[105, 106, 108, 109].

### 3.3VEGF Receptors and its signaling

VEGF binds to VEGFRs which are members of the receptor tyrosine kinases (RTKs) superfamily and are equipped with an approximately seven immunoglobulin-(Ig)-like domains in the extracellular domain. VEGF-A binds to both VEGFR-1(Flt-1) and VEGFR-2(Flk-1/KDR) which are primarily expressed in vascular endothelial cells, whilst VEGF-C and D bind to VEGFR-3(Flt-4) which is exclusively expressed in lymphatic endothelial cells. VEGFs also interact with a family of co-receptors, such as neuropilins (NRP) and HSPG[105, 107, 108]. In the signaling system we studied in the thesis, we mainly focus on VEGF binds to VEGFR-2. VEGFR-2 is type ш transmembrane kinase receptors, and is closely related to the platelet-desired growth factor receptors (PDGFRs). Binding of VEGF to the receptor induces dimerization and autophosphorylation of specific intracellular tyrosine residues. Phosphorylation of specific tyrosine residues in the receptor causes for the recruitment of specific intracellular proteins via their Src homology 2 (SH2) domains. The main tyrosine residues that are activated through this pathway are Y1175, Y1214, Y951, Y1054 and Y1059. Activation of intracellular signaling cascade results in proliferation, migration, survival and increased permeability. Y1214 and Y1175 are in the C-terminal tail of the receptor. The phosphorylation of Y1175 creates its binding to the adaptor protein called Shb. This binding regulates activation of FAK (focal adhesion kinase) and PI3K (phosphoinositide 3-kinase). This pathway leads to the survival and permeability of the cells. On the other side, binding of Y1175 to PLC-γ protein will lead to the activation of Erk ½ (extracellular regulated kinase 1 and 2) which results in the proliferation of the cells. Phosphorylation of Y1214 creates a binding site for the adaptor protein Nck, which results in activation of Cdc42 and p38 MAPK. This pathway leads to the migration of endothelial cells[105-107].

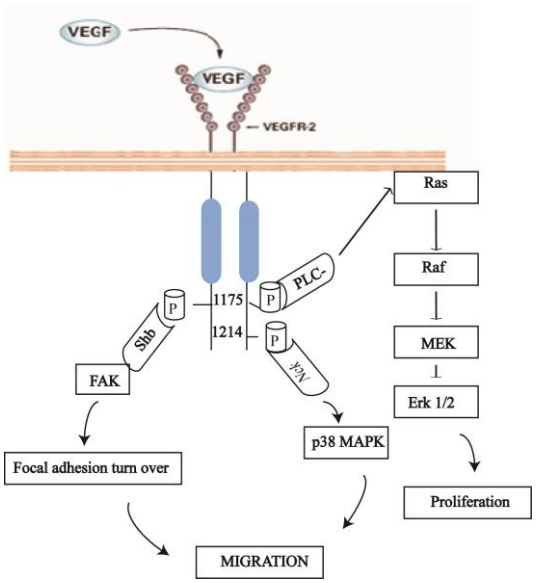


**Fig.3.1.** Representation of downstream cellular effects of the dimerization and activation of the VEGF/VEGFR-2 complex. The p38MAPK pathway, which promotes endothelial cell migration; and the Raf pathway, which induces endothelial cell proliferation[110].

### 3.4 Signaling of VEGFR-2 leads to cell behavior (tip cells/stack cells)

The understanding of the role of VEGF in the angiogenesis process has been growing, but the mechanism by which the process is initiated and controlled is still vague. In a healthy adult, vessels are in their quiescent form and signals for angiogenic response are low. Vessels provide oxygen and nutrients to the organs of the body, so the lack of oxygen is an inducible factor that stimulates angiogenic factors such as VEGF. The quiescent endothelial cells that are formed in a monolayer and are connected by junctional molecules such as VE-cadherin are called phalanx cells. In the presence of angiogenic factors such as VEGF, pericytes first detach from the basement membrane and endothelial cell junction loosens up by matrix metalloproteinases (MMPs). One endothelial cell becomes selected as “tip cell” and will take the lead. Tip cells migrate towards VEGF high concentration and using integrin adheres to the extracellular matrix. The neighboring

cells which are called stalk cells proliferate and elongate form lumen. These cells are prevented from becoming tip cells through Dll4/Notch signaling, which will be described later. These stalk cells then later attract pericytes to cover the lumen and allow perfusion of neovessels. The maturation of pericytes then resumes quiescence by promoting a phalanx phenotype. When one of the endothelial cells specialized to become tip cell in the presence of VEGF gradient and migrate, the inhibition of other cells to do so is due to tip-to stalk cell communication by Dll4/Notch signaling. Endothelial cells express various Notch ligands (Dll4, Dll1, Jagged 1, and Jagged2) and Notch receptors (Notch 1, 3, 4). The activation of VEGFR-2 upregulates Dll4 expression on tip cell surface, activating the Notch receptor on neighboring cells. Dll4 binds to Notch and downregulates the VEGFR-2 signaling. This causes the stalk cells to be less responsive to VEGF, inhibiting their migration and their phenotype switch into tip cells. Another Notch ligand, Jagged 1, contains a PDZ-binding motif that facilitates adhesion and migration of the tip cells. Other than VEGFR-2 and Dll4, tip cells are characterized by the expression of VEGFR-3 and platelet-derived growth factor (PDGF)-BB. VEGFR-3 expression is mostly limited to filopodia extensions at the tip cells at the edge of the vessel sprout, thus affecting the sprouting and branching process. The role of tip cells is to sense their micro-environmental cues and translate them into a dynamic process of cell movement through lamellipodia and filopodia. An attractive cue induces F-actin polymerization and cause the filopodia to extend. This filopodia adhere and form focal contact points to connect to the extracellular matrix (ECM). These results in stress fiber of actin filament production in the cytosol, pulling the cell and inducing forward movement at the edge of the filopodia to further extend it[14, 111-113].

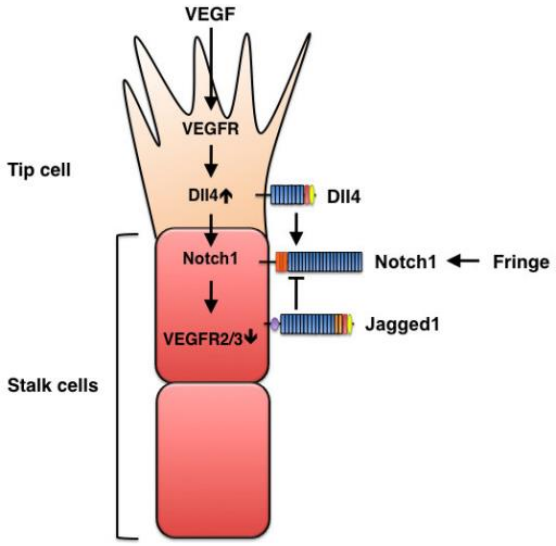


**Fig.3.2.**Opposing effects of Dll4 /Notch on the sprouting process of angiogenesis. VEGF signaling induces Dll4 expression on tip cells, and Dll4, in turn, activates Notch signaling in stalk cells, reducing stalk-cell sensitivity to VEGF stimulation and, consequently suppressing the tip-cell phenotype. Conversely, Jagged1 antagonizes Dll4-mediated Notch activation in stalk cells to increase tip cell numbers and enhances vessel sprouting. The antagonistic effects of the two ligands are controlled by Fringe-dependent modulation of Notch signaling[114].

### 3.5 Synergy strategy (co-localization)

In the previous chapter, we discussed the effect of ECM modulation on vascularization. Synergy in the downstream signaling pathways of VEGFRs is crucial for vascularization, but also the combined activation of integrins and VEGFR. Integrins are αβ heterdimeric cell-surface transmembrane receptors that link the ECM ligands to the actin cytoskeleton. They are responsible for cell adhesion and remodeling of ECM. They are known to play a critical role in angiogenesis[115-117]. Among the integrins, $\alpha_v\beta_3$ and $\alpha_v\beta_5$ and $\alpha_5\beta_1$ have been considered to positively regulate the angiogenic switch, because their pharmacological antagonists suppress pathological angiogenesis[118, 119]. In particular, interaction between VEGFR-2 and $\alpha_v\beta_3$ integrin is required for a full phosphorylation of VEGFR-2[107, 120]. However, it has been evidenced that mice lacking $\beta_3$ show normal vessel growth but increased tumor angiogenesis. In addition, gene deletion studies have demonstrated that both Fn and VEGF, and their cognate receptors $\alpha_5\beta_1$ and VEGFR-2 are critical for vascular development[121, 122].

### 3.5.1Fusion proteins

Hubbell's research group has studied endothelial cell attachment and spreading using FNIII10 fused to VEGF-A165[123]. They developed a bi-functional protein fusing VEGF and Fn type 10 domains III (FNIII10). This tends to preferentially bind to integrin $\alpha_v\beta_3$. They further investigated the effect of their system *in vivo* by using a diabetic mouse wound healing model. They demonstrated that blood vessels developed within 10 days post-injury were mature and in the fused FNIII10-VEGF condition compared to just VEGF[123]. Also, they showed that engineering the ECM environment with different domains of Fn (the $9^{th}$ to $10^{th}$ type III FN repeat and the $12^{th}$ to $14^{th}$ type III FN repeat), with the incorporation of VEGF and PDGF-BB, respectively results in skin repair and bone repair[124]. They showed that the two fragments of Fn (FN III9-10 and FN III12-14) closely presented in the same polypeptide chain was associated to an enhanced tissue regeneration, in both a mouse model of chronic wounds in diabetic condition, and in a rat model of critical-size bone defects[124]. Another group has showed that a fused protein with VEGF and the immunoglobulin Fc domain enhanced HUVECs growth[125].

### 3.5.2 VEGF with Fn

Errol et al have shown that Fn fragments containing both the $\alpha_5\beta_1$ integrin-binding domain (III 9 to 10) and the VEGF-binding domain (III 13 to 14) significantly enhanced VEGF-induced EC migration and proliferation and induced strong phosphorylation of the VEGF receptor and Erk.[126]

Fn is one of the main components of the ECM that binds to integrin receptors. It has been shown that Fn and VEGF are key regulators of blood vessel growth[108, 127, 128]. Their results suggest that the mechanism of Fn-induced enhancement of VEGF activity is due to the formation of an extracellular complex interacting with the cell surface receptors and the resulting promotion of co-stimulatory signaling from integrin and VEGF receptor[126]. It is also observed that directional endothelial cell migration was increased on the combined gradients of both VEGF and Fn as compared to the

VEGF alone or Fn alone[99]. With all these observations discussed in chapter 6, we will design a system in which we incorporate Fn fragment provided by Prof. Barker from the Georgia Institute of Technology. It's structure is stabilized by the fusion of the domain 9 and 10 of the Fn III, called FN III9*-10 ($Leu^{1408}$ to Pro) or FNV1, that preferentially binds $\alpha_5\beta_1$[117]. We will discuss the subject in detail in chapter 6.

**3.6 Summary**

VEGF has been known to be one of the most important pro-angiogenic factors, taking the lead in the initiation and the control of the angiogenesis process. VEGF initiates the stimulation of endothelial cells and provoked the ECs phenotype switch to specialized tip cells. The mechanism of this process is still poorly understood. Another parameter that needs to be considered in the understanding of the angiogenic process is the presentation and the 3D distribution of VEGF, affecting the regulation of vessel sprouting and branching. In the next chapter, we will investigate the role of different presentations of VEGF, by modulating its clustering conformation on heparin based-nanoparticles and its effect on ECs downstream signaling and the tip cell phenotype. The results obtained *in vitro* motivated the translation to *in vivo* model of cerebral ischemia in a young adult mouse, where VEGF nanoparticles of different densities will be injected within the stroke cavity. In the following chapter, we use the same system to incorporate Fn within the hydrogel system previously established, to assess the synergic effect of integrin receptors and the VEGR-2. In this last *in vitro* study, both results obtained at the molecular level and cellular level can be translated to an *in vivo* model to assess the effect of the VEGF/Fn synergy on tissue regeneration through controlled vascular branching and sprouting.

# Chapter 4

# *Utilizing Cell-matrix Interactions to Modulate Gene Transfer to Stem Cells inside Hyaluronic Acid Hydrogels*

## 4.1 Introduction

As we discussed in the earlier Chapter, We previously reported on a matrix metalloproteinase degradable hyaluronic acid hydrogel scaffold for stem cell culture[40]. Here we use this hydrogel scaffold to investigate how cell-matrix interactions modulate gene transfer. Matrices with different mechanical properties and RGD presentations are used to determine how these parameters affect gene transfer to cells seeded in three dimensions (inside the hydrogel scaffold). For these studies poly (ethylene imine) (PEI) was used as a transfection reagent. We believe that the use of gene based bioactive signals to guide stem cell differentiation or cell trans-differentiation in 3D hydrogel scaffolds will be a powerful approach for tissue engineering and tissue regeneration

applications.

## 4.2 Materials and Methods

### 4.2.1 Materials

Peptides Ac-GCRDGPQGIWGQDRCG-NH2 (MMPxl) and Ac-GCGWGRGDSPG-NH2 (RGD) were obtained from (Genescript, Piscataway, NJ). Sodium hyaluronan was a gift from Genzyme Corp. (Boston, MA). Gaussia luciferase expression vector (pGluc, New England BioLabs, Ipswich, MA) was expanded using an endotoxin free Giga Prep kit from Qiagen following the manufacturer's instructions. Linear PEI (25 kg/mol) was purchased from Polysciences (Warrington, PA). All other products were purchased from Fisher Scientific unless noted otherwise.

### 4.2.2 Cell culture

Mouse bone marrow cloned mesenchymal stem cells (mMSCs, D1, CRL12424) were purchased from ATCC (Manassas, VA) and cultured in DMEM (Invitrogen) supplemented with 10% bovine growth serum (BGS, Hyclone, Logan, UT) and 1% penicillin/streptomycin (Invitrogen, Grand Island, NY) at 37°C and 5% CO2. The cells were split using trypsin following standard protocols.

### 4.2.3 Hyaluronic acid modification

Acrylated hyaluronic acid (HA-AC) was prepared using a two-step synthesis to provide acrylate functionalities to the hyaluronan sodium. Briefly, hyaluronic acid (60,000 Da, Genzyme Corporation, Cambridge, MA) (2.0 g, 5.28 mmole, 60 kDa) was reacted with 18.0 g (105.5 mmole) adipic dihydrazide (ADH) at pH 4.75 in the presence of 4.0 g (20 mmole) 1-ethyl-3-[3-dimethylaminopropyl] carbodiimide hydrochloride (EDC) overnight and purified through dialysis (8000 MWCO) in DI water for 2 days. The purified intermediate (HA-ADH) was lyophilized and stored at -20 $^{o}$C until used. 40.46% of the carboxyl groups were modified with ADH based on the

trinitrobenzene sulfonic acid (TNBSA, Pierce, Rockford, Illinois) assay. HA-ADH (1.9 g) was reacted with N-Acryloxysuccinimide (NHS-AC) (1.33 g, 4.4 mmole) in HEPES buffer (pH 7.2) overnight and purified through dialysis in DI water for 2 days before lyophilization. The degree of acrylation of 10% was determined using $^{1}$H-NMR ($D_2O$) by taking the ratio of multiplet peak at $\delta$ = 6.2 corresponding to the cis and trans acrylate hydrogens to the singlet peak of the acetyl methyl protons in HA ($\delta$ = 1.6).

**4.2.4 DNA loaded HA hydrogel formation and characterization**

HA hydrogels were formed by Michael-type addition of bis-cysteine containing MMPxl peptides onto HA-AC functionalized with cell adhesion peptides (RGD). A lyophilized aliquot of RGD peptides (0.1 mg) was dissolved in 15 µL of .3M TEOA buffer (pH=8.7), mixed with HA-AC and allowed to react for 20 minutes at room temperature. The HA-RGD solution was kept on ice until used. DNA/PEI polyplexes were formed by mixing 5µg plasmid DNA with 4.57µg PEI in nuclease-free water, vortexing for 15 s and incubating for 10 min at room temperature. Polyplexes were cooled on ice prior to gelation. Immediately before adding the polyplex solution to the hydrogel precursors ice cooled 3M TEOA (pH=8.2) was added to bring the final concentration of buffer in the polyplexes to .3M TEOA. A lyophilized aliquot of the crosslinker (0.91 mg MMPxl) was then diluted in 18.2 µL of .3M TEOA buffer (pH=8.2) immediately before mixing with DNA/PEI polyplexes, HA-RGD (final concentration of 100 µM RGD) and the cell solution (500,000 cells per 100 µl final gel volume). The final gel solution had a pH=8.1 and all precursors were kept on ice prior to mixing. Gelation was achieved by placing a drop of the precursor solution between sigmacoted glass slides for 30 min at 37 °C. The final gel was placed inside 96-well plates for culture. Thorough mixing was used to ensure the polyplexes were uniformly distributed throughout the hydrogel.

Hydrogels with variable stiff nesses were prepared by changing the ratio of thiols to

acrylates (r ratio) or the concentration of HA used (see Table 1 for conditions and resulting storage moduli). To generate hydrogels with different RGD presentations different portions of HA-AC were first mixed with the constant amount of RGD peptide. The HA-RGD was then mixed with unmodified HA-AC. Thus homogenous RGD represents the condition were 100% of the HA-AC was mixed with the RGD peptide. For the RGD presentation studies a constant concentration of 100 μM RGD was used.

| Hydrogel ID | HA% | R ratio[1] | G' (+DNA) |
|---|---|---|---|
| 1 | 3 | 0.7 | 100.0±2.11 |
| 2 | 3 | 1.05 | 260.0±1.3 |
| 3 | 3.5 | 1.05 | 839±12.30 |
| 4 | 4 | 1.05 | 1360±11.73 |
| 5 | 5 | 1.05 | 1730±45.62 |

[1] The r ratio represents the moles of _SH over the moles of AC

Table 3.1. Hydrogel Formation Conditions and Overall Storage Modulus

To visualize the distribution of the polyplexes inside the HA hydrogels, gels were formed using the same protocol as described above but in the absence of cells. The hydrogels were stained with ethidium bromide post hydrogel formation and imaged using a fluorescence inverted microscope. The images were taken using the fluorescent (Observer Z1 Zeiss) microscope with 10x magnification.

### 4.2.5 Characterization of HA hydrogel mechanical properties (Rheology)

The storage and loss modulus were measured with a plate-to-plate rheometer (Physica MCR 301, Anton Paar, Ashland, VA) using a 8 mm plate under a constant strain of 0.03 with a frequency range of 0.1 to 10 rad/s. Hydrogels were made as detailed above and cut to a size of 8.0 mm in diameter to fit the plate. A humid hood was used to prevent the hydrogel from dehydrating during the test and the temperature was kept at (37°C).

### 4.2.6 Radiolabeling DNA

Plasmid DNA was radiolabeled with $^{3}$H-dCTP (100 µCi, MP Biomedicals, Santa Ana, CA) using a Nick translation kit (Roche, Indianapolis, IN) as per the manufacturer's protocol. Briefly, an equimolar mixture of dATP, dGTP, dTTP, and $^{3}$H-dCTP was prepared and added to the DNA (1 µg) solution. Once the enzyme solution was added to the mixture, the final solution (200 µl) was gently mixed by pipetting and incubated for 2 h at 15 °C. The reaction was stopped by addition of 10 µl 0.2 M EDTA (pH=8.0) and heating to 65 °C for 10 min. The DNA was purified using the mini Prep kit from Qiagen following the manufacturer's instructions. The final DNA concentration was 0.04µg/µl.

### 4.2.7 DNA/PEI polyplex release kinetics and activity

In order to determine the extent of release of the encapsulated polyplexes and their activity post encapsulation, gels were formed using the protocols indicated above with 1% radiolabeled DNA. To test the release kinetics, the gels were swelled in PBS for 2 h and the swelling solution was collected. The gels were then placed in 150 µL of release solution (PBS, 10 U/ml HAase and 0.50 U/ml Col I). At the indicated time points, 150 µL of the solution was removed and an additional 150 µL of fresh release medium was added. After 192 h, the Col I concentration was increased to 1 U/ml. Following the final release medium collection, the gels were incubated with 0.25% trypsin/EDTA to result in complete release of the DNA from the gel upon degradation. DNA concentrations were measured using a scintillation counter at the UCLA Chemistry core facility. The readout was analyzed using a standard curve.

To determine the activity of the encapsulated DNA/PEI polyplexes, a HA gel was prepared and swelled as indicated above using DNA encoding for Gaussia luciferase (pGluc). After swelling in PBS, the gel was degraded through incubation with 100 µL 0.25% trypsin at 37 °C for 10 min. To determine how much release solution should be added to add 0.5µg of DNA to mMSCs cultured

on a 48-well plate, the DNA concentration in the sample was measured using HOECHST dye (H33258). In a typical measurement, 100 µl heparin (10 mg/mL in PBS) was incubated with 10 µL of the degraded sample for 10 min at room temperature to displace the DNA from DNA/PEI complex.10 µL of the above solution was then mixed with 100 µL H33258 assay solution (0.1 mg/mL H33258 in TNE buffer (0.2 M NaCl, 10 mM Tris, 1.3 mM EDTA) and the fluorescence light intensity was read using a fluorometer equipped with a UV filter (Turner Biosystems, Sunnyvale, CA). The readout was analyzed using a standard curve measured using complexed DNA. The collected polyplexes from the degraded hydrogel sample was then used for a bolus transfection (0.5µg DNA for a 48 well-plate) and compared to freshly made polyplexes. The cell media was collected after 48 h and transgene expression was measured using the Gaussia Luciferase Assay Kit (New England BioLabs. Ipswich, MA) as described below (Gene transfer section).

**4.2.8 Cell viability, spreading and proliferation**

Cell viability in these hydrogels was studied using LIVE/DEAD viability/cytotoxicity kit (Molecular Probes, Eugene, OR). Briefly, 2 µl of ethidium homodimer-1 and 0.5 µL of calcein AM from the kit were diluted with 1 mL DMEM. Each gel was stained with 150 µL of this staining solution for 30 min at 37 $^{o}$C in the dark.

To better analyze cell spreading, separate gels were fixed for 30 min at RT using 4 % paraformaldehyde, rinsed with PBS, treated with 0.1 % triton-X for 10 min and stained for 90 min in the dark with DAPI for cell nuclei (500x dilution from 5 mg/ml stock) and rhodamine-phalloidin (5 µl per 200 µl final stain solution) in 1 % bovine serum albumin solution. The samples were then washed with 0.05 % tween-20. For both cell viability and cell spreading, an inverted Observer Z1 Zeiss fluorescence microscope was used to visualize samples. To better visualize the distribution throughout the hydrogel, multiple z-stacks 12-13 µm thick were taken for each image,

deconvoluted to minimize background, and presented as maximum intensity projections.

MTT assay (CellTiter 96$^{R}$ AQ$_{ueous}$ One Solution Cell Proliferation Assay, Promega, Madison, WI) was used to quantify the cell proliferation rate. 20 µL MTT reagent with 100 µL DMEM was added to each well (96-well plate) and incubated at 37 °C for 2 hrs. The cells were lysed after 2 h with addition of 10 % sodium dodecyl sulfate. The solutions were transferred to a new plate and absorbance was measured at 490 nm using a standard plate reader. Three gels for each condition were analyzed at each time point. Readings were normalized to day 2 readings for gels containing no DNA.

### 4.2.9 Gene transfer

pGluc/PEI nanoparticle loaded hydrogels with mMSCs were made as described above. Each day the media was collected and frozen immediately at -20$^{o}$C and fresh media was added to each gel. To quantify secreted Gaussia luciferase levels in the media, the samples were thawed on ice and assayed using a BioLux$^{TM}$ Gaussia Luciferase Assay Kit (New England Biolabs, Ipswich, MA) as per the manufacturer's protocol. Briefly, 20 µl sample was mixed with 50 µl 1x substrate solution, pipetted for 2-3 sec, and read for luminescence with a 5 sec integration. Background was determined with media from gels that did not contain any DNA and values were expressed as relative light units (RLU).

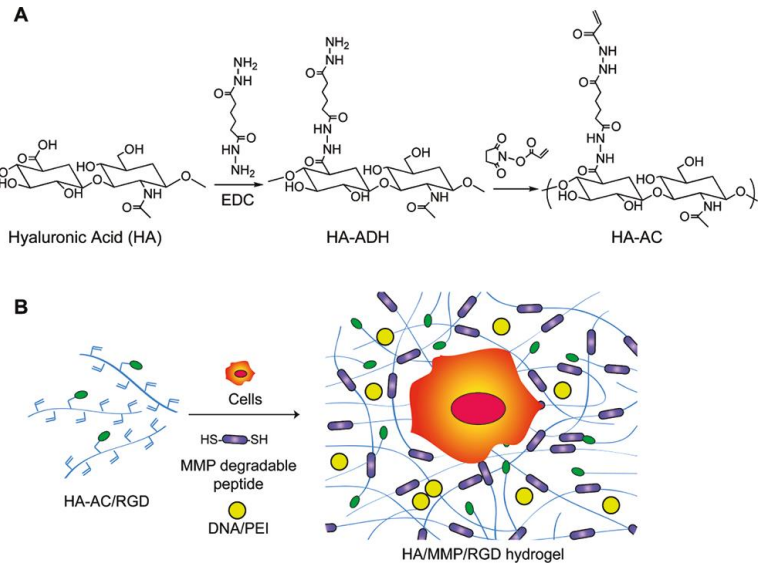


**Scheme 4.1**. Schematic of HA Modification and Hydrogel Formationa(A) HA-acrylate synthesis is a two-step process, first reacting HA with ADH and then using the pendant hydrazide to react with NHS-acrylate. (B) Schematic of DNA-loaded hydrogel formation. Liquid HA-AC is first modified with RGDpeptides using Michael type

addition. HA-RGD is then crosslinked using an MMP degradable peptide in the presence of DNA/PEI polyplexes.

## 4.3. Results

### 4.3.1Hydrogel preparation, DNA loading and characterization

Acrylates were conjugated onto the HA backbone through a two-step process (Scheme 1A). HA was first modified with adipic acid dihydrazide (ADH) using carboxylic acid/amine chemistry and the resulting hydrazide groups were then modified with NHS-acrylate (NHS-AC) to get acrylamide functionalities. An amine content assay (TNBSA assay) showed that 40.46% of the carboxylic acids were modified with ADHs. After reacting the HA-ADH with NHS-AC at pH 7.2 overnight, $^{1}$H-NMR showed that 10% of the hydrazide groups were modified with acrylate groups on the final products, resulting in approximately 15 acrylates per HA chain.

RGD adhesion peptides were incorporated through Michael-type addition of the cysteine side chain in the peptide to the acrylate groups on the HA backbone. The crosslinker was then added to form the hydrogels (Scheme 1B). Polyplexes were incorporated into the hydrogel during hydrogel gelation. Polyplexes were formed in a final volume of 20 µL by mixing equal volumes of PEI and DNA, vortexing for 15 seconds and incubating for 15 minutes. The full volume of the polyplexes was incorporated into 100 µL of hydrogel precursor solution to achieve a final DNA concentration of 0.05 µg DNA/µL hydrogel. Cells were also incorporated during gelation.

The storage (G') and loss moduli (G") of hydrogels with DNA polyplexes were measured at 37°C using plate-to-plate rheology with an 8 mm geometry. An evaporation blocker was utilized to avoid drying of the hydrogel sample. Results showed that the G' and G" did not cross at any measured frequency (0.1 to 10 Hz) and were frequency independent (Fig.4.1A), both of which are consistent with typical hydrogel characteristics. The loss tangent values (ratio of G" to G') were lower than 0.06 for all hydrogels tested, indicating that the hydrogels were highly elastic. The mechanical properties of the hydrogels were controlled by varying the percent of the HA solution

or the r ratio, resulting in a final range of mechanical properties from 100 to 1700Pa (Table 1, Fig. 4.1B).

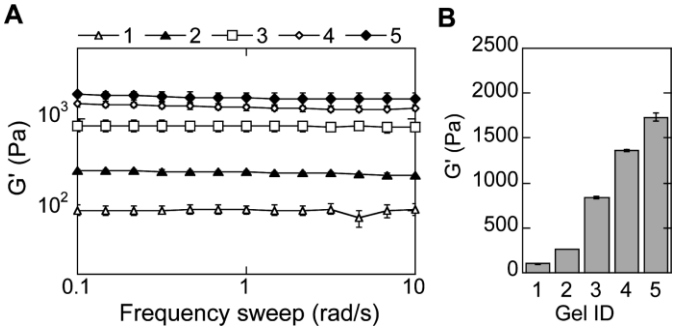


**Figure 4.1. Hydrogel mechanical properties.** The mechanical properties of the hydrogels were determined using plate-to-plate rheometry storage (A) and average (B) modulus over a frequency range of 0.1_10 rad/s at a constant strain of 0.03 and are shown for increasingly stiff hydrogels (Gel ID 1 < 2 < 3 < 4 < 5).

The activity of the entrapped polyplexes was estimated by synthesizing a polyplex-loaded hydrogel, degrading the hydrogel with trypsin and performing a bolus transfection with the released polyplexes (Fig.4.2A). The observed transfection was compared to that of fresh polyplexes, fresh polyplexes with trypsin added, and fresh polyplexes with a degraded hydrogel added. The amount of transgene expression decreased with the addition of trypsin but was the same for that of polyplexes exposed to hydrogel degradation products and released polyplexes indicating that the polyplexes were active inside the hydrogel. The distribution of the polyplexes inside the hydrogel scaffold was determined through the staining of the hydrogel with ethidium bromide post hydrogel formation. Polyplexes were observed mostly as unaggregated particles and uniformly distributed throughout the gel (Fig.4.2B).

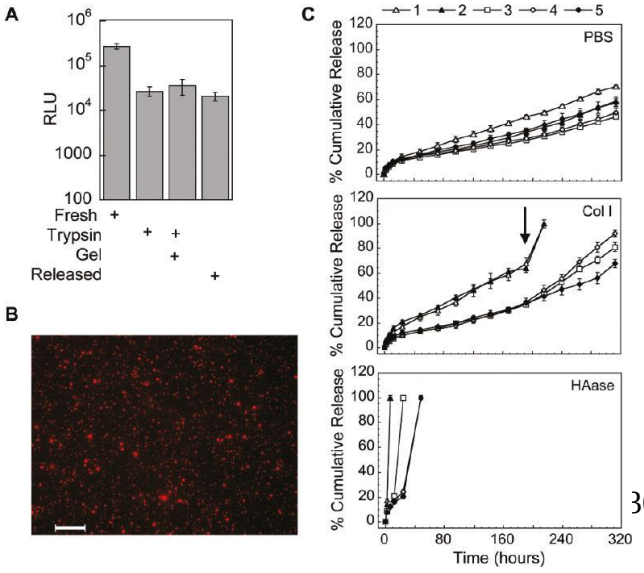


**Figure 4.2. Polyplex activity, distribution inside hydrogel scaffolds, and release.** (A) Activity of the entrapped polyplexes was determined through the release of the polyplexes post-hydrogel formation using trypsin and a subsequent bolus transfection with the released polyplexes. The gene transfer of the released polyplexes was compared to fresh polyplexes with trypsin added and fresh polyplexes with gel degradation products added. (B) DNA/PEI polyplexes were stained with ethidium bromide

post-hydrogel formation and imaged with a fluorescence microscope equipped with a z-stack capability. Scale bar = 100 μm.C) DNA release was determined using radiolabeled DNA. DNA/PEI loaded hydrogels were incubated in different release solutions, and at predetermined time points samples were gathered and analyzed for radioactivity using a scintillation counter. At the final day of the release assay the hydrogel was fully degraded with trypsin and the final activity measured. Data are plotted as the percentage of cumulative release.

To determine the release kinetics of the entrapped polyplexes, radiolabeled DNA was used. Release studies indicated that the hydrogel mechanical properties modulated the release rate of the polyplexes (Fig.4.2C). In general, stiffer materials resulted in lower release rates in PBS, collagenase I and hyaluronidase. DNA release in collagenase I and hyaluronidase were directly modulated by hydrogel stiffness, with hydrogels with 100 and 260 Pa resulting in faster release than hydrogels with higher storage modulus. At 192 hours a higher collagenase I concentration was added to induce faster release. However, even with this higher concentration stiff hydrogels did not result in complete hydrogel degradation and DNA release by 312 hours, with 81%, 92% or 68%, released for 839, 1360 and 1730 Pa gels, respectively. DNA release in PBS was also seen with the trend 70%, 59%, 46.4%, 50%, and 58%, for 100, 260, 839, 1360, 1730 Pa hydrogels respectively which was not as heavily dependent of the hydrogel stiffness.

### 4.3.2 Cell viability, proliferation and gene transfer as a function of N/P ratio

The toxicity of the DNA/PEI polyplexes was assessed using both the LIVE/DEAD and MTT assays as a function of nitrogen to phosphate (N/P) ratio (Fig.4.3A, B). Although all conditions contained some dead (red) cells, we observed minimal toxicity for cells cultured in hydrogels that did not contain polyplexes and for cells cultured inside hydrogels with polyplexes made with N/P 5 and N/P 7 ratios. However, by 8 days the images showed lower numbers of cells for the N/P 9 and N/P of 12 conditions. Cell spreading as a function of N/P ratio was also investigated (Fig.4.3A). Cell spreading was observed for all the conditions tested; however, N/P of 5, 7 and 9 had the most abundant cell spreading at day 8. The MTT assay was performed at days 2,

4 and 6 of transfection, supporting the results from the LIVE/DEAD and spreading images. It showed that the no DNA, N/P 5 and N/P 7 conditions contained more cells than the N/P 9 and 12 conditions. At day 2 there were a statistically lower number of cells in the N/P 12 condition ($p < 0.05$); however, all other conditions contained the same number of cells. By day 4 and 6 the no DNA condition contained statistically more cells than any other condition, while N/P 5 and 7 have statistically the same cell number with respect to each other but have statistically more cells than the N/P 9 condition ($p <$ at least 0.05).

**Figure 4.3. Gene transfer as a function of the N/P ratio.** The effect of the N/P ratio on transgene expression was studied for cells cultured inside MMP degradable HA hydrogels. For these studies a 3% hydrogel with an r ratio of 0.3 was used. The cell viability, ability of the cells to spread, and the metabolic activity of the cells were studied using the LIVE/DEAD assay, phalloidin staining (A), and MTT assay (B). Gene expression was determined over time using a reporter plasmid, pGluc, which is secreted by the cell when expressed (C). The cumulative expression at days 2 and 8 is plotted for ease of comparison (D). The statistical significance was determined using multiple comparisons and either the Dunnett or the Tukey multiple comparison's tests. The symbol ** indicates statistical significance at the level of 0.01 between the indicated condition and the corresponding no DNA control in B or between the indicated conditions in D. The symbols*, **, and *** indicate statistical significance at the level of 0.05, 0.01, and 0.001 between the indicated conditions in B. N/P= 0 represents the condition with no DNA polyplexes added to the hydrogel. Scale bar = 100 μm.

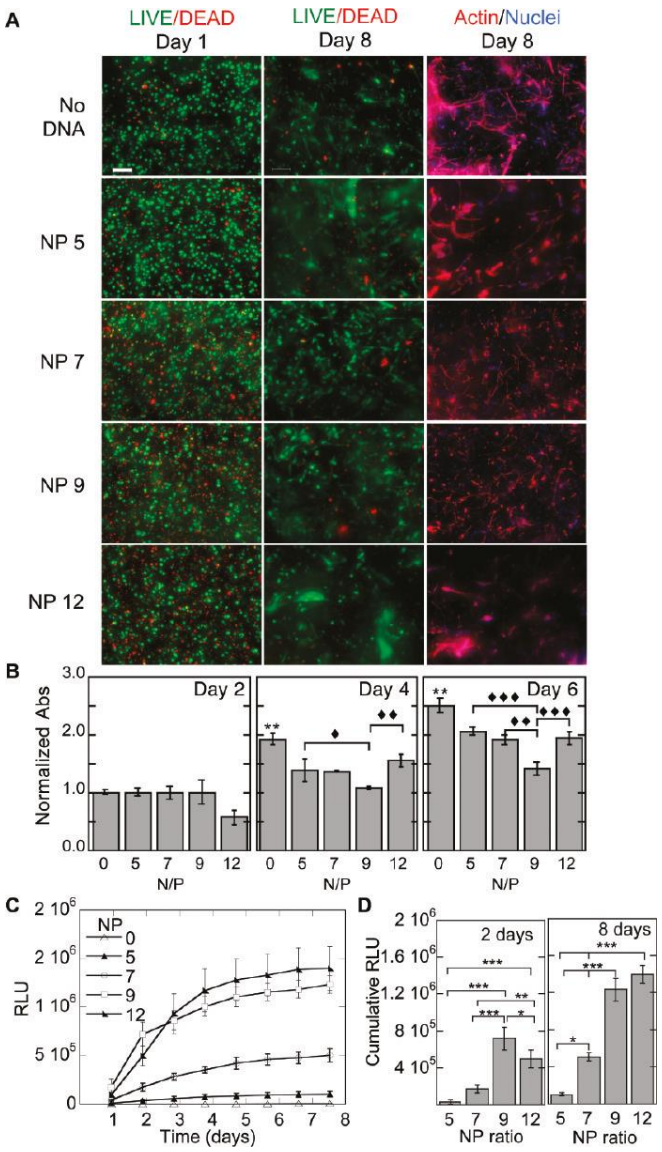

Surprisingly the N/P 12 condition recovered in cell number quicker than the N/P 9 condition suggesting that the polyplexes were released faster from this hydrogel and allowed the cells to grow again. Gene transfer was also assessed as a function of N/P ratio while keeping the amount of DNA constant at 5µg per 100µL of hydrogel. In general, transgene expression increased with increasing N/P (Fig.4.3C), with N/P of 12 and 9 achieving significantly more transgene expression than N/P of 5 and 7 (Fig.4.3D). At day 2, N/P of 9 and 12 transgene expression was statistically significantly more than N/P 5 and 7 ($p <$ at least 0.01) and N/P 9 was significantly more than N/P of 12 ($p < 0.05$). Similarly at day 8, transgene expression for N/P of 9 and 12 was statistically significantly more than N/P 5 and 7 ($p < 0.001$); however, there was also a significant difference between N/P 7 and N/P 5 ($p < 0.05$) with no statistical difference between N/P 9 and 12. To balance toxicity with gene transfer in our subsequent experiments N/P of 7 was used.

### 4.3.3Hydrogel mechanical properties influence cell proliferation, spreading and transgene expression

Hydrogels with different mechanical properties were synthesized and analyzed for their ability to modulate non-viral gene transfer. The viability of the cells at days 1 and 8 was assessed using the LIVE/DEAD stain and at 2, 4, and 6 days using the MTT assay (Fig.4.4A, B). The LIVE/DEAD stain showed minimal cell death at day 1 indicating that the hydrogel synthesis conditions did not affect cell viability. However, by day 8 significantly fewer cells were observed for the highest modulus hydrogels (gel ID 4 and 5). Cell spreading at day 5 was affected by hydrogel stiffness with 100 to 839Pa hydrogels resulting in substantial cell spreading, while hydrogel stiffness of 1350 and 1730 Pa resulted in reduced cell spreading (Fig.4.4A). The MTT assay agreed with the live/dead data (Fig.4.4B), showing significantly more metabolic activity at days 2 and 4 for the 100 Pa and 260Pa hydrogels compared to 1360 and 1730Pa hydrogels ($p$ at least $< 0.05$). Further, at days 2 and 4 there was no statistically significant difference between the

no DNA condition (gel ID 0) and the softest hydrogels (gel ID 1,2), while there was a statistical difference between no DNA and the stiffest samples (gel ID 4,5). By day 6 the softest hydrogel was significantly degraded, which resulted in the loss of cells and, therefore, showed a lower cell number. The 260Pa (gel ID 2) hydrogel remained higher in cell number than the two stiffest samples (gel ID 4, 5).

Transgene expression was a direct function of the hydrogel stiffness with softer hydrogels resulting in enhanced gene transfer compared to stiffer hydrogels (Fig.4.4C). Transgene expression at days 2 and 8 for 200 and 260 Pa hydrogels was also statistically significantly higher compared to the three stiffest hydrogels, with $p < 0.001$ and $p <$ at least 0.05 for 200 and 260 Pa comparisons, respectively (Fig.4.4D).

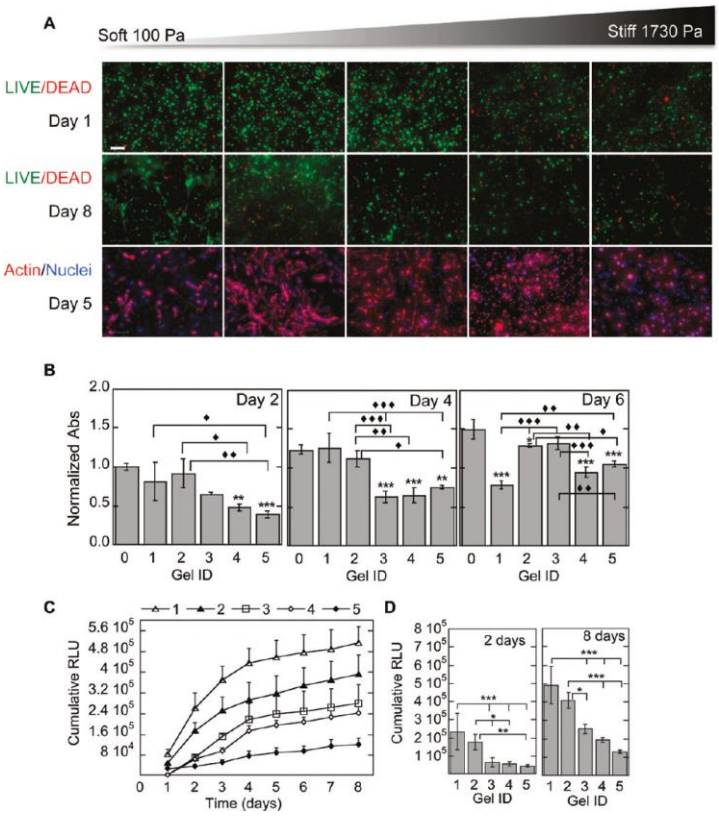


**Figure 4.4. Gene transfer as a function of hydrogel stiffness.** The effect of hydrogel stiffness on the ability of cells seeded inside the hydrogel to become transfected was studied for hydrogels with storage modulus ranging from 100 to 1730 Pa. The cell viability, ability of the cells to spread, and the metabolic activity of the cells were studied using the LIVE/DEAD assay, phalloidin staining (A), and MTT assay (B). None of the cell stiffness resulted in lower cellular viability. However, cell spreading was inhibited for stiffer hydrogels. Gene expression was determined over time using a reporter plasmid, pGluc, which is secreted by the cell when expressed (C). The cumulative expression at days 2 and 8 is plotted for ease of comparison (D). Matrix stiffness influenced transgene expression. The numbers 1_5 represent different hydrogel stiffness: 1 = 100 Pa, 2 = 260 Pa, 3 = 839 Pa, 4 = 1360 Pa, 5 = 1730 Pa. The statistical significance was determined using multiple comparisons and either the Dunnett or the Tukey multiple comparison's tests. The symbols ** and *** indicate statistical significance at the

level of 0.05, 0.01, and 0.001 between the indicated condition and the corresponding noDNAcontrol in B or between the indicated conditions in D. The symbols *,**, and *** indicate statistical significance at the level of 0.05, 0.01, and 0.001 between the indicated conditions in B. Gel ID 0 represents the condition with no DNA polyplexes added to the hydrogel. Scale bar = 100 μm.

### 4.3.4Effect of RGD concentration and presentation on gene transfer

In addition to the mechanical properties we also investigated how the concentration and presentation of RGD peptides on the hydrogel would affect the process of non-viral gene transfer. RGD concentrations of 10, 100 and 400 μM for the conditions containing DNA and 100μM for the condition with no DNA were tested. To look at the effect of RGD presentation the concentration of RGD was kept constant at 100μM but the fraction of the total HA it was reacted with was

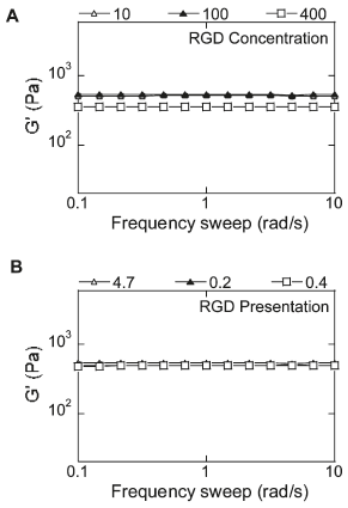


**Figure 4.5. Hydrogel mechanical properties for hydrogels with different RGD concentrations and presentations.** The mechanical properties of the hydrogels were determined using plate-to-plate rheometry storage (A, B) modulus over a frequency range of 0.1_10 rad/s at a constant strain of 0.03 are shown for hydrogels with variousRGDconcentrations and presentations, respectively. RGD presentation is displayed as the number of RGD/HA molecules with 4.7 RGD/HA being the most clustered condition and 0.2 RGD/HA being the least clustered/homogeneously distributed condition.

modulated to result in different numbers of RGD molecules per HA chain. For homogeneously dispersed RGD 100% of the HA was modified with RGD, however, for increasing degrees of RGD clustering lower and lower percentages of HA were reacted with the RGD. Thus, the trend of 0.2 < 0.4 < 4.7 for number of RGD per HA molecule represents an increase in clustering of RGD, with 4.7 RGD/HA representing the most clustered RGD condition. To ensure comparisons in transfection were due to the RGD concentration and presentation and not hydrogel

stiffness, mechanical properties were tested. Regardless of RGD clustering and at low RGD concentrations (10 and 100μM) the mechanical properties were independent of RGD presentation and concentration (Fig.4.5A, B). However, 400 μM RGD hydrogels were slightly softer (360 Pa for 400 μM compared to 516 and 541 Pa for 10 and 100 μM, respectively). This slight difference in modulus could not be avoided in order to be able to test a complete range of RGD concentrations.

The viability of the cells at days 1 and 8 was assessed using the LIVE/DEAD stain and at 2, 4, and 6 days using the MTT assay (Fig.4.6A, B). The LIVE/DEAD stain showed minimal cell death at day 1 indicating that the RGD conditions did not affect cell viability. By day 8 spreading were observed in all conditions (Fig.4.6A). The MTT assay for various RGD concentrations showed that the number of cells in the hydrogel was the same as the no DNA condition for low concentrations of RGD peptide at days 2 and 4, while at day 4 the highest concentration of RGD tested showed a lower metabolic activity than the no DNA condition (Fig.4.6B). At day 4 the 10 and 100μM RGD concentrations were statistically higher in metabolic activity than the 400μM condition. By day 6 all conditions showed lower metabolic activities than the sample with no DNA ($p < 0.001$), although the 10μM condition continued to show a higher metabolic activity than the 400μM condition ($p < 0.05$). RGD concentration affected transgene expression with the 100μM RGD concentration showing higher levels of transgene expression followed by 10, which was followed by 400μM RGD (Fig.4.6C). At day 8 the 100μM RGD concentration was statistically higher than the 400μM condition ($p < 0.05$, Fig.4.6D). RGD presentation was also assessed as a possible factor to influence cell viability, proliferation, and transfection efficiency. The viability of the cells at days 1 and 8 was assessed using the LIVE/DEAD stain and at 2, 4, and 6 days using the MTT assay (Fig.4.7A, B). The LIVE/DEAD stain showed minimal cell death at day 1 indicating that RGD clustering conditions did not affect cell viability. By day 8 spreading were also observed in all conditions (Fig.4.7A).

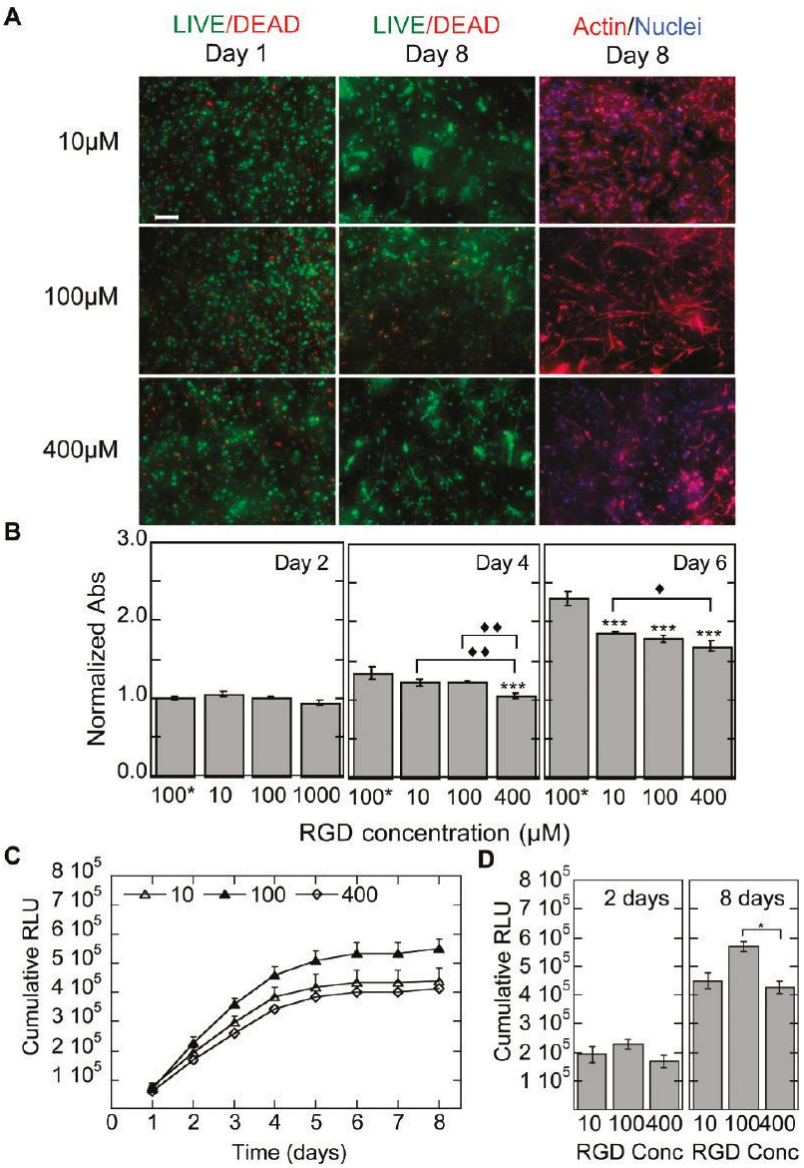


**Figure 4.6. Gene transfer as a function of RGD concentration.** The effect of RGD concentration on the ability of cells seeded inside the hydrogel to become transfected was studied for hydrogels with RGD ranging from 10 μMto 400 μM. The cell viability, ability of the cells to spread, and the metabolic activity of the cells were studied using the LIVE/DEAD assay, phalloidin staining (A), and MTT assay (B). Gene expression was determined over time using a reporter plasmid, pGluc, which is secreted by the cell when expressed (C). The cumulative expression at days 2 and 8 is plotted for ease of comparison (D). Different RGD concentration influenced transgene expression. The statistical significance was determined using multiple comparisons and either the Dunnett or the Tukey multiple comparison's tests. The symbol *** indicates statistical significance at the level of 0.001 between the indicated condition and the no DNA control in B or between the indicated conditions in D. The symbols *, **, and *** indicate statistical significance at the level of 0.05, 0.01, and 0.001 between the indicated conditions in B. 100* represents the condition with no DNA polyplexes added to the hydrogel. Scale bar = 100 μm.

The MTT assay for RGD presentation showed that the degree of RGD clustering influenced the metabolic activity with the highest clustered condition (4.7 RGD/HA molecule) resulting in higher MTT readings than the lower clustering conditions (.4 and .2 RGD/HA molecule, Fig.4.7B). At day 2 there is a significantly higher MTT reading than for the 4.7 RGDs per HA molecule than the 0.4 and 0.2 RGD clustering conditions ($p < 0.01$). By day 6 all the conditions were again lower than the no DNA condition (p at least < 0.01) and the highest clustered condition continued to have higher

MTT values than the lower clustering conditions.

Transgene expression was also affected by the RGD presentation in the scaffold, with an intermediate RGD clustering resulting in optimal transgene expression (Fig.4.7C). The trend observed was 0.4 > 4.7 > 0.2 RGD per HA molecule, with .4 RGD/HA resulting in the greatest transgene expression. The 0.4 clustering condition was statistically higher than the 0.2 (homogeneous RGD) clustering condition ($p < 0.01$, Fig.4.7D).

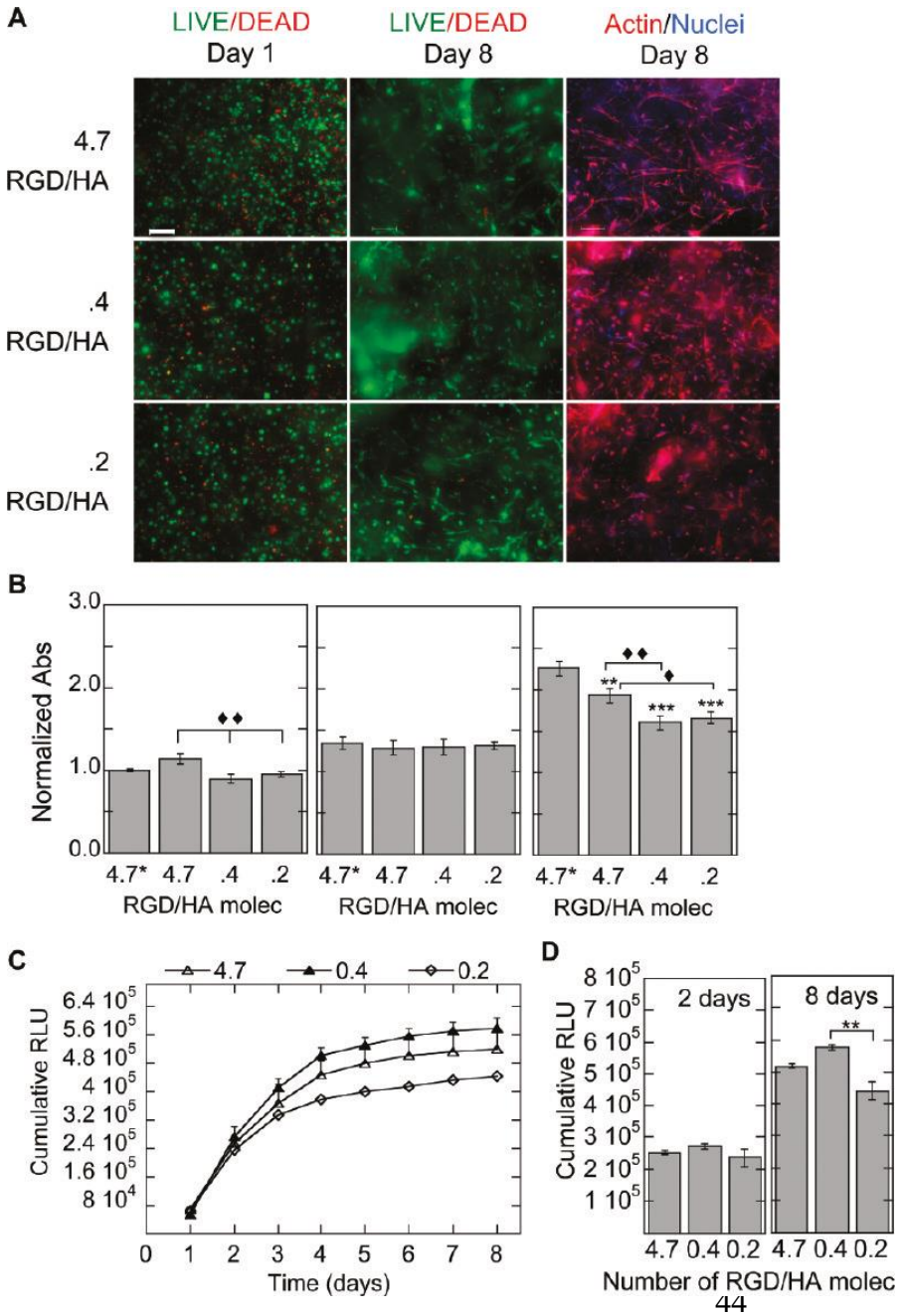


**Figure 4.7. Gene transfer as a function of RGD presentation.** The effect of RGD presentation on the ability of cells seeded inside the hydrogel to become transfected was studied for hydrogels with 100 μM RGD displayed either homogeneously (100% HA-RGD, 0.2 RGD/HA molecule) or as RGD clusters (52% to 4.3% HA-RGD, 0.4 and 4.7 HA/RGD molecule, respectively). RGD clustering is achieved by reacting different amounts of HA-AC with the same amount of RGD and then mixing the resulting HA-RGD with unmodified HA. The cell viability, ability of the cells to spread, and the metabolic activity of the cells were studied using the LIVE/DEAD assay, phalloidin staining (A), and MTT assay (B). Gene expression was determined over time using a reporter plasmid, pGluc, which is secreted by the cell when expressed (C).The cumulative expression at days 2 and 8 is plotted for ease of comparison (D). RGD presentation influenced transgene expression. The statistical significance was determined

using multiple comparisons and either the Dunnett or the Tukey multiple comparison's tests. The symbols ** and *** indicates statistical significance at the level of 0.01 and 0.001 between the indicated condition and the corresponding no DNA control in B and between the indicated conditions in D. The symbols * and ** indicate statistical significance at the level of 0.05 and 0.01 between the indicated conditions in B. 4.7* represents the condition with no DNA polyplexes added to the hydrogel. Scale bar = 100 μm.

### 4.4Discussion

Cell-matrix interactions are increasingly being utilized to guide stem cell differentiation [129-131] and have been previously implicated with DNA/PEI non-viral gene transfer[44, 56] for cells plated on top of hydrogel materials (in two dimensions). We are interested in introducing gene based bioactive signals to aid in the differentiation of either transplanted or endogenous stem cells from within 3-dimensional hydrogel scaffolds. Here HA-RGD was crosslinked with a MMP labile peptide using Michael type addition to form hydrogels that were degradable through a combination of hyaluronidases and MMPs. In addition, DNA/PEI polyplexes and mouse mesenchymal stem cells were encapsulated during gelation. The role of cell-matrix interactions on DNA/PEI non-viral gene transfer for cells seeded within hydrogel scaffolds was investigated here (in three dimensions). Using a range of mechanical properties from 100 ± 2.11 to 1730 ± 45.62 Pa, we observed that gene transfer was strongly influenced by mechanical properties, with softer hydrogels resulting in optimal transgene expression. We further studied if the concentration and presentation of RGD cell adhesion peptides affected gene transfer in three dimensions. An intermediate RGD clustering resulted in the most effective transgene expression.

The activity of the entrapped polyplexes was as high as fresh polyplexes mixed with trypsin and hydrogel degradation products, indicating that the encapsulation process does not inactivate the polyplexes (Fig. 2A). However, compared to fresh polyplexes without trypsin and hydrogel degradation products the activity was lower. This indicates that the presence of trypsin in the polyplex solution negatively affects transfection. The distribution of the polyplexes inside the

hydrogel was studied through the labeling of the DNA post hydrogel formation. The presence of DNA clusters indicates that the polyplexes are present in the hydrogel (Fig. 2A). Naked DNA would show a uniform fluorescence inside the hydrogel. Although some larger aggregates are observed the majority of particles were found to not be aggregated. This result is consistent with our previous studies showing that concentrations of DNA below 0.1μg DNA/μL hydrogel do not result in severe polyplex aggregation[58, 80]. As expected the polyplex physical properties affected the rate of non-viral gene transfer for cells seeded inside hydrogel scaffolds with increasing N/P ratio resulting in higher transgene expression, but also higher toxicity (Fig. 3). This is the same trend observed for polyplexes grown in two-dimensional surfaces[132, 133]. Thus, although we observed two fold higher transgene expressions for N/P of 9 and 12, an N/P of 7 was used in the remaining studies to ensure minimal toxicity was observed.

For cells cultured on two-dimensional surfaces cell area[44, 56] has been previously been linked to non-viral gene transfer, with increased cell area also increasing transgene expression. For cells cultured in three-dimensions the migration rate[57, 58] of cells through the material has previously been implicated with effective non-viral gene transfer. Based on these findings we postulated that hydrogel scaffolds that allowed for extensive cell spreading and migration would result in enhanced gene transfer over hydrogels that did not allow for substantial cell spreading or migration. We previously published on culture of MSCs inside HA/MMP hydrogels. In that study it was observed that soft hydrogel materials allowed for extensive spreading and migration, while stiff materials did not[40]. Here we find that soft hydrogel materials result in more effective transfection of encapsulated cells compared to those within stiff hydrogels (Fig. 4), suggesting that cell spreading and migration also play a role in gene transfer to cells seeded inside hydrogels. It should be noted that for cells seeded on top of the hydrogel material (in two dimensions), stiff substrates have been shown to promote more efficient gene transfer than cells cultured on soft

substrates[44].

The lack of efficient gene transfer on stiff hydrogels is attributed to decreased migration rates, spreading, and actin polymerization, all of which have been implicated with enhanced transfection[44, 56-58, 134]. Further, to achieve stiff hydrogels higher HA percentages were used to form the hydrogels, which decreased the pore size. Higher stiffness did slow down cellular metabolic activity and cell spreading; thus, nutrient diffusion and slowed matrix degradation could be a reason for lower gene transfer especially at early time points.

One possibility to enhance transfection further in our soft hydrogels is to prevent polyplex release from our hydrogel scaffolds. Extensive release was observed even when release was performed in PBS. Thus, if more DNA was retained throughout the 8-day incubation period (and beyond) more transgene expression might be observed.

We next wanted to study the role of the concentration and presentation of RGD peptide on non-viral gene transfer in three-dimensions. As mentioned RGD presentation was found to be important for gene transfer in 2 dimensions[56]. Because each molecule of HA in our system has on average 64 acrylate groups and < 7% of those groups are used for conjugating RGD many sites are still available to crosslink without compromising mechanical properties. As expected the mechanical properties of these hydrogels remained approximately constant (Fig. 5). An intermediate RGD concentration of 100μM was found to achieve the most efficient transgene expression compared to 10μM and 400μM, suggesting that there is an optimal degree of spreading and migration rate associated with transgene expression inside hydrogel scaffolds (Fig. 6C,D). RGD concentration was not found to affect cell viability as determined by the LIVE/DEAD assay, however, the MTT metabolic activity assay showed lower metabolic activity for 400μM RGD compared to lower RGD concentrations. This could explain why 400μM RGD resulted in the lowest transgene expression of the three tested RGD concentrations.

To cluster RGD we used a similar approach used by the Mooney group to cluster RGD in alginate hydrogels[56, 131]. In this approach, a fraction of the total polymer is modified with RGD and then mixed with unmodified polymer. By changing the ratio of modified to unmodified polymer, while keeping the overall concentration constant, the RGD presentation is modulated. Using 100% modified HA would result in homogeneously displayed RGD and 0.2 RGDs per HA molecule, while using 4.3% modified HA and 95.7% unmodified HA would result in our most RGD clustered condition with 4.7 RGDs per HA molecule. RGD presentation was found to significantly influenced transgene expression with an intermediate clustering achieving the more efficient transgene expression (Fig. 7C, D). Metabolic activity was the highest for the most clustered condition; however, this condition did not achieve the most efficient gene transfer. Another complementary explanation for the effect of RGD presentation ion transgene expression is integrin clustering. Clustering of integrins has been implicated with stem cell differentiation [135], enhanced bone formation in vivo [136], enhanced nanoparticle targeting [137] and enhanced transgene expression [56, 138], suggesting that the clustering of integrins may be playing a role in making the cells more susceptible to transfection.

**4.5 Conclusion**

In conclusion, we explored the role of matrix stiffness and RGD presentation on gene transfer to cells seeded inside hydrogel scaffolds. Both matrix stiffness and RGD presentation significantly influenced transgene expression with an intermediate stiffness and RGD clustering resulting in maximal transgene expression. We believe that the knowledge gained through this *in vitro* model can be utilized to design better scaffold-mediated gene delivery for local gene therapy for *in vivo* applications.

## 4.6 Protocols

### 4.6.1HA Modification with Acrylates

Materials

- Hyaluronic acid (HA, 60kDa, Genzyme Corp.)
- Adipic acid dihydrazide (ADH)
- 1-ethyl-3-[3-dimethylaminopropyl] carbodiimide hydrochloride (EDC)
- N-Acryloxysuccinimide (NHS-Acrylate)
- HEPES
- NaCl
- EDTA
- DMSO
- DI H2O
- 6000-8000 MWCO Dialysis tubing

Protocol

Part 1: Reaction of HA to produce HA-ADH

1. Dissolve 2.00g hyaluronic acid (HA) (60kDa) in 400ml DI water (keep fixed concentration of 1g/200ml) and stir.
    a. Note: Do not scale up beyond 2g. Issues with mixing will occur.
2. Add 36.77g adipic acid dihydrazide (ADH, 40 molar excess over carboxylic acid groups), dissolve completely and adjust the pH to 4.75 with 1N HCl.
3. Add 4.00g 1-ethyl-3-[3-dimethylaminopropyl] carbodiimide hydrochloride (EDC, 3.95 molar excess over carboxylic acid groups) as a catalyst.
4. Maintain the pH at 4.75 until it becomes stable (~2hrs) and let it react overnight with stirring.
5. Dialyze for 4-5 days against 100mM NaCl -> DI H2O (use 25mM gradients over day 1 and water for the following 3-4 days).
6. Filter HA-ADH solution using .22um filter to remove precipitates (may be slightly viscous here).
7. Lyophilize! (requires 3-4 days to be completely dry!) Dry HA-ADH can be stored at -20°C until the next step.
    a. Characterize final HA-ADH sample by NMR -> 400µl of 10mg/ml in D2O.

Part 2: Reaction of HA-ADH to produce HA-Ac

8. Make reaction buffer: 10mM HEPES with 150mM NaCl and 10mM EDTA at pH 7.4.
9. Dissolve all HA-ADH in 400ml reaction buffer. Mix using a stir bar and plate for about 2hrs to completely dissolve (pH usually drops to 7.1-7.2 here).
10. Weigh out 4.46g N-Acryloxysuccinimide (NHS-Ac, 5 molar excess over carboxylic acid groups) and dissolve in DMSO at 100mg/ml.
11. Add dissolved NHS-Ac to HA-ADH. Here pH usually drops to 5.8-5.9. Bring pH to 6.0 and maintain it for ~2hrs. Let it react overnight with stirring.
12. Dialyze for 3-4 days against 100mM NaCl -> DI H2O (use 25mM gradients over day 1 and water for the following 2-3 days).
13. Filter HA-ADH solution using .22um filter to remove precipitates (usually there is no problem here!)

14. Lyophilize! (Requires 3-4 days to be completely dry!) Dry HA-Ac can be stored at -20°C until ready for use.
    a. Characterize final HA-Ac sample by NMR -> 400µl of 10mg/ml in D2O.

### 4.6.2Porous and Nano HA-MMP Hydrogels with CnE Polyplexes

MATERIALS

- HA-Ac (10-15% modified with acrylates)
- RGD aliquots (.1mg RGD)
- Cross-linker aliquots (.1-1mg)
- .3M Triethanol amine (TEOA) buffer pH 8.2–8.8 (sterile)
    - NOTE: Appropriate pH needs to be chosen based on HA batch!
    - Final gel solution pH should be 7.8–8.0 for gelation to occur within 30min.
    - If cells are not being encapsulated, higher pH buffers can be used.
- CnE polyplexes (sterile)
- Sigmacote® (silicon solution, Sigma-Aldrich, SL-2, 100mL, store at 2-8°C) glass slides and spacers
    - Coated slides can be reused about 3 times
- PMMA bead templates
- Regular and positive displacement pipets and tips (sterile)
- Ice

Protocol

1. Prepare RGD and MMP crosslinker aliquots in .1% TFA at least 1 day before making gels prepare Sigmacote® coated glass slides by immersion of slides in Sigmacote® solution using a 50ml conical tube for 1min and air drying for 3min. Repeat this 3x for each slide.
    - After use, pour the Sigmacote® back into a dark glass bottle (not back into the clean stock solution). This Sigmacote can be re-used 3-4x.
    - After the 3rd coating, place slides into oven above 100$^{o}$C for 2hrs-overnight to allow for complete drying
2. Prior to preparing gels, prepare all supplies in tissue culture hood: vortex, microcentrifuge, pipets, positive displacement pipets, tips, slides, spacers, clips, and spatulas.
3. Spray down all supplies, including slides, with ethanol and wipe dry with Kim wipes.
4. Take out buffer (TEOA from -20$^{o}$C and place it on ice to thaw). Check pH prior to use.
5. Weigh out HA-Ac into 1.5ml microcentrifuge tube.
6. Dissolve the HA-AC in buffer for a final concentration of .08mg/ul. Vortex, spin down, and incubate at 37°C for 10min to allow HA to completely dissolve. Pipet with positive displacement pipet if needed to help with dissolving/mixing
7. Take out .1mg RGD aliquot from -20$^{o}$C freezer immediately before use.
8. Pipet 15ul of HA-Ac solution to RGD (all HA-Ac will not be directly mixed with RGD - only 15ul HA-Ac results in clustering of RGD throughout the HA gel).
9. Vortex, spin down, and incubate at 37°C for 20-25min to allow HA-Ac to react with RGD - this is HA-RGD. Keep remaining HA-AC at 37$^{o}$C for this period as well. After this time place stocks on ice until ready to use. Longer incubation will result in gelation by unreacted amines and acrylates.
10. Mix unreacted HA-Ac (A) with HA-RGD (B), and additional buffer (D) and place on ice - this is the gel precursor solution.

11. Start preparing polyplexes.
12. For CnE samples (made previously used attached protocol at least 2 days before), place lyophilized polyplexes into 1.5ml centrifuge tube using tweezers.
13. Take out crosslinker aliquot from -20$^{o}$C freezer and place on ice.
14. Now be fast!
15. To CnE polyplexes: add the entire gel precursor solution to the lyophilized polyplexes, mix vigorously with a positive displacement pipet (solution will be very viscous), and spin down to remove bubbles.
16. Dissolve the crosslinker in buffer for a final concentration of .05mg/µl, vortex, and spin down
17. Immediately add crosslinker (C) to gel precursor mixture, mix well with positive displacement pipet.
18. (Nano gels) Pipet 20ul gel solution onto a glass-slide with cover glass spacers (made with 3 slides generally) on each end. Puncture bubbles with the pipette tip. Place a glass slide gently on top and place one clip on each end of the slide.
19. (Porous gels) Pipet 20ul gel solution onto center of bead template. Place a glass slide gently on top and place one clip on each end of the slide. Immediately centrifuge down gel into void space for 6min at 4°C at 1500rpm
20. Place the slide in the incubator at 37°C for 30 minutes for polymerization to take place.
21. Add 20ul of medium gently in between the glass slides and remove the clips
22. Carefully move a spatula in between the slides and the gel to detach it from the slides.
23. Transfer the gel into non-TC treated 96-well plate. Add 150ul PBS to well.
24. Keep in PBS

### 4.6.3Radiolabeling plasmid DNA with $^{3}$H-dCTP and measuring radioactivity

Materials

- Nick Translation Kit (Roche)
    - control DNA 20 µl (pBR322 DNA- 50 µg/µl)
    - dATP 50 µl (.4 mM 2'-deoxycytidine-5'- triphosphate in tris buffer)
    - dCTP 50 µl (.4 mM 2'-deoxycytidine-5'- triphosphate in tris buffer)
    - dGTP 50 µl (.4 mM 2'-deoxycytidine-5'- triphosphate in tris buffer)
    - dTTP 50 µl (.4 mM 2'-deoxycytidine-5'- triphosphate in tris buffer)
    - 10x buffer 100 µl (10x concentrated nick translation buffer)
    - Enzyme mixture consisting of DNA polymerase 1 and DNAase in 50% glycerol (v/v)
    - dCTP-$^{3}$H (67.2 Ci/mmol – batch dependent, 1mCi/ml – always constant, MP Biomedicals)
- EDTA stop solution (.2 M EDTA, ph=8)
- Ice
- DNA Clean & Concentrator$^{TM}$-5 Kit (Zymo Research, catalog #D4013)
- Nuclease-free water
- Appropriate protection for low energy β-radiation (gloves, lab coat, goggles)

Protocol (for labeling 5 µg DNA with 50 µCi dCTP-$^{3}$H)

1. Dilute DNA to 1 µg/µl in a clean microcentrifuge tube – add 5 µl to sample tube
2. Place nick translation kit tubes on ice to thaw
3. Add the following to 5 µl DNA sample:
4. 15 µl dNTPs (5 µl of each dATP, dTTP, dGTP corresponds to 2 nmol of each dNTP)
5. 3.14 µl regular dCTP (corresponds to 1.256 nmol (adjust so total with dCTP-$^{3}$H will be 2 nmol); will need to adjust based on concentration of provided dCTP-$^{3}$H – calc. based on 67.2 Ci/mmol)
6. 50 µl dCTP-$^{3}$H (corresponds to .744 nmol based on 67.2 Ci/mmol)
7. 10 µl 10x buffer (final 1x)
8. 6.86 µl water (nuclease-free)
9. 10 µl Enzyme mixture (add last!
10. Mix gently by pipetting up and down - do not vortex!
11. Spin briefly to bring contents to bottom of tube
12. Incubate for 2 hr at 15$^{o}$C (or 16$^{o}$C)
13. Stop the reaction by adding 5 µl 0.2 M EDTA (pH=8.0) and by heating the sample to 65° C for 10 min.
14. Final samples volume becomes 105 µl
15. Purification:

Note: Each column from DNA Clean & Concentrator$^{TM}$-5 Kit can only purify up to 5 µg DNA so if purification of more DNA is required, may need to use several columns

1. Load 100 µl binding buffer into a ZYMO-SPIN COLUMN and place column into a 2ml collection tube.
2. Centrifuge at full speed ( >10000 *g) for 30s.
3. Discard flow-through.
4. Add 210 µl (2x DNA sample volume) binding buffer to labeled DNA sample (105 µl).
5. Load mixture into a ZYMO-SPIN COLUMN and place column into a new 2ml collection tube.
6. Centrifuge at full speed ( >10000 *g) for 30s.
7. Collect the flow through and keep it as "binding solution."
8. Wash with 200 µl Buffer PE to the QIA quick column and spin for 30s.
9. Collect the flow through and keep it as "wash 1."
10. Wash with 200 µl Buffer PE to the QIA quick column and spin for 30s.
11. Collect the flow through and keep it as "wash 2."
12. Place the column into a new 1.5 ml tube. Add 25 µl of nuclease-free water directly to the column and spin to elute the DNA.
13. DNA will be at a concentration of 5 µg /25 µl (.2 µg/µl)
14. For reading add 1 ul of each step (binding solution, wash 1, wash 2, sample and blank) to the 2 ml of cocktail and read using scintillation counter (chemistry building, 5$^{th}$ floor) – can also place entire column into a vial to test for lost 3H-DNA
15. Must also read a negative control
16. Calculate DPM (disintegrations per minute) based on the following:

    1. i. DPM = (CPM – CPMneg)/.5

2. ii. CPM = counts per minute (scintillation counter output)
3. iii. .5 = scintillation counter efficiency
4. Note scintillation reads an absolute value (reading here will be for total radiation in 1ul)
5. Calculate final uCi from DPM standard curve (1ul in 2ml cocktail)

DNA loading and release from hydrogels:

1. Incorporate a fraction of radiolabeled DNA exactly as non-labeled DNA would be incorporated into hydrogels
2. Generally use ~1% radiolabeled DNA and 99% non-labeled since using all radiolabeled DNA is not (1) feasible or (2) necessary since the detection limit on the scintillation counter is very low
3. Place gels into release solution and collect solutions at various times
4. To read, add 30ul (or more if reading come out very low) release sample solution to 2ml scintillation cocktail and read as described above in step 14.
    1. Note: the same standard curve can be used even though 30ul of sample was used here
    2. Account for 30ul volume when calculating total uCi in 150ul (or Xul) release solution

### 4.6.4Transfection with Gaussia luciferase

Protocol for transfection from hydrogels

1. Incorporate pGluc into hydrogels with cells and place gels in 150ul media in a 96-well plate
2. Collect media from gels at specified times (e.g. every 24hrs) and replace with fresh media
3. For samples to be tested at a later time, immediately freeze at -20$^{o}$C and thaw only prior to testing
4. Use the BioLux Gassia Luciferase Assay Kit for quantification of secreted Gluc into media
5. Follow exact manufacturer's instuctions (New England Biosystems, cat #E3300L)
6. Thaw samples (and then keep on ice)
7. Thaw assay buffer in RT water bath
8. Prepare 1x substrate solution by adding 1ul Gluc substrate to every 100ul assay buffer (keep substrate and final solution out of light!)
    1. Calculate total amount of 1x substrate solution that will be needed that day and make one stock (50ul for each sample)
    2. Make sure to account for negative control samples
9. Using the same microcentrifuge tubes for all the samples, pipet 20ul of sample into each tube
10. Add 50ul of 1x substrate solution to the sample, quickly pipet up and down to mix (DO NOT VORTEX!), and immediately measure luminescence
11. Integration of luminescence should be between 5-10sec (longer times can be used for lower signals)
12. Luminometer -> Protocols -> Gluc5 -> 5sec integration
13. Try to get a rhythm going so pipetting and reading of each sample takes about the same time so the integration periods overlap between samples

14. Make sure to run 1-3 negative controls with just media or conditioned media from non-transfected cells – should be close to 1000RLU
15. Subtract background readings and report values as RLU or with respect to control samples
16. Gaussia luciferase is not available in protein form so at this time making a standard curve is not possible

# Chapter 5

# *High clustered VEGF promote angiogenesis in vitro and in vivo*

## 5.1. Introduction

Blood vessels nourish every organ of the body, so its insufficient growth can lead to several diseases such as stroke, myocardial infarction and neurodegeneration[14,139,140]. To form, function and regenerate a tissue after damage, a highly dynamic and complex array of biophysical and biochemical signals originating from the extracellular microenvironment is involved in the ultimate establishments of a mature vascular network[141]. One of the predominant regulators of this process is vascular growth factor (VEGF) which distinguishes itself from other angiogenic superfamilies by the largely non-redundant roles of its family members. VEGF family consists of five members, VEGF A, B, C, D and placenta growth factor (PLGF)[142]. We are focusing on VEGF A in this work. Alternative splicing of the VEGF A family members can give rise to different isoforms. The most

common include $VEGF_{121}$, $VEGF_{165}$, and $VEGF_{189}$. These isoforms differ based on their affinity for the extracellular matrix (ECM). For example $VEGF_{165}$ binds to the ECM while $VEGF_{121}$ remains soluble. We are focusing on $VEGF_{165}$ in this study.

Two distinct receptors that lead to divergent signaling outcomes have been identified for this isoform of VEGF on endothelial cells (ECs): VEGFR1 (also known as Flt-1) and VEGFR2 (Flk-1)[7,107].The binding of VEGFR2 to VEGF induces receptor dimerization and consequent phosphorylation of a subset of intracellular tyrosine residues which are involved in the angiogenic cascade. The expression of VEGFR-2 will stimulate specialized endothelial cells "tip cells" which are located at the forefront of vessel branches and cause them to migrate toward the gradients of guidance cues and form new vessels. Another pathway involved in tip cell formation through VEGF signaling is Notch pathway[143, 144]. The local high level of VEGF induces the expression of Delta 4 (Dll4), one of the notch ligands, at the surface of tip cells[145-147]. Dll4 binds to the notch receptor on neighboring ECs and downregulates VEGFR-2 signaling, thus controlling the tip cell phenotype switch and the number of branches during vessel formation. Another highly expressed protein at tip cells surface is VEGFR-3, known to have an effect on the number of branch points and EC proliferation[8, 148]. Although knowledge on the role of VEGF in tissue repair has been greatly acquired, its clinical effectiveness is still limited[149, 150]. Some of these limitations are due to the fast release and clearance of the VEGF and difficulties in achieving an appropriate dosage of VEGF which leads to immature and leaky neovessel formation[151].

The presence of VEGF as a cluster form is an approach that may provide a better duration of active signals locally and result in mature and functional blood vessel formation. Bioengineered scaffolds are a versatile tool in regenerative medicine that can be used to deliver cells and molecules[152]. Much progress has been made in developing both 3D artificial and natural matrices that incorporate adhesive signals as well as VEGF to induce blood vessel formation *in vitro*

[153,154,155]. In general, materials from natural sources are favorable because of their inherent properties of biological recognition, while bioartificial matrices are attractive because they provide a controlled and tailored environment[156]. Since fibrin is a natural ECM-derived biomaterial that is a clinically well-established matrix for wound healing purpose, it can be used as a promising scaffold to translate *in vitro* knowledge to *in vivo*[157]. In this chapter, we aim at developing a strategy to promote angiogenesis in vitro, by displaying VEGF in a clustered conformation. The effect of clustered VEGF will be studied at a cellular and molecular level, before being tested at a therapeutic level using a rodent stroke model. We hypothesize that controlling the discrete distribution of VEGF in an engineered matrix can promote the formation of functional and mature vessels by modulating the EC phenotype toward a tip cell phenotype and promoting vessel branching. In addition, we hypothesize that controlled vessel formation would lead to post-stroke angiogenesis in a mouse model of cerebral ischemia.

## 5.2. Materials and methods

### 5.2.1. Heparin nanoparticle synthesis and VEGF binding

Heparin was first modified as described in chapter 4. The final product was dissolved in a 100 mg/ml solution of sodium acetate at pH 4, and combined with Tween-80 and Span-80 (8% HLB) to form nanoparticles. The radical polymerization was initiated by sonication of the solution of heparin nanoparticles diluted in a ten-fold volume of hexane and combined with N,N,N',N'-tetramethyl-ethane-1,2-diamine (TEMED) and ammonium persulfate (APS). The resultant nanoparticles were purified via liquid-liquid extraction in hexane. Finally, the final stage of the extraction process consisted in using bubbling nitrogen gas to evaporate off the excess of hexane. The particles were then dialyzed in 100 kD MWCO dialysis units for few hours and stored until use. The amount of heparin in the solution was determined by lyophilizing a small aliquot of the solution. VEGF (20μg/ml) was mixed with different concentrations of heparin nanoparticles and

incubated overnight at 4°C to form VEGF nanoparticles of different packing density, before shining a 365 nm wavelength UV light for 10 minutes to lock VEGF covalently to the surface. The VEGF nanoparticles were then washed from excess with 0.05% Tween-20 in PBS, then with PBS, using a 100 kD MWCO dialysis units. The washes were collected to estimate the amount of VEGF bound to nanoparticles.

### 5.2.2. Heparin nanoparticle characterization

Dynamic Light Scattering (DLS) was used to characterize the diameter of heparin nanoparticles after each preparation step, formation, purification, and dialysis. Samples were loaded into a filtered DI water cleaned quartz cuvette and analyzed by a Malvern Zetasizer. Ten runs of three measurements each were performed, and data was reported as Z-average and polydispersity index (PDI). In order to analyze the morphology and size distribution of nanoparticles, a Transmission Electron Microscopy (TEM) with a T12 Quick CryoEM was performed at the Electron Imaging Center for NanoMachines (EICN). Briefly, a drop of sample solution (1 mg/mL) was placed onto a 300 mesh copper grid coated with carbon. About 2 min after deposition, the grid was tapped with filter paper to remove surface water, followed by three washes with three droplet of DI water and air-drying. The nanoparticles, deposited on the grid, were then negatively stained by 2 wt % photungstic acid (PTA) solution, followed by three washes and air-drying.

### 5.2.3. Enzyme linked immunosorbant assay (ELISA) and Dot Blot

To quantify the amount of VEGF immobilized on nanoparticles, a standard ELISA technique was used. A high binding 96-well plate was coated overnight at room temperature with 1 µg/ml VEGF capture antibody (R&D Systems, Minneapolis, MN). Then non-specific binding sites were blocked with blocking buffer (1% BSA in PBS, pH 7.4) for 1 h at room temperature. Samples collected from the washes were added to the wells and incubated for 2 h at room temperature.

Washes with a solution of 0.05% Tween-20 in PBS at pH 7.4 were performed before adding a biotinylated detection antibody (1 µg/ml in blocking buffer, R&D Systems, Minneapolis, MN) for 2 h at room temperature. Finally, streptavidin-HRP (200 µg/ml in blocking buffer, R&D Systems, Minneapolis, MN) was added and incubated for 20 min at room temperature,, then exposed to TMB substrate (Cell Signaling Technology, Boston, MA) for 20 min at room temperature. The resulting absorbance at 645 nm (applying a correction at 570 nm) was measured using a plate reader (BioTek PowerWave XS, Winooski, VT). To confirm the results obtained by Elisa on the washes, a Dot blot was also performed. In this method, a 2µl drop of the final heparin nanoparticles of VEGF sample was deposited on a nitrocellulose membrane. The membrane then was soaked in blocking buffer (1% BSA in PBS, pH 7.4) for 1 h at room temperature before addition of the biotinylated detection antibody, followed by streptavidin-HRP. The samples were then visualized by chemifluorescence (ECL detection reagents, GE Healthcare) using a Molecular Imager Chemi Doc XRS+ scanner (Bio Rad). Images of the stained membrane were analyzed using Image Lab software.

**5.2.4. VEGFR-2 phosphorylation assay**

Human Umbilical Vein Endothelial Cells (HUVECs) were grown to confluency in a 6 well plate, and submitted to serum depravation for 5 h before cell lysis with 0.1 mM sodium vanadate for 5 min. The cells were then treated with 5 ng/ml of either soluble or bound VEGF at 37 °C for 5 min. The cells were rinsed twice with ice cold PBS supplemented with 0.2 mm sodium vanadate. After aspirating all remnants of liquid from the wells, 100 µl of lysis buffer (1% Non-idet, 10 mm Tris–HCl, pH 7.6, 150 mm NaCl, 30 mm sodium pyrophosphate, 50 mm sodium fluoride, 2.1 mm sodium orthovanadate, 1 mm EDTA, 1 mm phenylmethylsulfonyl fluoride, and 2 µg/ml of aprotinin) was added to the surface and scraped. Insoluble cell material was removed by centrifugation at 4 °C for 10 min at 14,000 rpm (Beckman Coulter Microcentrifuge 22R). Equal amounts of cell lysate (DC assay, Bio-Rad) were mixed with NuPAGE LDS sample buffer (4x) and

NuPAGE Reducing Agent (10x) (Novex, life technology) with the ratio of 2.5:1, boiled for 10 min at 70 °C, separated by SDS-PAGE (4-12% resolving, 1 h at 200 V), and transferred to nitrocellulose membranes (2 h at 350 mA). Membranes were incubated in blocking buffer (5% milk in 0.1% Tween-20 in TBS) for 1 h at room temperature before overnight incubation with primary antibodies. Phosphorylated proteins were detected by immunoblotting using anti-phosphotyrosine antibodies (pVEGFR-2/1175 Cell Signaling, pVEGFR-2/1214 Invitrogen, in blocking buffer) followed by secondary antibodies coupled with horseradish peroxidase (200 ng/ml, Invitrogen, 1 h at room temperature) and visualized by chemifluorescence (ECL detection reagents, GE Healthcare) using a Molecular Imager Chemi Doc XRS+ scanner (Bio Rad). The images were analyzed with Image Lab software.

**5.2.5. Tube formation assay and quantification**

HUVECs were grown in a T25 flask until confluency. Meanwhile, cytodex beads were autoclaved and then coated with fibronectin (Millipore, Temecula, CA) in an incubation solution of 10 μg/ml fibronectin at 37 °C for 2 h. The cells were trypsinized and combined with the cytodex beads at a ratio of 1 million cells per 2500 beads for 4 h at 37 °C with occasional agitation. The HUVEC-coated cytodex beads were cultured overnight in a T25 flask, and then combined in the pre-gel solution at a concentration of 500beads/ml. Fibrinogen was diluted from its stock to 2 mg/ml and supplemented with aprotinin. VEGF nanoparticles at 200ng/ml were combined with the fibrinogen and cytodex bead/HUVEC solution. Fibrin gel formation was initiated by adding 1.25 U/ml of thrombin in a 10% v/v ratio. The gels were allowed to stand for 15 min at room temperature, and then incubated at 37 °C for 15 min. Meanwhile, fibroblast cells were trypsinized and plated at 20,000 cells per condition. The cells were cultured in VEGF withdrawn EGM-2 media for 7 days. The soluble VEGF condition was refreshed every other day with new soluble VEGF (200ng/ml). Phase micrographs captured the tube formation, and quantification was

completed in ImageJ. For each condition, 10 beads were analyzed. Branching points were considered where two tubes grew out of a single tube. Sprouts were measured as tubes originating from the cytodex bead. Total network length was calculated by measuring the distance from the bead to the end of the sprout, and summing up all the sprouts on the bead. The tube thickness was measured across the vessel away from its base (interface with the bead).

### 5.2.6. RNA Isolation and Real Time q-PCR

HUVECs were grown in complete EGM media (Lonza, Switzerland) in a 24 well plate at 70% confluency. Cells were submitted to serum depravation for 5 h., before exposing them to fetal bovine serum basal EGM-2 media at different time points (2, 4, 6 h). Cells were trypsinized and the cell pellet was collected. Lysis buffer from the RNAqueous micro total RNA isolation kit (Ambion, Life Technologies) was immediately added to cell pellet. Total RNA was isolated from the cells following the manufacturer's protocol. RNA concentration was evaluated by UV absorbance ($\lambda$ = 260 nm). Reverse transcription was carried out by loading 0.25 µg RNA per reaction of the iScript Advanced cDNA synthesis kit (Bio-Rad). Quantitative real-time PCR (qPCR) was carried out using 10 ng cDNA per reaction of the Maxima SYBR Green/ROX qPCR master mix (Thermo Scientific, Pittsburgh, PA, USA) following the manufacturer's recommended protocol for three-step cycling using the StepOnePlus real-time PCR system (Applied Biosystems, Life Technologies). Primer pairs used for qPCR were reported previously in Each 20-µl reaction contained 5µl of cDNA, 12.5 µl SYBR Green master mixes (life technology), 250 nM forward and reverse primers, and nuclease free water. Threshold cycles ($C_T$) were evaluated by the bundled software and expression fold change was calculated using the delta-delta $C_T$ method assuming 100% efficiency. GAPDH was used as the housekeeping gene.

### 5.2.7. Proliferation assay

Proliferation rate of HUVEC cells exposed to different clusters of VEGF was measured by

the CyQUANT® Cell Proliferation Assay Kit (Invitrogen). Briefly, cells were grown in complete EGM-2 media in a 96 well-plate for 2-4 hrs for cell attachment and exposed to VEGF nanoparticle of different cluster density, in basal EBM media with 2% fetal bovine serum (Lonza, Basal, Switzerland) and compared to a negative control condition containing no VEGF. After 48 h, cells were lysed with Cyquant lysis buffer and the relative fluorescence was measured at 485 nm excitation and 528 nm emissions.

### 5.2.8. Stroke animal model

#### 5.2.8.1 Hyaluronic acid modification and hydrogel gelation

Hyaluronic acid (60,000 Da, Genzyme, Cambridge, MA) was functionalized with an acrylate group using a two-step synthesis as previously described[45]. After dissolving the HA (2.0 g, 5.28 mmol) in water, it was reacted with adipic dihydrazide (ADH, 18.0 g, 105.5 mmol) in the presence of 1-ethyl-3-(dimethylaminopropyl) carbodiimide hydrochloride (EDC, 4.0 g, 20 mmol) overnight at a pH of 4.75. The hydrazide-modified hyaluronic acid (HA-ADH) was purified with decreasing amounts of NaCl (100, 75, 50, 25 mmol) for 4 hours each via dialysis (8,000 MWCO). The solution was then purified via dialysis (8000 MWCO) in deionized water for 2 days. After 2 days purifying against deionized water, the HA-ADH was lyophilized. The HA-ADH was re-suspended in 4-(2-hydroxyethyl)-1-piperazine ethane-sulfonic acid (HEPES) buffer (10 mM HEPES, 150 mM NaCl, 10 mM EDTA, pH 7.4) and reacted with N-acryloxysuccinimide (NHS-AC), 1.33 g, 4.4 mmol) overnight. After purification via dialysis as described earlier, the acrylated HA (HA-AC) was lyophilized. The product was analyzed with 1H NMR ($D_2O$) and the degree of acrylation (14.9%) determined by dividing the multiplet peak at $\delta = 6.2$ (cis and Trans acrylate hydrogens) by the singlet peak at $\delta = 1.6$ (singlet peak of acetyl methyl protons in HA).

This hydrogel was chosen because of its biocompatibility with human tissue, as it is constituted of naturally occurring brain extracellular matrix constituents. It remains liquid for a

period after mixing, such that it can be injected into the brain through a minimally invasive needle; and will gel within the stroke cavity, conforming to the boundaries of this damaged brain tissue. The mechanical properties of this hydrogel are similar to those of normal brain. Finally, HA has been shown to promote angiognesis in a mouse model of skin wound healing[158, 159].

**5.2.8.2 Gelation**

The hydrogel was made by dissolving the lyophilized HA-AC in 0.3 M HEPES buffer for 15 minutes at 37°C. Studies with stroke mice contained 500 μM of the adhesion peptide Ac-GCGYGRGDSPG-$NH_2$ (RGD, Genscript, Piscataway, NJ). We have previously found that clustered bioactive signals such as the adhesion peptide RGD results in significant differences in cell behaviour when encapsulated inside three-dimensional HA[54]. The highest degree of cell spreading, integrin expression and proliferation of encapsulated mouse mesenchymal stem cells was obtained with a ratio of 1.17 mole of RGD-reacting HA for 1 mole of RGD. The RGD peptide was dissolved in 0.3 M HEPES and added to 16% of the total HA-AC required to obtain a degree of clustering of 1.17, and reacted for 20 minutes at room temperature before being added to the rest of non-RGD reacting HA-AC. 200 ng of soluble VEGF, hcV, mcV, lcV or heparin nanoparticles alone were then added to the gel precursor solution and compared to a control group that contains no VEGF and no heparin. To crosslink the gels, an aliquot of the desired crosslinker (Ac-GCREGPQGIWGQERCG-$NH_2$, MMP-degradable or Ac-GCREGDQGIAGFERCG-$NH_2$, MMP-nondegradable) was dissolved in 0.3 M HEPES and added to the gel precursor solution. For viability and animal injections, the precursor was loaded into the Hamilton syringe directly after mixing in the desired crosslinking peptide.

**5.2.8.3 Animal model of stroke**

Animal procedures were performed in accordance with the US National Institutes of Health

Animal Protection Guidelines and the University of California Los Angeles Chancellor's Animal Research Committee. Focal and permanent cortical stroke was induced by a middle cerebral artery occlusion (MCAo) on young adult C57BL/6 male mice (8-12 weeks) obtained from Jackson Laboratories. Briefly, under isoflurane anesthesia (2–2.5% in a 70% N2O/30% O2 mixture), a small craniotomy was produced over the left parietal cortex. One anterior branch of the distal middle cerebral artery was then exposed, electrocoagulated and cut to be permanently occluded. Bilateral jugular veins were clamped for 15 min. Body temperature was maintained at 36.9 ± 0.4 °C with a heating pad throughout the operation. In this model, ischemic cellular damage is localized to somatosensory and motor cortex[160].

#### 5.2.8.4 Hydrogel and VEGF intracranial transplantation

Five days following stroke surgery, 6 μL of RGD – functionalized HA hydrogel previously incubated with the different VEGF/heparin nanoparticle conditions was loaded into a 25 μL Hamilton syringe (Hamilton, Reno, NV) connected to a syringe pump. The solution was then injected in liquid form directly into the stroke cavity using a 30-gauge needle at stereotaxic coordinates 0.26 mm anterior/posterior (AP), 3 mm medial/lateral (ML), and 1 mm dorsal/ventral (DV) with an infusion speed of 1 μL/min. A control group was injected with the same volume of PBS (Blank). The needle was withdrawn from the mouse brain immediately after the injection was complete. This time point for VEGF delivery was chosen because it falls within the time frames of post-stroke ipsilateral VEGF up-regulation and the peak of peri-infarct microvascular density[161]. These neoangiogenesis phenomenon have been shown to be associated with post-stroke reactive astrogliosis. Thus, the microenvironment of the infarct core at day 5 post-stroke has stabilized a boundary of reactive astrocytes around the stroke cavity that can allow the hydrogel implantation without further damaging the adjacent tissue. Ten days following the hydrogel transplantation,

animals were given the DNA synthesis marker 5-bromo-2'-deoxyuridine (BrdU, Sigma, St Louis, MO; 100 mg/kg in 0.9% NaCl) intraperitoneally 4 and 2 hours before euthanasia to assess cell proliferation. In all experiments, the researchers were blind to the treatment given to each animal (n=7-9/group).

**5.2.8.5 Mouse tissue processing and immunohistochemistry**

At 2 weeks post-stroke (10 days after transplantation), mice were transcardially perfused with 0.1 M PBS followed by 40 mL of 4% (wt/vol) paraformaldehyde (PFA). After isolation, the brain was post-fixed in 4% PFA overnight, cryoprotected in 30% sucrose in phosphate buffer for 24 hours and frozen. Tangential cortical sections of 25 μm-thicks were sliced using a cryostat and directly mounted on gelatin-subbed glass slides. Brain sections were then washed in PBS and permeabilized and blocked in 10% Normal Donkey Serum and 0.3% Triton before being immunohistochemically stained. Primary antibodies were as follows: Rabbit anti-Glucose Transporter 1 (Glut-1-) (1:200; Abcam, Cambridge, MA) for vascular Endothelial Cells; goat anti-Platelet-derived Growth Factor Receptor β (1:400; PDGF-Rβ, R&D system (R&D Systems, Minneapolis, MN) for pericytes; rat anti-BrdU (1:300; Abcam, Cambridge, MA). Primary antibodies were incubated overnight at +4°C followed by alexa fluor 594-labeled secondary antibody (Molecular Probes, Cergy-Pontoise, France, 1:400) for 1 h at room temperature. Cell nuclei were then counterstained with the nuclear marker 4', 6-diamidino-2-phenylindole (DAPI, 1:500, Invitrogen) for 10 minutes at room temperature. After 3x 10 minute washes in PBS, the slides were dehydrated in ascending ethanol baths, and dewaxed in xylene and coverslipped over fluorescent mounting medium (Dako). Sections stained for BrdU were pretreated with 2N HCl for 30 min and neutralized with sodium borate buffer, pH 8.4, before incubation in primary antibody[162].

#### 5.2.8.6 Microscopy and Morphoanalysis

Analyses were performed on microscope images of 3 coronal brain levels at +0.80 mm, -0.80 mm and -1.20 mm according to bregma, which consistently contained the cortical infarct area. Each image represents a maximum intensity projection of 10 to 12 Z-stacks, 1 um apart, captured at a 20x magnification with a Nikon C2 confocal microscope using the NIS Element software. The endothelial (Glut-1) and pericyte coverage (PDGFR β) positive area in the infarct and peri-infarct areas were quantified in 4 to 8 randomly chosen regions of interest (ROI of 0.3 $mm^2$). In each ROI, the positive area was measured using pixel threshold on 8-bit converted images (ImageJ v1.43, Bethesda, Maryland, USA) and expressed as the area fraction of positive signal per ROI. Values were then averaged across all ROI and sections, and expressed as the average positive area per animal.

#### 5.2.8.7 Statistics

Data are expressed as mean ± SD. Individual comparisons were performed using unpaired, paired Student's *t*-test or by one-way ANOVA with post hoc Tukey test. A value of $P<0.05$ was considered significant (Prism 5.03, graph Pad, San Diego, USA).

## 5.3. Results

### 5.3.1. Heparin nanoparticle synthesis and characterization

To understand the effect of VEGF presentation on vessel branching morphogenesis and tip cell phenotype switch in an engineer matrix, different VEGF clustering density on heparin nanoparticles were made as outlined in (Fig. 5.1).

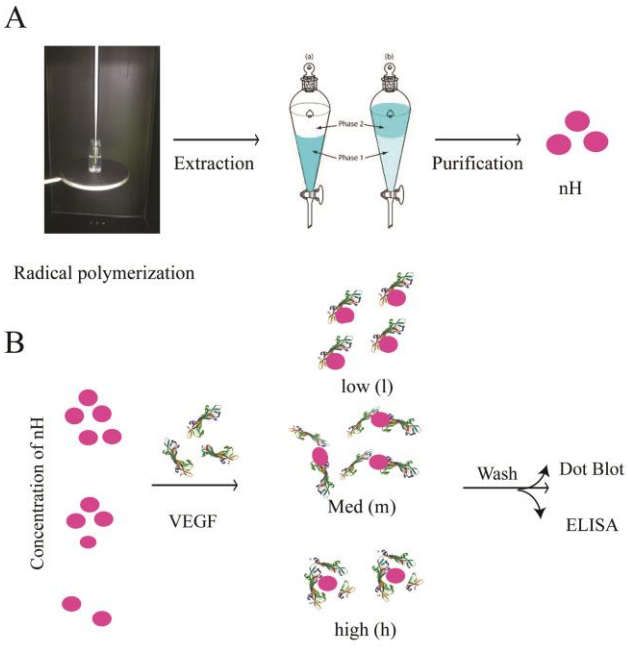


| Sample | Diameter (nm) |
|---|---|
| nH in water | 95.97 ± 2.68 |
| nH in hexane | 219 ± 5.897 |
| nH in surfactant | 46.607 ± 3.51 |
| h-cV | 768.5 ± 2.68 |
| m-cV | 578 ± 5.897 |
| l-cV | 669.5 ± 3.51 |

nH = heparin nanoparticles, h-cV = high VEGF cluster, m-cV= medium VEGF cluster and l-cV= low VEGF cluster

**Fig. 5.1. Heparin nanoparticle formation and VEGF binding and characterization.**(A) After modification of heparin, it is combined with surfactants into a hexane solution for sonication. During the inverse emulsion sonication process, radical initiators (APS) are added to the solution to generate radical polymerization. The purification of heparin nanoparticles is perfomred through a liquid-liquid extraction process and then move to the next step for binding to VEGF (B) VEGF is incubated with heparin at 4°C overnight so that VEGF interact with heparin and forms its specific electrostatic interaction. Then, UV light activates the crosslinker, which covalently binds to VEGF. The heparin-binding domain of VEGF has many available amines on the lysine groups that interact with the sulfate groups on heparin. To form different VEGF presentation, the same amount of VEGF is mixed with different amount of heparin particles. After washes and purification, Dot Blot and ELISA is used to quantify the amount of VGEF that is bound to heparin. (C) TEM is used to measure the size of the particles. TEM shows homogenously distributed of heparin nanoparticles which is consistent with the result from DLS. (B) DLS characterization of heparin nanoparticles shows a size of about 100 nm with the PDI of 0.2. Also, measurement of these particles after each step and also after binding to VEGF with different densities has been collected.

Nanoparticles were developed using an inverse emulsion process. The polymer solution was added to a ten-fold volume of hexane with surfactants Tween-80 and Span-80, and sonicated with addition of radical initiator ammonium persulfate (APS) and the catalyzer *N*,*N*,*N*',*N*'-tetramethyl-ethane-1,2-diamine (TEMED). The heparin nanoparticles formed from this radical polymerization in the template of the nanoemulsion generated during the sonication treatment. (Fig. 5.1A) The heparin nanoparticles were then incubated with VEGF with different density of heparin nanoparticles, and then exposed to UV light to induce covalent immobilization of the growth factor

to the nanoparticles and create different clustering densities of VEGF (Fig.5.1B) on the particles.

Dynamic light scattering (DLS) measurements confirmed the formation of nanoparticles of a Z-average size of 95.97 nm, and a PDI of 0.268. A low PDI observed in the measurement shows relatively homogenous distribution of heparin nanoparticles. The Transmission electron microscopy (TEM) images also confirmed the measurement observed from DLS and no significant aggregation was observed during the process (Fig. 5.1C, D). In addition, the size of nanoparticles was measured after each step of the radical polymerization process by DLS, showing an increase in diameter for heparin loaded with VEGF, as expected (Fig. 5.1.C).

### 5.3.2. VEGF nanoparticle loading characterization

VEGF was incubated with different concentrations of heparin nanoparticles, to form three different clustering densities of the growth factor on the particle's surface: high (hcV), medium (mcV) and low (lcV). The heparin nanoparticles were then washed and the washes were analyzed for VEGF content. Indirect Elisa was performed on the washes as well as on the VEGF bound to heparin nanoparticles. Dot Blot also was performed on the VEGF bound to heparin nanoparticles for further investigation of the direct binding of VEGF to heparin nanoparticles for high, medium and low binding densities. Results obtained from Elisa were normalized to the amount of heparin to show the different clustering densities (Fig.5.2A).

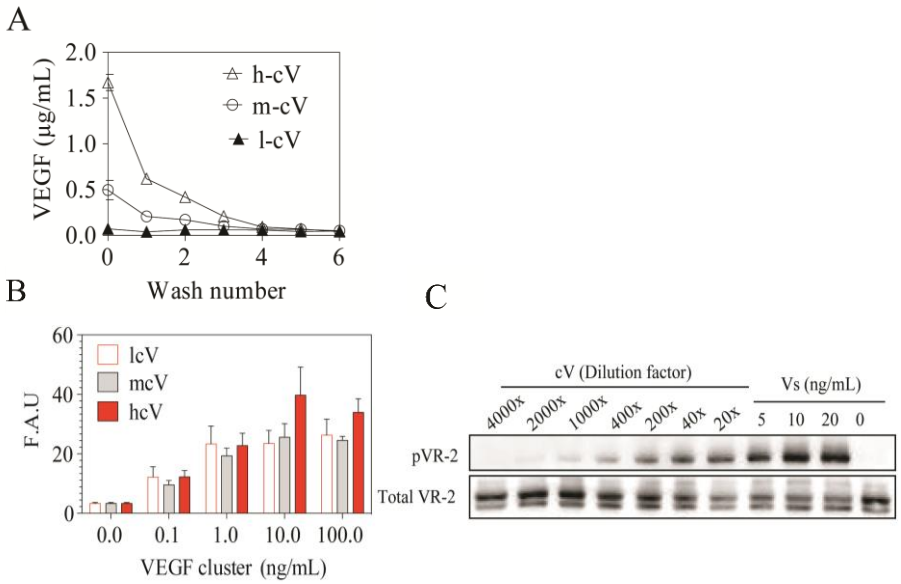


**Fig. 5.2. VEGF binding and activity characterization.** VEGF binding to different amount of particle was characterized using ELISA on the successive washes as well as ELISA and Dot Blot on the samples. Also, for the activity of VEGF bound to particles, proliferation assay and western blot were performed. (A) In direct ELISA was performed on all the washes to quantify the amount of VEGF that is bound to mg of heparin. Also the plot confirms the high cluster formation of VEGF to heparin by having the most unbound VEGF amount in the washes to show that heparin reached to its saturation binding to VEGF. (B) Proliferation assay for different concentration of VEGF is confirmed the activity of VEGF bound to different densities of heparin. (C) VEGFR-2 phosphorylation assay also confirms the activity of the bound VEGF. Binding of VEGF to particles enriches Y1175 signaling for the medium cluster formation at different dilutions of the VEGF as well as for the soluble VEGF as a positive control.

### 5.3.3. Proliferation of HUVECs in response to different presentation of VEGF

HUVECs were cultured in a 96 well plate and the cells were attached after 2-4 hours of incubation in the cell incubator. Cells were exposed to hcv, mcV and lcV at different concentration of VEGF (0; 0.1; 1; 10; 100 ng/ml) basic media + 2% FBS for 48 h. The Cyquant proliferation assay was then used to quantify the number of proliferative cells showing a significant increase in the number of proliferative cells with the increase of VEGF concentration (Fig.5.2C).

### 5.3.4. VEGF activity after bound to heparin nanoparticles

The activity of covalently bound VEGF was tested by measuring the phosphorylation of its receptor on Y1175 using western blot. HUVEC cells cultured in a 6 well-plate were exposed to different concentration of VEGF nanoparticles for 5 min and compared to a control group condition with soluble VEGF. A western blot was performed on lysates, showing a phosphorylation of the

VEGF receptor on Y1175 at all concentrations of clustered VEGF tested, indicating that the activity of the growth factor is not altered when displayed in its clustered conformation, even at a low concentration of VEGF with a 40x dilutions (Fig.5.2D).

### 5.3.5. VEGFR-2 phosphorylation and downstream signaling activation of different presentation of VEGF bound heparin nanoparticles

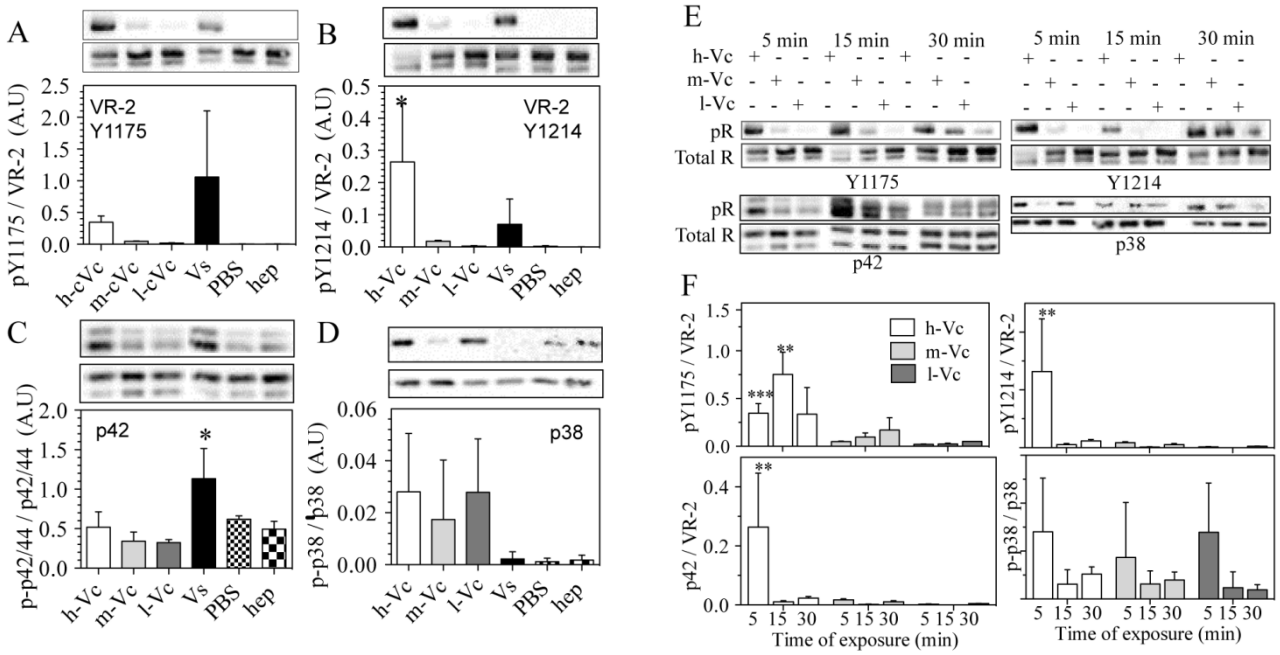


**Fig. 5.3 VEGFR-2 phosphorylation assay.** Plot quantifies phosphorylated VEGFR-2 band intensities and is normalized to total VEGFR-2 for each condition (n = 3 blots). Top band shows pVEGFR-2 and bottom band shows total VEGFR-2.Western blot data is shown for phospho-VEGFR-2 at Y1175 at 5min (A), for Y1214 at 5 min (B), phospho Erk ½ at 5 min (C) and phospho p-38 at 5 min (D). Western blot data for all has been shown for different time points (5, 15, 30 min)(E) and the quantification of those data has been plotted in (F). Data show increased activation of phospho Y1175 and Y1214 for hcV over the other two conditions. Also, hcV show sustained activation of pY1175 at 15 min compared to mcV and lcV.

VEGF-induced activation of VEGFR-2 in HUVECs is known to result in the phosphorylation of a number of tyrosine residues at the cytoplasmic side of the membrane receptor. In particular, Y1175 and Y1214 are major phosphorylation sites associated with the activation of the MAPK pathways in cells[163]. Here, we looked at the phosphorylation of these two tyrosine

residue as well as downstream activation of ERK1/2 MAPK pathway and p38 MAPK pathway to response to different presentation of VEGF formed as low/high/medium clusters. As expected, VEGF soluble results in a large spike in VEGFR-2 phosphorylation at Y1175 (pY1175/VEGFR-2) within 5 min (Fig.5.3A). The intensity of VEGFR-2 phosphorylation at Y1214 has a large spike for high cluster VEGF compared to other conditions as well as the soluble VEGF within 5 min (Fig.5.3B). The phosphorylation profile for Y1175 over time in the presence of high cluster VEGF (hcV) exhibited a stronger and sustained activation compared to other presentation of VEGF (low/medium) up to 30 min (Fig.5.3E, F). The phosphorylation profile for Y1214 over time was less pronounced for different VEGF cluster after 5 min.Activation of the ERK1/2 MAPK pathway following Y1175 phosphorylation is typically associated with the proliferative response in HUVECs. Evaluation of ERK1/2 phosphorylation at the 5 min time point confirms that the ERK1/2 pathway was activated in the presence of soluble VEGF (Fig.5.3C). This shows the same results obtained for pY1175/VEGFR-2(Fig.5.3A). On the other hand, activation of the p38 MAPK pathway following Y1214 phosphorylation is associated with the migration response in HUVECs. Interestingly, the activation of p38 was also higher for the hcV compared to other conditions, but because of the high error bars which are a reflection of the background level of p38/VEGFR-2, there are no statistical differences between conditions (Fig.5.3D). Activation of p38 pathways in the presence of hcV were sustained over 30 min incubation periods as compared to low and medium clusters, despite the error bars. This data would suggest that a higher presentation of VEGF as a cluster may be critical for sustained activation of the MAPK pathways.

### 5.3.6. VEGF presentation inside fibrin hydrogels modulates HUVEC branching

To determine the effect of VEGF presentation on endothelial tube formation, a sprouting bead assay was performed. Briefly, cytodex beads were coated with HUVEC cells and encapsulated in a fibrin hydrogel scaffold, where fibroblast cells were seeded on top to further

mimic a physiologic environment (Fig.5.4A)[27, 164]. During the fibrin gel formation hcV, mcV and lcV at a concentration of 200ng/ml were added and compared to a positive control condition containing 5ng/ml of soluble VEGF and a negative condition containing only heparin nanoparticles where no VEGF was attached. The endothelial tubes formed from the beads were then quantified for branching points, sprouts, thickness, and total vessel network length (Fig.5.4B, C). The number of sprouts was significantly increased in the hcV condition compared to the 2 other cluster densities and to the heparin nanoparticles condition alone (Fig.5.4B, C). In addition, the number of branching points in the hcV condition was significantly increased compared to mcV and lcV, indicating that the presentation of VEGF on nanoparticles affected the architecture of the vessels formed in the fibrin gel. Furthermore, the number of branching point was significantly increased in all clustered VEGF conditions compared to the nanoparticles only, suggesting that heparin particles are not sufficient to promote controlled vessel branching. Finally, the total network length was quantified by measuring the length of individual sprouts from the beads to their end point, and summing up all the values obtained for each bead (Fig.5.4B, C). The total network length for hcV was statistically increased compared to lcV and mcV, indicating that the presentation of the VEGF in fibrin hydrogel modulates the extent of the vascular network formed. No difference was observed between mcV and lcV.

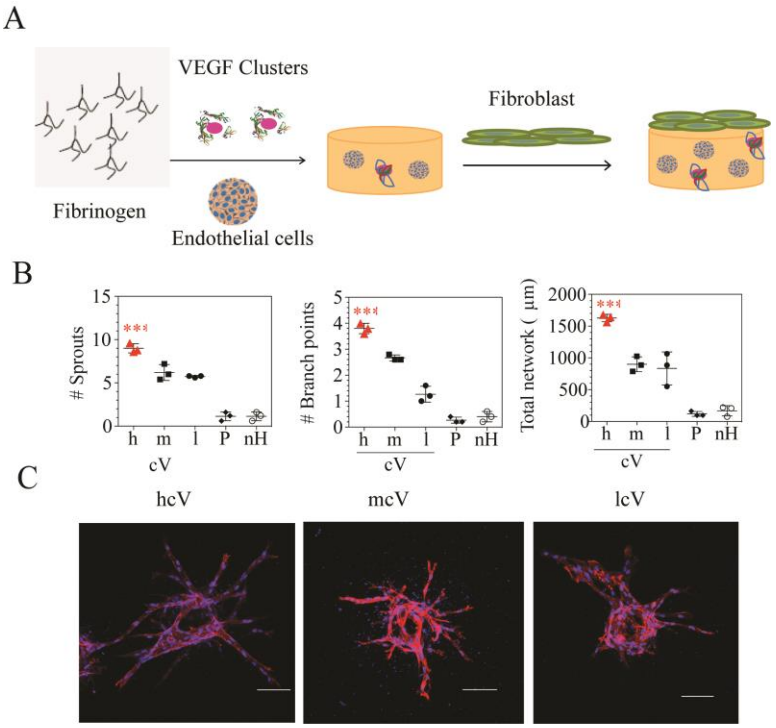


**Fig. 5.4.Tube formation assay with different VEGF clusters**. (A)Different VEGF clusters are introduced to a fibrin gel with endothelial cell-coated cytodex beads, while fibroblast are cultured on top of the gel. Sprouting was analyzed over the course of 7 days for number of branching, number of sprouts and total network. (B) in all the analysis, hcV leads to a significant increase in branching points for endothelial cells as well as number of sprouts and total network over mcV and lcV. (C) Flourescent images of different sproutinf from cytodex beads. Endothelial cells are stained with pholloidain actin and DAPI and images are representing of different cluster VEGF branching inside fibrin gel.

### 5.3.7. Gene expression of VEGF receptors and Notch ligands

The Notch receptor-ligand pathway forms a close counterpart to the VEGF receptor-ligand pathway in directing endothelial cell response during sprouting angiogenesis[165]. In particular, the Notch ligands Dll4 and Jag1 are known to form an antagonistic pair in regulating tip and stalk cell phenotype switch, with Dll4 predominantly expressed in tip cells and DII4/Jag1 in the adjacent stalk cells[166, 167]. Our data indicates that Dll4 gene expression levels peaked at 30 min and 4 h post incubation for hcV at a high concentration of VEGF (100ng/ml). Since Dll4 gene expression is associated with the tip cell phenotype, this could suggest a stronger competition for the tip cell position under this condition (Fig5.5A). HUVECs express three VEGF receptors, namely VEGFR-1, VEGFR-2, VEGFR-3, all of which are involved in the regulation of angiogenesis among which VEGFR-3 has been found to be upregulated in tip cells but its role in angiogenesis has been less

well studied[168]. Our data suggests that there is no significant fold change in VEGFR-3 gene expression levels under the conditions tested (fig.5.5B).

In contrast, under lower concentration of VEGF (20ng/ml), there was a significant fold changes in Jag1, Dll4 and VR-3 gene expression levels for medium cluster compared to the other conditions. Jag1 is associated with the stalk cell phenotype, and is synthesized in response to Notch signaling (Fig.5.5C).

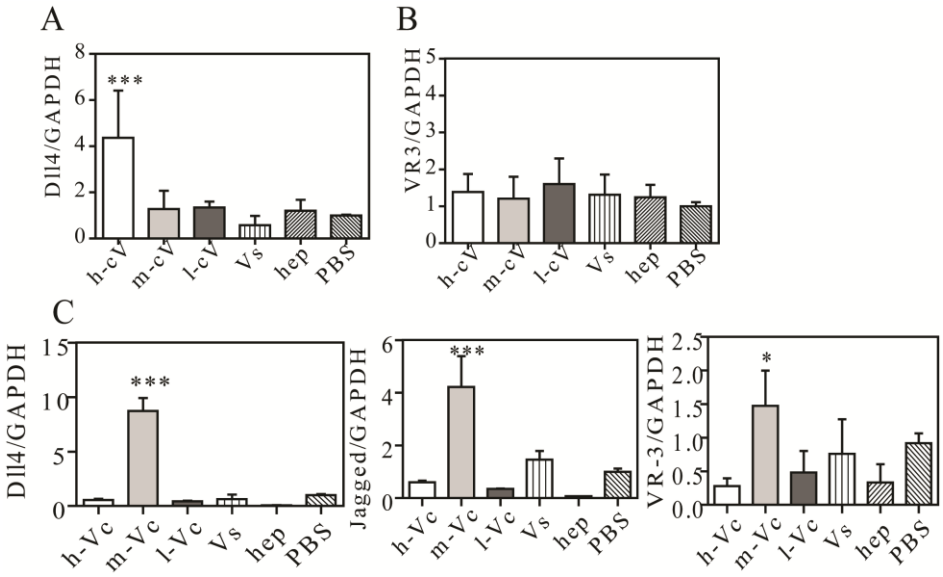


**Fig. 5.5. Gene expression of Notch ligands and VEGFRs for different cluster formation.** (A, B) Data indicate gene expression level of Dll4 and VEGFR-3 at the high concentration of VEGF (100 ng/ml) after 30 min exposure time and 4 hours post-incubation time. Gene expression of Dll4 level shows an increase for hcV over mcV and lcV and even soluble VEGF. (C) Data indicate an increase for mcV at lower concentration of VEGF (20ng/ml) for gene expression level of Dll4 and VR-3 over hcV.

### 5.3.8. Post-stroke angiogenesis within the infarct core

The main activity was to perform an in vivo experiment to figure out the baseline angiogenic response to our materials in the stroke brain. Animals were subjected to a permanent distal middle cerebral artery occlusion and a transient bilateral common carotid occlusion to generate a permanent and focal ischemic stroke. Five days post stroke induction, hyaluronic acid-RGD hydrogel alone (HA-RGD), HA-RGD plus 200ng of soluble VEGF (Vs), HA-RGD plus

heparin nanoparticles (nH), or HA-RGD plus covalently bound VEGF to heparin nanoparticles (cVc) were injected directly into the stroke cavity. Ten days post implantation, the animals were perfused with paraformaldehyde and the brain was collected and processed. The sections were stained to quantify vessel infiltration (Glut-1) and the pericyte coverage (PDGFRß).

The mouse brain sections were stained for Glut-1, a glucose transporter specifically expressed on brain endothelial cell surface. Our study shows that endothelial cell infiltration in the infarct and the peri-infarct areas is significantly higher in the hcV group compared to the other groups (Fig.5.6). The number of double-labeled cells for Glut-1 and BrdU, a proliferation marker, was assessed and the results shows that the number of endothelial cell in the proliferation phase is also significantly increased in the hcV condition (Fig.5.7). In addition, the % area of positive staining for PDGFRß in the infarct area as well as in the peri-infarct area was statistically significantly greater for the HA-RGD/cVc condition compared to all other conditions (Fig.5.8). No other condition had vessels growing in the stroke cavity.

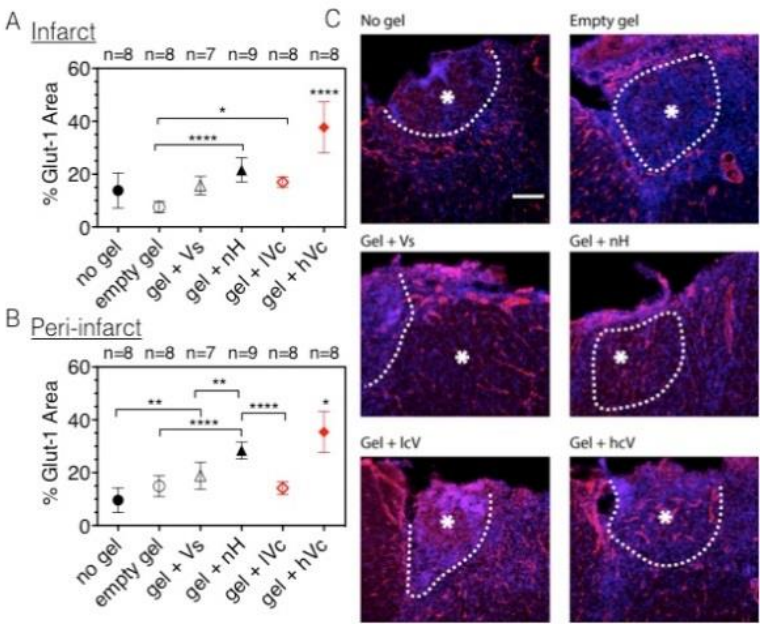


**Fig. 5.6. Endothelial cell infiltration within the infarct core.** Mice brain were fixed in a solution of 4% paraformaldehyde, cryo-protected in sucrose and frozen. Sections of 25 µm were obtained using a cryostat, and stained for Glut-1 in a blocking buffer. The positive area for the brain endothelial marker was quantified in 3 sections per animal, in the infarct (A) and the peri-infarct (B) areas for each transplanted group (n=7-9). Pictures (C) of the immunofluorescent staining were taken using confocal microscopy at 20 x. Scale bar, 100 µm. The dotted line delimitates the stroke core (*) from the peri-infarct area.

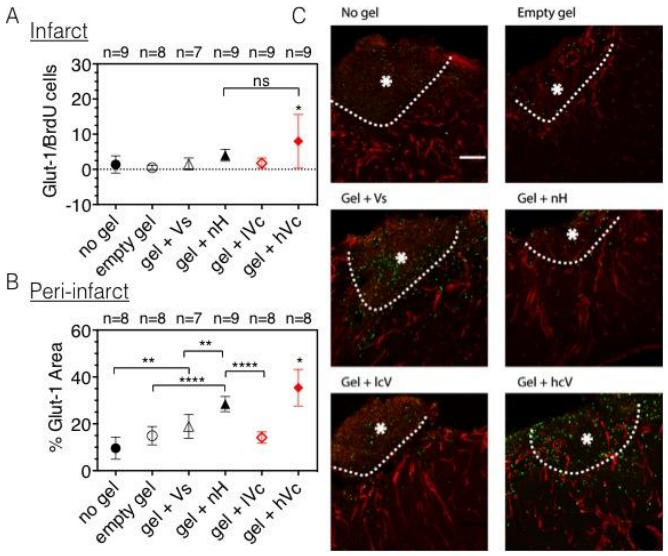


**Fig. 5.7. Endothelial cell proliferation within the infarct core.** Mice brain were fixed in a solution of 4% paraformaldehyde, cryo-protected in sucrose and frozen. Sections of 25 µm were obtained using a cryostat, and stained for Glut-1 and for BrdU in a blocking buffer. The number of double labeled cells for both markers, the endothelial and the proliferation markers, was quantified in 3 sections per animal, in the infarct (A) and the peri-infarct (B) areas for each transplanted group (n=7-9). Pictures (C) of the immunofluorescent staining were taken using confocal microscopy at 20 x. Scale bar, 100 µm. The dotted line delimitates the stroke core (*) from the peri-infarct area.

These data demonstrate that our proposed VEGF clusters can promote the re-vascularization of the stroke cavity within 2 weeks. This first experiment showed that the baseline angiogenic response from blank gel (HA-RGD) and blank gel plus either soluble VEGF or plain heparin nanoparticles (HA-RGD + Vs or HA-RGD + nH) resulted in low levels of vascularization than the hcV condition.

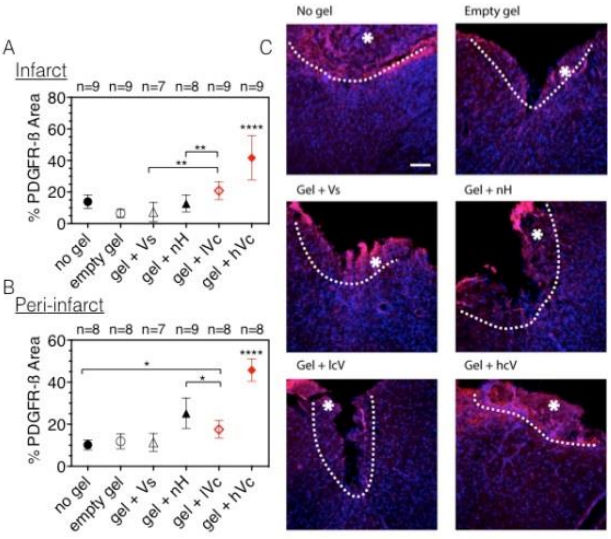


**Fig. 5.8. Vascular maturity of newly formed vessels.** Mice brain were fixed in a solution of 4% paraformaldehyde, cryo-protected in sucrose and frozen. Sections of 25 µm were obtained using a cryostat, and stained for PDGFRb in a blocking buffer. The positive area for the pericyte marker was quantified in 3 sections per animal, in the infarct (A) and the peri-infarct (B) areas for each transplanted group (n=7-9). Pictures (C) of the

immunofluorescent staining were taken using confocal microscopy at 20 x. Scale bar, 100 µm. The dotted line delimitates the stroke core (*) from the peri-infarct area.

### 5.4. Discussion

Vascular endothelial growth factor (VEGF) is widely known as a key regulator to promote vascularization at damaged or diseased sites in pro-angiogenic therapies applications[98,164]. In this current report, we investigated the consequences of displaying VEGF in a clustered conformation endothelial cells phenotype and controlled vessel branching in an engineered matrix. VEGF was covalently bound to nanoparticles and encapsulated in a fibrin hydrogel, containing HUVECs-coated cytodex beads. Three different clustering densities of VEGF on heparin nanoparticle surface were tested. The obtained results show that the high density clusters of VEGF (hcV) was associated with significantly increased tube branching, sprouts, and total vessel network length compared to the medium (mcV) and low (lcV) VEGF cluster conditions. Our study shows that controlling the 3 dimensional presentation of VEGF by controlling its discrete distribution on heparin nanoparticles affects blood vessel formation and branching in an engineered matrix.

In order to make different presentation of VEGF, VEGF was incubated with different amounts of particle. The result is different densities of VEGF on the particles that have been controlled using the ELISA on the washes from the purification process.

To determine if the covalent immobilization of VEGF affects its biological activity, HUVEC cells were exposed to the different clusters and the proliferation and VEGFR-2 phosphorylation were measured. The proliferation rate was pronounced at higher concentration of VEGF for all the conditions (Figure 1c), indicating that the VEGF remains active throughout the process of particle modification. Interestingly, the phosphorylation level of Y1175 in the hcV condition was enhanced over a time course of 30 min was and sustained for a longer time compared to the other conditions. The phosphorylation of this residue results in the activation of the ERK1/2

pathway and is known to promote cell proliferation[169-171], while the phosphorylation of the Y1214 residue results in the activation of the p38 pathway and is known to promote cell migration[172, 173].

Studies at a molecular level lead to a better understanding of the clusters effect on vessel branching. The Dll4/Notch1 signaling pathway has been evidenced to play a crucial role in the tip cell/stalk cell phenotype switch within the angiogenic sprout, inhibiting the formation of new sprouts in response to VEGF.[146,] This lateral inhibition regulates the ratio between tip and stalk cells, promoting the formation of a controlled vessel sprouting and branching, leading to the formation of a functional and mature vascular network. In our study, if the level of VEGFR-3 mRNA expression didn't show any significant difference between groups, the high cluster of VEGF was associated with a significantly increased Dll4 mRNA expression level, suggesting an effect on the modulation of endothelial cell phenotype in favor to tip cell phenotype.

**5.5. Conclusion**

Our study shows that controlling the 3 dimensional presentation of VEGF by displaying the growth factor in a clustered conformation and controlling its discrete distribution on heparin nanoparticles affects blood vessel formation and branching in an engineered matrix. We showed that covalently bound and clustered VEGF in a high packing density on the surface of nanoparticles leads to the endothelial cell activation, and sprout formation by modulating the balance between tip/stalk phenotype in favor of tip cell. Our data also evidence the effect of such presentation of VEGF on post-stroke angiogenesis by promoting endothelial cell infiltration within the infarct core at 2 weeks, when injected within a biomaterial containing the clustered adhesive peptide RGD. Indeed, we showed that the hcV condition was associated with an increased number of proliferative vascular cells, and an increased area of covered vessels by pericytes, which indicates the formation of a more mature and functional vascular network in the damaged brain. These results represent a promising therapeutic strategy to promote brain tissue regeneration after such a damaging trauma.

# Chapter 6

# *Clustered VEGF with fibronectin domains promote angiogenesis in vitro*

## 6.1 Introduction

As discussed in chapter 3, ECM proteins trigger synergistic signaling between growth factor receptors and integrins, in addition to their ability to cause GFs retention [124, 174, 175]. Crosstalk between growth factors and integrins is critical to regulate blood vessel growth. Fn has been shown to be a ubiquitous ECM protein for several integrins. $\alpha_v\beta_3$ and $\alpha_5\beta_1$ integrins are the two key Fn receptors that are essential for vascular development[119, 126]. The objective of this aim is to evaluate whether the presence of ECM proteins can locally modulate cellular responses to growth factors. To answer this question, we incorporated Fn fragments with a high affinity for $\alpha_5\beta_1$ to hydrogels containing our VEGF clusters from Aim 2 and studied its effect on the activation of VEGFR-2 and the induction of the tip cell phenotype. The Fn fragments were generously provided by Prof. Barker

from Georgia Institute of Technology. It's structure is stabilized by the fusion of the domain 9 and 10 of the Fn III, called FN 9*-10 ($Leu^{1408}$ to Pro) or FNV1, and preferentially binds $\alpha_5\beta_1$. We hypothesize that the addition of Fn fragments to VEGF clusters in an engineered matrix can influence the magnitude and duration of ECs intracellular signaling, leading to controlled vascular sprouting and branching in 3D.

## 6.2 Materials and Methods

### 6.2.1 Heparin nanoparticle synthesis for VEGF and Fn fragment binding

The first part of the reaction is the same as described in chapter 5. The modified heparin was then reacted with k-peptide in MES buffer (pH 6.0) and was reacted overnight at room temperature to allow all the maleimide groups on EMCH to react with k-peptide. Following dialysis the next day, the solution was lyophilized for another day.

To form heparin nanoparticles, the final product was dissolved in sodium acetate, pH 4, at 100 mg/ml and combined with Tween-80 and Span-80 (8% HLB). The solution was placed in a ten-fold volume of hexane and combined with N,N,N',N'-tetramethyl-ethane-1,2-diamine (TEMED) and ammonium persulfate (APS) during sonication to initiate radical polymerization. The resultant nanoparticles were purified via liquid-liquid extraction in hexane. In the final stage of the extraction process, bubbling nitrogen gas into the nanoparticle solution evaporated off excess hexane. The particles were then dialyzed in 100 kD MWCO dialysis units for few hours and stored until use. The amount of heparin in the solution was determined by lyophilizing a small aliquot of the solution. A constant concentration of VEGF (20μg/ml) was incubated with three different concentration of Fn fragment (9*10) (1, 5, 10 μg/ml) in presence of heparin nanoparticles and activated FXIII, at 4°C overnight to facilitate the binding of Fn fragment to heparin.

The following day, samples were exposed to a 365 nm wavelength UV light for 10 minutes to activate the covalent attachment of VEGF to the particles surface. The excess of VEGF and Fn

fragments were washed three times with 0.05% Tween-20 in PBS using a 100 kD MWCO dialysis units, followed by three PBS washes. The washes were collected to estimate the amount of bound VEGF.

### 6.2.2. Heparin nanoparticle characterization

Dynamic Light Scattering (DLS) was used to characterize the size of the heparin nanoparticles. Heparin nanoparticles were analyzed in a Malvern Zetasizer to determine particle diameter after each preparation step. Heparin nanoparticles were analyzed after formation, purification, and dialysis. Samples were loaded into a filtered DI water cleaned quartz cuvette. Ten runs each comprised three measurements, and data was reported as Z-average with polydispersity index (PDI). Transmission Electron Microscopy (TEM) was performed using T12 Quick CryoEM in Electron Imaging Center for NanoMachines (EICN).this method has been described in the previous chapter.

### 6.2.3. Enzyme linked immunosorbant assay (ELISA) and Dot Blot

To quantify the amount of VEGF and Fn fragments immobilized on nanoparticles, a standard ELISA technique as well as a Dot Blot were used. The protocol is described in the previous chapter.

### 6.2.4. Proliferation assay

For cell proliferation experiments, cells were grown in complete EGM-2 media in a 96 well-plate for 2-4 h for cell attachment. The three Fn cluster conditions were added to a basal EBM media containing 2% fetal bovine serum depleted in Fn andVEGF (Lonza, Basal, Switzerland) and compared to a positive control group where cells were exposed to soluble VEGFor heparin nanoparticle alone. After 48 h, cells were lysed and the cell density was determined using CyQUANT® Cell Proliferation Assay Kit.

### 6.2.5. VEGFR-2 phosphorylation assay

HUVECs were grown to confluency in a 6 well plates, and then serum starved for 5 h prior to growth factor treatment. Cells were treated with 0.1 mm sodium vanadate for 5 min, then with 20 and 100 ng/ml of either soluble or bound VEGF at 37 °C for 5 min. Cells were rinsed twice with ice cold PBS supplemented with 0.2 mm sodium vanadate. A 100 µl of lysis buffer (1% Non-idet, 10 mm Tris–HCl, pH 7.6, 150 mm NaCl, 30 mm sodium pyrophosphate, 50 mm sodium fluoride, 2.1 mm sodium orthovanadate, 1 mm EDTA, 1 mm phenylmethylsulfonyl fluoride, and 2 µg/ml of aprotinin) was added to the plate and scraped. Insoluble cell material was removed by centrifugation at 4 °C for 10 min at 14,000 rpm (Beckman Coulter Microcentrifuge 22R). A Western blot protocol was followed as described in the previous chapter. Phosphorylated proteins were detected by immunoblotting using anti-phosphotyrosine antibodies (pVEGFR-2/1175 Cell Signaling, pVEGFR-2/1214 Invitrogen, in blocking buffer) followed by secondary antibodies coupled with horseradish peroxidase (200 ng/ml, Invitrogen, 1 h at room temperature). In addition, Integrin linked kinase activation and focal adhesion kinase activation were studied. The images were visualized by chemifluorescence (ECL detection reagents, GE Healthcare) using a Molecular Imager Chemi Doc XRS+ scanner (Bio Rad) and analyzed with Image Lab software.

### 6.2.6. Tube formation assay and quantification

A tube formation assay protocol was performed as described in the previous chapter. The Fn content was depleted from the FBS. HUVECs were cultured in a fibrin gel as a clot and fibroblasts were grown on top of the gels. Clustered VEGF and VEGF/Fn were bound to the matrix at the concentration of 200 ng/ml. The soluble VEGF condition was refreshed every other day with 200ng/ml VEGF. Phase images of the newly formed vascular tube were captured, and the quantification in terms of number of sprouts, branching and total vessel length was made using ImageJ. In addition, samples were stained for Actin (conjugated with phalloidin) and DAPI to have

a better understanding of the intracellular cytoskeleton network and thus, the formation of filopodia. In each condition, 10 beads were analyzed. Was considered a branching point the observation of tubes growing out of a single tube. Sprouts were measured as tubes originating from the cytodex bead. The total network length was calculated by measuring the distance from the bead to the end of the sprout, and summing for all the sprouts on the bead. The thickness of vessels was measured across the vessel away from its base (interface with the bead).

## 6.3 Results

### 6.3.1 Heparin nanoparticle synthesis and characterization

Integrins are receptors for extracellular matrix proteins that are involved in reciprocal crosstalk with growth factor receptors.[176] Here, in order to investigate the synergy effect of the VEGF receptor and integrins, we developed a clustering system that would allow us to incorporate both elements, VEGF and Fn fragments designed to bind selectively VEGF through the domains (9*10).

During the heparin modification process, a new step was added to provide functional groups on heparin to bind the Fn fragments. After lyophilization and before the heparin nanoparticle formation, k-peptide was reacted with heparin to allow its binding to the Fn fragment. The reaction between the thiol groups on k-peptide and maleimide group on EMCH is almost 90% efficient and the NMR confirms that maleimide groups are replaced by k-peptide.A TNBS assay was used to determine the quantity (in mmoles) of amine remained on the k-peptide, detecting a total amount of 25 mmoles. Nanoparticles were then developed using an inverse emulsion process. Heparin nanoparticles were formed using a radical polymerization process and a nanoemulsion generated during the sonication treatment. Heparin nanoparticles were then incubated with a constant concentration of VEGF and different concentrations of Fn fragments in the presence of activated FXIII, and then exposed to UV light to induce a covalent attachment of the growth factor to the

nanoparticles.

Dynamic light scattering (DLS) measurements confirmed the formation of heparin nanoparticles with a Z-average size of 78 nm, and a PDI of 0.21 (Fig.6.1A). A low PDI was observed, showing a relatively homogenous distribution of heparin nanoparticle sizes. Transmission electron microscopy (TEM) images also confirmed the measurement observed from the DLS and almost no aggregation was observed in the formation of particles. (Fig.6.1B)

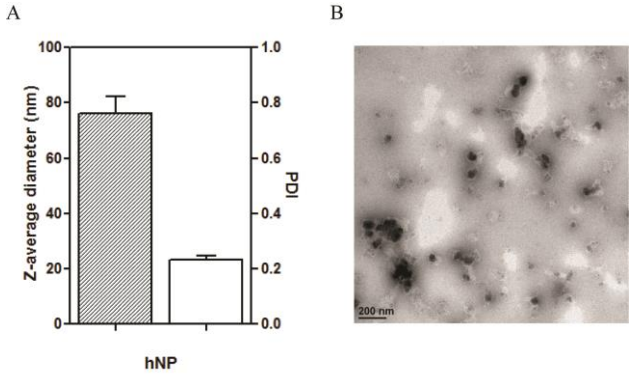


**Fig. 6.1. Physical characterization of heparin nanoparticles.** (A) DLS measurements of heparin nanoparticles show an average size of 78 nm with a PDI of 0.21, a low PDI indicating a homogenous distribution of heparin nanoparticle sizes. (B) TEM image of heparin nanoparticle.

### 6.3.2 VEGF nanoparticle loading characterization

VEGF was loaded onto the heparin nanoparticles as well as Fn fragments at different concentration to determine the effect of this factor on the synergy between VEGFR and integrins. Heparin nanoparticles were then washed and the washes analyzed for both VEGF and Fn fragment content. Dot Blot also was performed on the VEGF and fragment bound to heparin nanoparticles for further estimate the amount of bound elements to nanoparticles. ELISA and Dot blot both confirmed their binding to nanoparticles, confirming that the attachment of Fn fragments did not alter the attachment of VEGF. For this study, we decided to further investigate the effect of double loaded nanoparticles using the VEGF clustering condition that showed the best results in terms of ECS growth, migration, proliferation and tube formation which: the high VEGF cluster with a total of 1100µg VEGF/mg heparin. (Table 6.1)

| Methods | cV/[Fn]1[µg/m] | cV/[Fn]5[µg/ml] | cV/[Fn]10[µg/ml] | cV[µg/ml] |
|---|---|---|---|---|
| Indirect ELISA-VEGF | 18.91 | 19.29 | 18.28 | 18.5 |
| DotBlot-VEGF | 16.53 | 18.53 | 17.53 | 19.27 |
| Indirect ELISA-Fn | 2.54 | 5.19 | 6.38 | |
| Dot Blot-Fn | 4.32 | 4.67 | 8.53 | |

**Table 6.1. Characterization of VEGF loading.** ELISA and Dot blot were performed for both VEGF and Fn fragments to confirm and quantify the amount bound to heparin nanoparticles.

### 6.3.3 Proliferation of HUVECs in response to different VEGF/Fn loading

HUVECs were cultured in a 96 well plate and the cells were attached after 2-4 h of incubation in the cell incubator. Media was replaced with basic media + 2% FBS (Fn and VEGF depleted) and the different VEGF/Fn cluster condition were added. Cells were incubated in these solutions for 2 days, lysed and studied for proliferation using the proliferation assay (CYQUANT) was performed to quantify the number of proliferative cells after being exposed for 48 h. Two different concentrations of bound VEGF (10,100 ng/ml) were tested. The results show that when exposed to the low concentration of bound VEGF (10ng/ml), all the groups where the double loaded VEGF/Fn nanoparticles were added, showed a significant increase in proliferation at 2 days, compared to the high cluster of VEGF. However, when exposed to the high concentration of bound VEGF (100 ng/ml), no significant differences between all the conditions was observed (Fig.6.2).

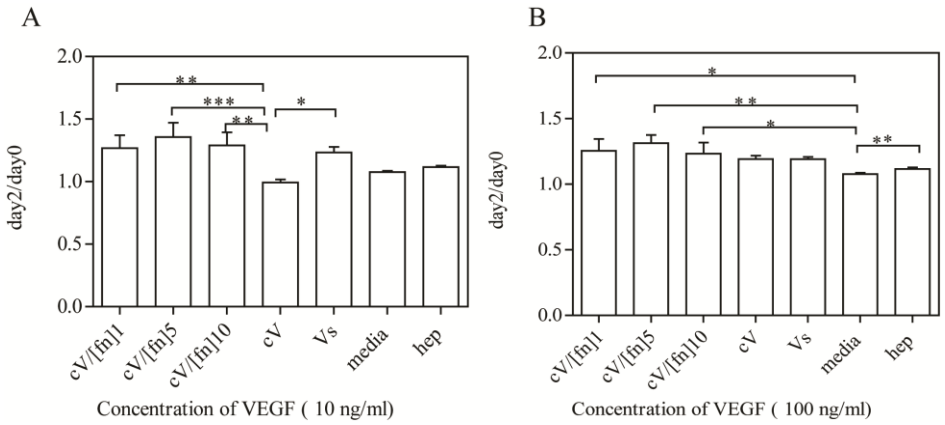

**Fig. 6.2. Proliferation assay.** To test the effect of double loaded Fn/VEGF nanoparticles on cell proliferation, HUVECs were exposed to different VEGF/Fn clusters where the concentration of Fn differs. (A) Cells were exposed to a low concentration of bound VEGF, showing a significant increase in the number of cells after 2 days compared to the high cluster of VEGF and the soluble VEGF conditions. (B) The exposure of a high concentration of bound VEGF didn't show any significant effect on ECs proliferation.

### 6.3.4 VEGFR-2 phosphorylation and downstream signaling activation of VEGF/FN cluster

It has previously been shown that VEGF/Fn complexes prolonged cell signaling[177]. Therefore, our results suggest that different pathway in the VEGFR-2 downstream signaling could be involved in the synergy effect of integrins and the VEGF receptor. We further studied the effect of different concentration of VEGF and of Fn fragments of the double loaded particles, on the activity of Erk ½ and the phosphorylation of VEGFR-2 on the tyrosine residue Y1175. Different controls were used for this experiment: soluble VEGF, high cluster VEGF, soluble Fn fragments and soluble VEGF /soluble Fn fragments. We hypothesize that the immediate vicinity between integrins and VEGFR-2 is small enough to allow the synergy interaction. The results obtained from the controls support this idea. Soluble VEGF results in a strong proliferation effect, associated with an enhanced phosphorylation of VEGFR-2 on Y1175 (pY1175/VEGFR-2) within 5 min. The western blot results show that a high concentration of bound Fn fragments on double loaded VEGF/Fn heparin nanoparticles was associated with an enhanced VEGFR-2 activation for all the Fn concentrations under 5 µg/ml (Fig.6.3A, B). However, a Fn fragment concentration over 5 µg/ml shows a decrease in the VEGFR-2 activation. In addition, we can notice that a stronger phosphorylation of Y1775 was observed for all the VEGF/Fn cluster conditions compared to the exposure of VEGF nanoparticles only. The quantification of ERK ½ activation at 5 min time point

confirmed the same result (Fig.6.3C, D). To further investigate the integrin binding effect, we tested the activation of the Integrin linked kinase and the Focal adhesion kinase in all the conditions after exposing cells for 5 min. A significant increase in the phosphorylation of the integrin linked kinase was observed in the VEGF/Fn nanoparticle conditions compared to the high VEGF cluster nanoparticle only and the soluble VEGF.

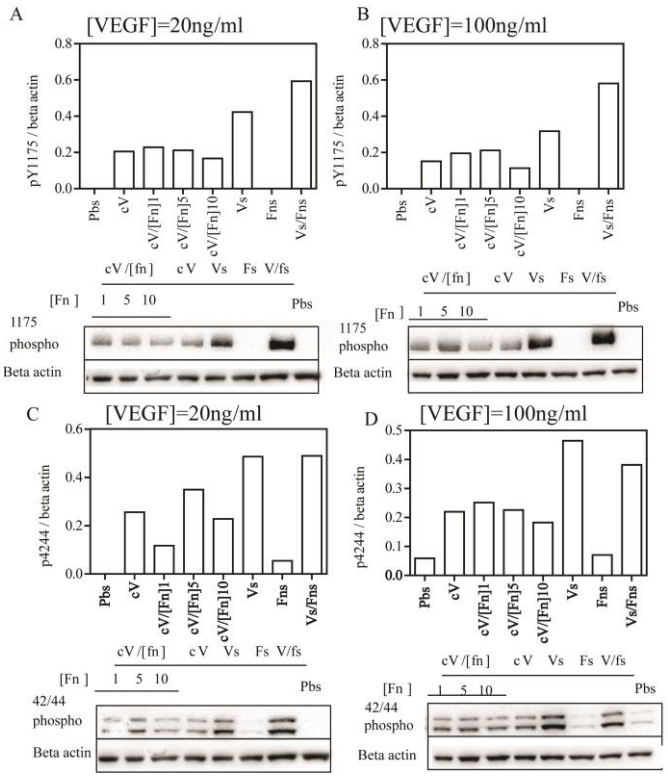


**Fig. 6.3.VEGFR-2 phosphorylation assay.** Western blot data for two different concentration of VEGF(20, 100 ng/ml) for phosphorylation of Y1175 is shown in (A) and (B) respectively. Plot quantifies phosphorylated VEGFR-2 band intensities and is normalized to Beta actin each condition. Top band shows pVEGFR-2 and bottom band shows Beta actin. (C) and (D) Western blot data for downstream signaling of activation of Erk ½ for two different concentration of VEGF. Data indicate the activity of VEGF after binding to heparin nanoparticles.

This can be a confirmation for the activity of Fn fragment and also its effect compared to the VEGF cluster that has no fragment. For the focal adhesion activity, because of the background in the negative control, we can't get a clear conclusion. All the conditions seem to have an activation of focal adhesion kinase as well as the negative control which is just PBS. All these results confirm the activity of VEGF and Fn fragment after their binding. (Fig.6.4)

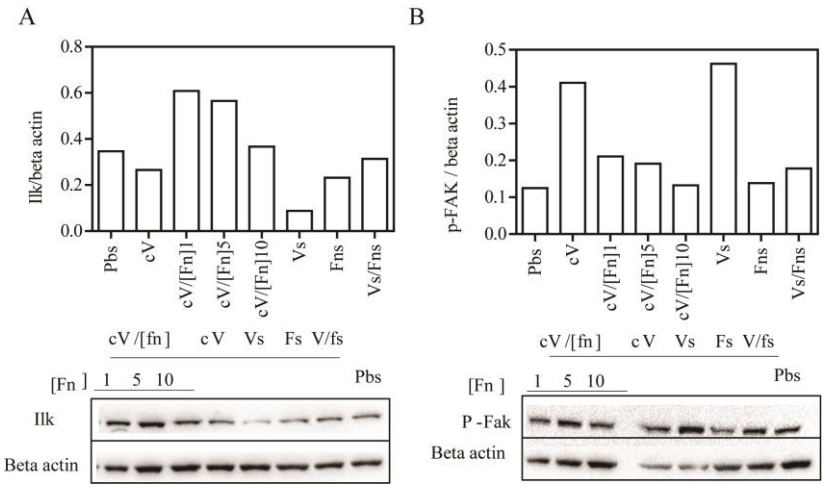


**Fig. 6.4 Western Blot data for phosphor focal adhesion kinase and integrin linked kinase.** (A) Western blot data and plot for integrin linked kinase for different conditions indicate the activity of Fn fragments after clustering with VEGF on the heparin. There is no significantly difference between different conditions. (B) Western blots data for phosphorylation of focal adhesion kinase for different conditions. All the data is normalized to Beta actin.

### 6.3.5 VEGF presentation inside fibrin hydrogels modulates HUVEC branching

To determine the effect of incorporating Fn to the VEGF presentation on the tip cell phenotype switch and branching morphology, a sprouting bead assay was used in which cytodex beads were coated with endothelial cells and placed in a fibrin hydrogel scaffold, while fibroblast cells were seeded on top[27, 164]. During the fibrin gel formation, 200 ng/ml of bound VEGF in VEGF/Fn were encapsulated within the hydrogel and compared to a control where 5ng/ml of soluble VEGF was added to the media. HUVEC-derived tubes from the cytodex beads were then quantified for branching points, sprouts, thickness, and total vessel network length. There is no significant differences between conditions.

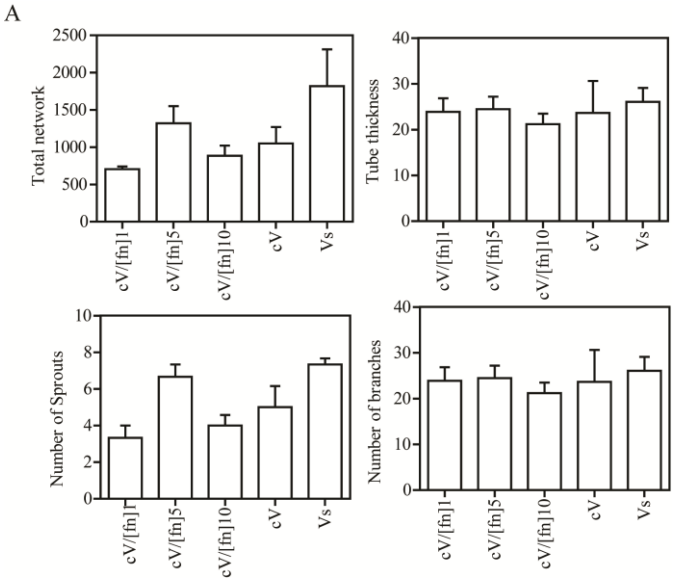


**Fig. 6.5.Tube formation assay with different VEGF clusters**. Different conditions are introduced to a fibrin gel and analyzed the data for different branching formation. (A) there is no significant differences between different conditions. This could be explained

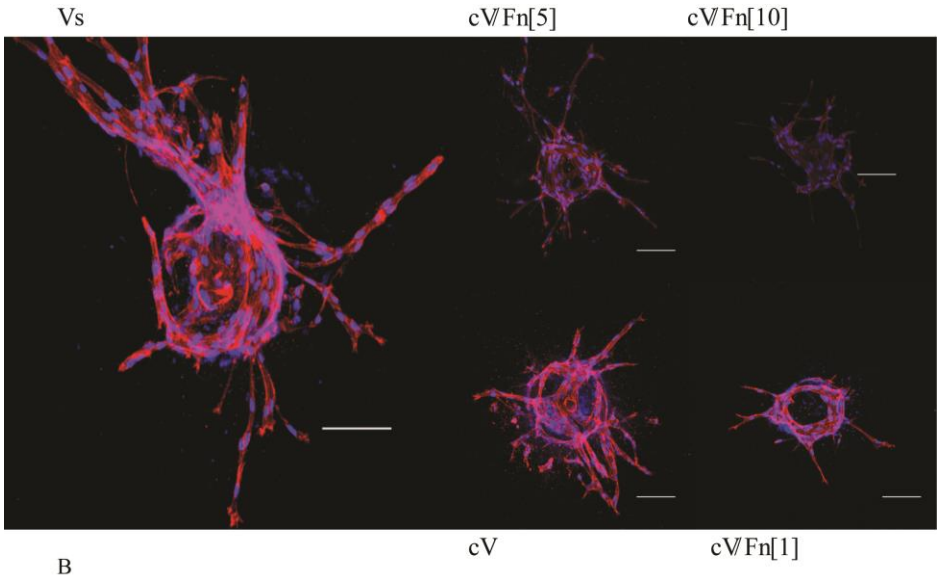


by the presence of Fn in the fibrinogen gel that inhibits the effect clustered Fn/VEGF on vascular branching. (B) Fluorescent staining images of different sprouting conditions from the cytodex beads. Endothelial cells were stained with actin (conjugated with Phalloidin) and DAPI.

Results showed that no significant differences between groups in term of branching points as well as total network length. To explain the absence of effect on vessel branching, we hypothesize that Fn from the biomaterial itself could inhibit the effect of bound Fn. To further investigate the accuracy of the hypothesis, we suggest to repeat the experiment using a Fibrinogen biomaterial depleted in Fn. This study is actually in progress.

**6.4 Discussion**

Interactions between cells and extracellular matrix (ECM) are very important in blood vessel development. The earliest ECM protein expressed in the embryo during vasculogenesis is fibronectin (FN)[178, 179]. Integrins which are the main receptors for Fn ligand have shown to play critical role in the initiation and the development of a functional vasculature when they are co-clustered with growth factor receptors. Gene deletion studies have confirmed the role of Fn and its integrin receptors, $\alpha_5\beta_1$, in angiogenesis and vasculogenesis in developing embryo[180, 181]. The integrin $\alpha_5\beta_1$ is an important Fn-specific integrin that can be found in different adhesion structures. To remain functional, $\alpha_5\beta_1$ requires the presence of an integrin-biding sequence (RGD) located in

the 10th domain of type III Fn (FN III10) repeat unit, but also requires to be in vicinity of the "synergy sequence" (PHSRN) in the 9th type III repeat (FN III9). However, for the functionality of $\alpha_v\beta_3$, PHSRN is not required[182]. Interestingly, type III repeats are stabilized only by hydrogen bonding and van der Waals forces[183,117]. Recent studies aiming at unfolding the FNIII9-10, have achieved the stabilization of the intermediate structural state before completely unfolding the 10th type III repeat[184]. In this intermediate state, the distance between the PHSRN-to RGD doesn't allow to synergistically bond the same receptor. This results in a preferential binding to $\alpha_v\beta_3$ receptors rather than $\alpha_5\beta_1$[185]. The conformational stability of FN III9 will affect the regulation of $\alpha_5\beta_1$ and one way to stabilize the FN III9 domain attributed to a single human to mouse ($Leu^{1408}$ to Pro) mutation is to enhance both conformational stability of FN III9–10 and affinity for $\alpha_5\beta_1$.[186, 187]Because $\alpha_5\beta_1$ binding requires this critical and sensitive domain conformation, we used this specific conformation with Fn fragments provided by the Prof. Barker laboratory. They structurally stabilized FN III9*-10 ($Leu^{1408}$ to Pro) or FNV1 that will preferentially binds $\alpha_5\beta_1$. We used this fragments throughout the last chapter of this thesis to test the synergy effect of integrins with VEGF receptors by displaying the Fn fragments and VEGF in a clustered conformation.

In order to cluster VEGF/Fn fragments, we first synthesized heparin nanoparticles and then introduced another functional group, the k-peptide, to facilitate the binding of Fn to heparin. From the results obtained in the previous chapter, we chose to further continue working with the high VEGF clusters. In order to bind VEGF and Fn to heparin, VEGF and Fn were incubated with heparin nanoparticles. In addition, different concentrations of Fn were used. The clusters were characterized using the ELISA and Dot blot method. In all the conditions, soluble VEGF was used as a control. To determine if the process of immobilization affects VEGF activity, HUVECs proliferation and VEGFR-2 phosphorylation induced by VEGF modified nanoparticles or soluble VEGF were compared. The proliferation rate was increased at lower concentration of VEGF for all

the conditions, indicating that the VEGF remains active throughout the process of particle modification.

A number of mechanisms have been suggested for integrin/growth factor synergism, many emphasizing pathways for intracellular signaling crosstalk. Signaling from $\alpha_5\beta_1$ ligation (and syndecan engagement) can support or reinforce the downstream signaling from VEGFR-2 to Erk ½ [177]. Here, at the molecular level, VEGFR-2 phosphorylation level of Y1175 for a different concentration of Fn clustering VEGF was enhanced over the time point of 5 min compared to just high VEGF cluster. It has also been observed that there is an optimum concentration for Fn fragment to be involve in the effect of crosstalk receptors. Phosphorylation at Y1175 results in the activation of the ERK ½ pathway and cellular proliferation. The same trend was observed for the activation of ERK ½ pathways. These results may reflect the isolated contribution of the co-stimulatory signaling pathways that are known to exist between $\alpha_5\beta_1$ and VEGFR-2 downstream to Erk. However, the current data suggest that these cooperative pathways are capable of a much more robust response when their receptors are occupied by a specialized VEGF/Fn complex. This can be investigated at different time points.

In addition, Integrin complexes have been studied to recruit a number of proteins, including growth factor receptors, and stimulate tyrosine phosphorylation of FAK[176]. Thus, we looked at the activation of Integrin linked kinase and also the phosphorylation of focal adhesion kinase to investigate the effect of Fn fragment. Our data show that the activity of the Integrin linked kinase remain stable and didn't show any significant difference with the control conditions, the high VEGF cluster and soluble VEGF, showing that the attachment of Fn fragment to heparin nanoparticle didn't affect the activity of those fragments. For the phosphorylation level of focal adhesion kinase, the background for the negative control was too high to conclude on the results of the other groups.

At the cellular level, VEGF/Fn clusters were incorporated inside fibrin hydrogels, which contained HUVECs bound to cytodex beads. Fibroblast cells were plated on top of the fibrin gel to further mimic a physiologic environment. The observations from the tube formation assay suggests more branching points as well as more sprouts for the medium concentration of Fn fragment bound to the high clusters of VEGF. Although there were no significantly differences, the results show tendencies between conditions. One of possible explanation is that the fibronectin contained in fibrinogen jeopardized the effects of the bound Fn fragments, thus covering any effect when associated with bound VEGF on heparin nanoparticles. For future directions, we suggeste the use of fibrinogen-depleted fibronectin as a biomaterial.

**6.5 Conclusion**

This study investigates the effect of the degree of $\alpha_5\beta_1$ engagement in the context of angiogenesis in engineered matrices. For this purpose, we developed a 3D system that allows the incorporation of VEGF as well as Fn fragments that preferentially bind to $\alpha_5\beta_1$, to investigate the synergy effect of integrins and growth factor receptors at the surface of ECs. Heparin nanoparticles were engineered and both VEGF and Fn were bound covalently to heparin backbone. The particles were characterized for the amount of bound VEGF and bound Fn fragments, as well as the activity of the growth factor after attachment. The results obtained in this last chapter did not show any effect of the double loaded VEGF/Fn fragments on vessel branching or cell proliferation, but this might be explained by the utilization of a non-appropriate biomaterial that contains a significant amount of fibronectin that might interfere with the results.

# Chapter 7

# *Conclusion*

## 7.1 Introduction

The research described in this thesis aimed at developing a system to study the mechanism of VEGF presentation and the synergy effect of the integrin with growth factor receptor on the vascular formation. Also, developing hydrogels for gene transfer to stem cells was studied in the earlier chapter. The following sections re-visit the proposed specific aims and hypotheses, followed by the major conclusions and possible future experimental directions.

## 7.2 Specific aim 1

This aim used the encapsulated non-viral DNA nanoparticle strategy to design scaffolds to enhance gene transfer to mouse mesenchymal stem cells by utilizing cell-matrix interactions.

*Hypothesis (Chapter 4)*: Design of hydrogel scaffolds is crucial in effective delivery of DNA to stem cells. Parameters such as higher N/P ratios, softer hydrogels and higher RGD concentration concentration will lead to higher gene transfer.

Hyaluronic acid hydrogels were used to encapsulate DNA/PEI polyplexes and transfect encapsulated stem cell as varying different parameters of the scaffolds. Previously, it has been shown that Cell-matrix interactions have effect on stem cell fate such as differentiation and gene transfer in 2D dimensional system. Here, we are interested to investigate the effect of cell-matrix interactions on gene transfer on 3D hydrogel systems. We investigated the effect of gel stiffness, RGD concentration and N/P ratio on the effective gene transfer from the HA hydrogel scaffolds. HA-RGD was crosslinked with a MMP labile peptide using Michael type addition to form hydrogels that were degradable through a combination of hyaluronidases and MMPs. In addition, DNA/PEI polyplexes and mouse mesenchymal stem cells were encapsulated during gelation. We have found that both matrix stiffness and RGD presentation significantly influenced transgene expression with an intermediate stiffness and RGD clustering resulting in maximal transgene expression. Moreover, the polyplex physical properties affected the rate of non-viral gene transfer for cells seeded inside hydrogel scaffolds with increasing N/P ratio resulting in higher transgene expression, but also higher toxicity. We observed two fold higher transgene expressions for N/P of 9 and 12, minimal toxicity was observed for N/P 7.

### 7.3 Specific aim 2

The goal of specific aim 2 was to study the effect of different presentation of VEGF on tube formation and downstream signaling as well as tip cell phenotype. Also, we investigate the effect of VEGF presentation to promote angiogenesis *in vivo* on an ischemia stroke model.

> *Hypothesis (chapter 5):* VEGF clusters result in enhanced level of phosphorylated VEGF receptor-2 and tip cell phenotypes compared to soluble VEGF and the transplantation of fibrin based hydrogel containing VEGF clusters in cerebral ischemia will enhance vessel formation and maturation.

To probe the validity of this aim, we first designed different presentation of VEGF, by introducing the same amount of VEGF to different concentration of heparin nanoparticles. The high VEGF density resulted in high VEGF clusters showing a more extensive vessel network *in vitro* and *in vivo*. This condition also showed a sustained activation of Y1175 and Y1214 on VEGFR-2 at 15 min. HUVECs express different ligand and receptors to specify the tip cell/stalk cell phenotype. Dll4/Notch signaling is known to initiate and modulate vessel branching through the control of this ECs phenotype switch. The levels of gene expressed in tip cells were quantified. Among all, Dll4 showed an enhanced mRNA level of DII4 expressed. The use of a lower concentration of VEGF (20ng/ml), shoed no significant changes Dll4 and VR-3 gene expression levels for medium cluster compared to the other conditions.

### 7.4 Specific aim 3

We hypothesized that Fn might be a unique biological partner with VEGF: when Fn complexes with VEGF, their coordinated binding to their cognate receptors enhances the specific cellular responses to VEGF. These extracellular events might be an important step in modulating the complex signaling pathways that lead from receptor ligation to cellular response. So, we made our third hypothesis.

> *Hypothesis (Chapter 6): T*he introduction of Fn fragments into heparin nanoparticles will enhance the effect of VEGF cluster on the VEGFR-2 phosphorylation through synergistic signaling between growth factor (GF) receptors and integrins.

Here, we use the system developed in aim 2, and modified it by introducing an additional element to heparin nanoparticles, Fn fragments. We aimed at studying the synergy effect of VEGFR-2 and the integrin $\alpha_5\beta_1$. The amount of each protein loaded to heparin nanoparticle is controlled and confirmed using two methods; ELISA and Dot Blot. The phosphorylation level of Y1175 as well as activation of Erk ½ was both enhanced with the incorporation of Fn fragment to the VEGF clusters at 5 min. Also, the activation of Integrin linked kinase for VEGF/Fn confirmed the activity of the Fn fragment post binding. From the tube formation assay, the results suggested an increased in the number of vascular network for the cluster conditions that include the Fn fragments compared to just VEGF clusters. However, because of the presence of fibronectin in the fibrin gel, there was no significantly a difference between conditions.

### 7.5 Future direction

The ultimate goal of this project was to translate the developed system for presentation of VEGF to clinical application and use this system for further binding dual growth factors or growth

factor/Fn as we have started in previous chapter. Progress has been made but more work needs to be done before the full therapeutic potential of this approach can be achieved. The main advantage of this system is the presence of heparin as a backbone of the system. Heparin is a proteoglycans that present in the mammalian tissues. They have a crucial role in maintaining homeostasis and pathological processes. From our *in vitro* and *in vivo* study in chapter 6, we have proved that clustering VEGF will promote angiogenesis compared to soluble VEGF. In order to translate this system to a clinical trial and important behavioral studies should be performed. The ultimate goal is to be able to regenerate the most part of the damaged tissue and recovery, for that reason, behavioral studies are extremely important. These studies were performed in Dr Carmichael's laboratory under the supervision of Dr Lina Nih and the results are highly anticipated. Indeed, the *in vitro* study was then translated to a mouse model of cerebral ischemia where the engineered particles were transplanted within a hydrogel, directly into the stroke cavity to promote post-stroke tissue regeneration through the development of a functional and organized vascular network in the stroke. The results show that the high cluster of VEGF nanoparticles significantly enhanced the infiltration of ECs, but also enhanced the number of proliferative ECs and the pericyte coverage of the newly formed vessels in the stroke area, compared to all the other conditions used: no gel transplanted, the transplantation of an empty gel, the gel loaded with soluble VEGF, gel loaded with naked heparin nanoparticles, but also a low cluster of VEGF.

Alternatively, there are observations suggest the critical role for FN and its integrin receptor, $\alpha_5\beta_1$in angiogenesis. What we have shown in this thesis is that we can apply this system to bind Fn fragment and VEGF co-cluster to see the synergy effect of the integrin receptor and the VEGFR-2 together in vessel formation. The engineering part of the system can be more developed. We have confirmed the binding and activity of both the VEGF and Fn fragment after clustering to the heparin. But experiments can be done to the optimum ratio of the VEGF/Fn to get the

maximum result in enhancement of the phosphorylation of the VEGFR-2 as well as controlling the vessel formation. Also, the *in vivo* studies should be done to confirm the results achieved *in vitro*. A wound healing db/db mice has already been conducted and it's in the process of analyzing data which seems to be promising.

# Chapter 8

## *References*


1. Novosel, E.C., Kleinhans, C. & Kluger, P.J. Vascularization is the key challenge in tissue engineering. *Adv Drug Deliver Rev* **63**, 300-311 (2011).

2. Novosel, E.C., Kleinhans, C. & Kluger, P.J. Vascularization is the key challenge in tissue engineering. *Adv Drug Deliv Rev* **63**, 300-311 (2011).

3. Hermann, D.M. & Zechariah, A. Implications of vascular endothelial growth factor for postischemic neurovascular remodeling. *J Cereb Blood Flow Metab* **29**, 1620-1643 (2009).

4. Greenberg, D.A. Angiogenesis and stroke. *Drug News Perspect* **11**, 265-270 (1998).

5. Hermann, D.M. & Zechariah, A. Implications of vascular endothelial growth factor for postischemic neurovascular remodeling. *J Cerebr Blood F Met* **29**, 1620-1643 (2009).

6. Eming, S.A. & Hubbell, J.A. Extracellular matrix in angiogenesis: dynamic structures with translational potential. *Exp Dermatol* **20**, 605-613 (2011).

7. Chen, T.T. et al. Anchorage of VEGF to the extracellular matrix conveys differential signaling responses to endothelial cells. *J Cell Biol* **188**, 595-609 (2010).

8. De Smet, F., Segura, I., De Bock, K., Hohensinner, P.J. & Carmeliet, P. Mechanisms of vessel branching: filopodia on endothelial tip cells lead the way. *Arterioscler Thromb Vasc Biol* **29**, 639-649 (2009).

9. Horowitz, A. & Simons, M. Branching morphogenesis. *Circ Res* **103**, 784-795 (2008).

10. Gerhardt, H. et al. VEGF guides angiogenic sprouting utilizing endothelial tip cell filopodia. *J Cell Biol* **161**, 1163-1177 (2003).

11. Estrach, S. et al. Laminin-binding integrins induce Dll4 expression and Notch signaling in

endothelial cells. *Circ Res* **109**, 172-182 (2011).

12. Martino, M.M. et al. Engineering the growth factor microenvironment with fibronectin domains to promote wound and bone tissue healing. *Sci Transl Med* **3**, 100ra189 (2011).

13. Auger, F.A., Gibot, L. & Lacroix, D. The Pivotal Role of Vascularization in Tissue Engineering. *Annu Rev Biomed Eng* **15**, 177-200 (2013).

14. Carmeliet, P. & Jain, R.K. Molecular mechanisms and clinical applications of angiogenesis. *Nature* **473**, 298-307 (2011).

15. Laschke, M.W. & Menger, M.D. Vascularization in Tissue Engineering: Angiogenesis versus Inosculation. *Eur Surg Res* **48**, 85-92 (2012).

16. Laschke, M.W. et al. Angiogenesis in tissue engineering: Breathing life into constructed tissue substitutes. *Tissue Eng* **12**, 2093-2104 (2006).

17. Lee, K., Silva, E.A. & Mooney, D.J. Growth factor delivery-based tissue engineering: general approaches and a review of recent developments. *J R Soc Interface* **8**, 153-170 (2011).

18. Fischbach, C. & Mooney, D.J. Polymers for pro- and anti-angiogenic therapy. *Biomaterials* **28**, 2069-2076 (2007).

19. Adeloew, C., Segura, T., Hubbell, J.A. & Frey, P. The effect of enzymatically degradable poly(ethylene glycol) hydrogels on smooth muscle cell phenotype. *Biomaterials* **29**, 314-326 (2008).

20. Reed, D.M. et al. Endothelin-1 Release from Human Embryonic Stem Cell Derived-Endothelial Cells (Hesc-Ec): Comparisons with Human Endothelial Cells. *Inflamm Res* **60**, 224-224 (2011).

21. Iyer, P., Walker, K.J. & Madihally, S.V. Increased matrix synthesis by fibroblasts with decreased proliferation on synthetic chitosan-gelatin porous structures. *Biotechnol Bioeng* **109**, 1314-1325 (2012).

22. Liu, Y. et al. In Vitro Construction of Scaffold-Free Bilayered Tissue-Engineered Skin Containing Capillary Networks. *Biomed Res Int* (2013).

23. Park, S.H., Choi, B.H., Park, S.R. & Min, B.H. Chondrogenesis of Rabbit Mesenchymal Stem Cells in Fibrin/Hyaluronan Composite Scaffold In Vitro. *Tissue Eng Pt A* **17**, 1277-1286 (2011).

24. Park, J.S., Yang, H.N., Woo, D.G., Jeon, S.Y. & Park, K.H. Chondrogenesis of human mesenchymal stem cells in fibrin constructs evaluated in vitro and in nude mouse and rabbit defects models. *Biomaterials* **32**, 1495-1507 (2011).

25. Seliktar, D. Designing Cell-Compatible Hydrogels for Biomedical Applications. *Science* **336**, 1124-1128 (2012).

26. Kong, S.W. et al. Surface modification with fibrin/hyaluronic acid hydrogel on solid-free form-based scaffolds followed by BMP-2 loading to enhance bone regeneration. *Bone* **48**, 298-306 (2011).

27. Nakatsu, M.N., Davis, J. & Hughes, C.C. Optimized fibrin gel bead assay for the study of angiogenesis. *J Vis Exp*, 186 (2007).

28. Fraser, J.R., Laurent, T.C. & Laurent, U.B. Hyaluronan: its nature, distribution, functions and turnover. *J Intern Med* **242**, 27-33 (1997).

29. Leach, J.B., Bivens, K.A., Patrick, C.W. & Schmidt, C.E. Photocrosslinked hyaluronic acid hydrogels: Natural, biodegradable tissue engineering scaffolds. *Biotechnology and Bioengineering* **82**, 578-589 (2003).

30. Park, Y.D., Tirelli, N. & Hubbell, J.A. Photopolymerized hyaluronic acid-based hydrogels and interpenetrating networks. *Biomaterials* **24**, 893-900 (2003).

31. Shu, X.Z., Liu, Y.C., Palumbo, F.S., Lu, Y. & Prestwich, G.D. In situ crosslinkable hyaluronan hydrogels for tissue engineering. *Biomaterials* **25**, 1339-1348 (2004).

32. Yeo, Y. et al. In situ cross-linkable hyaluronic acid hydrogels prevent post-operative abdominal adhesions in a rabbit model. *Biomaterials* **27**, 4698-4705 (2006).

33. Chung, C. & Burdick, J.A. Influence of Three-Dimensional Hyaluronic Acid Microenvironments on Mesenchymal Stem Cell Chondrogenesis. *Tissue Engineering Part A* **15**, 243-254 (2009).

34. Gerecht, S. et al. Hyaluronic acid hydrogel for controlled self-renewal and differentiation of human embryonic stem cells. *Proc Natl Acad Sci U S A* **104**, 11298-11303 (2007).

35. Kim, J. et al. Characterization of low-molecular-weight hyaluronic acid-based hydrogel and differential stem cell responses in the hydrogel microenvironments. *Journal of Biomedical Materials Research Part A* **88A**, 967-975 (2009).

36. Kim, J. et al. Synthesis and characterization of matrix metalloprotease sensitive-low molecular weight hyaluronic acid based hydrogels. *Journal of Materials Science-Materials in Medicine* **19**, 3311-3318 (2008).

37. Pan, L.J., Ren, Y.J., Cui, F.Z. & Xu, Q.Y. Viability and Differentiation of Neural Precursors on Hyaluronic Acid Hydrogel Scaffold. *Journal of Neuroscience Research* **87**, 3207-3220 (2009).

38. Aruffo, A., Stamenkovic, I., Melnick, M., Underhill, C.B. & Seed, B. CD44 is the principal cell surface receptor for hyaluronate. *Cell* **61**, 1303-1313 (1990).

39. Sherman, L., Sleeman, J., Herrlich, P. & Ponta, H. Hyaluronate Receptors - Key Players in Growth, Differentiation, Migration and Tumor Progression. *Current Opinion in Cell Biology* **6**, 726-733 (1994).

40. Lei, Y., Gojgini, S., Lam, J. & Segura, T. The spreading, migration and proliferation of mouse mesenchymal stem cells cultured inside hyaluronic acid hydrogels. *Biomaterials* (2011).

41. Peyton, S.R. & Putnam, A.J. Extracellular matrix rigidity governs smooth muscle cell motility in a biphasic fashion. *J Cell Physiol* **204**, 198-209 (2005).

42. Jha, A.K., Xu, X.A., Duncan, R.L. & Jia, X.Q. Controlling the adhesion and differentiation of mesenchymal stem cells using hyaluronic acid-based, doubly crosslinked networks. *Biomaterials* **32**, 2466-2478 (2011).

43. Hadjipanayi, E., Mudera, V. & Brown, R.A. Interface integration of rapidly engineered multilayer collagen scaffolds. *Tissue Eng Pt A* **14**, 748-749 (2008).

44. Kong, H.J. et al. Non-viral gene delivery regulated by stiffness of cell adhesion substrates. *Nat Mater* **4**, 460-464 (2005).

45. Lei, Y.G., Gojgini, S., Lam, J. & Segura, T. The spreading, migration and proliferation of mouse mesenchymal stem cells cultured inside hyaluronic acid hydrogels. *Biomaterials* **32**, 39-47 (2011).

46. Ghajar, C.M., Blevins, K.S., Hughes, C.C.W., George, S.C. & Putnam, A.J. Mesenchymal stem cells enhance angiogenesis in mechanically viable prevascularized tissues via early matrix metalloproteinase upregulation. *Tissue Eng* **12**, 2875-2888 (2006).

47. Kniazeva, E., Kachgal, S. & Putnam, A.J. Effects of Extracellular Matrix Density and Mesenchymal Stem Cells on Neovascularization In Vivo. *Tissue Eng Pt A* **17**, 905-914 (2011).

48. Kong, H.J., Kim, E.S., Huang, Y.C. & Mooney, D.J. Design of biodegradable hydrogel for the local and sustained delivery of angiogenic plasmid DNA. *Pharm Res* **25**, 1230-1238 (2008).

49. Kleinman, H.K., Philp, D. & Hoffman, M.P. Role of the extracellular matrix in morphogenesis. *Curr Opin Biotechnol* **14**, 526-532 (2003).

50. Bottaro, D.P., Liebmann-Vinson, A. & Heidaran, M.A. Molecular signaling in bioengineered tissue microenvironments. *Ann N Y Acad Sci* **961**, 143-153 (2002).

51. Dhaliwal, A., Lam, J., Maldonado, M., Lin, C. & Segura, T. Extracellular matrix modulates non-viral gene transfer to mouse mesenchymal stem cells. *Soft Matter* **8**, 1451-1459 (2012).

52. Tokatlian, T., Cam, C., Siegman, S.N., Lei, Y.G. & Segura, T. Design and characterization of microporous hyaluronic acid hydrogels for in vitro gene transfer to mMSCs. *Acta Biomater* **8**, 3921-3931 (2012).

53. Prowse, A.B.J., Chong, F., Gray, P.P. & Munro, T.P. Stem cell integrins: Implications for ex-vivo culture and cellular therapies. *Stem Cell Res* **6**, 1-12 (2011).

54. Lam, J. & Segura, T. The modulation of MSC integrin expression by RGD presentation. *Biomaterials* **34**, 3938-3947 (2013).

55. Wang, X. et al. Effect of RGD nanospacing on differentiation of stem cells. *Biomaterials* **34**, 2865-2874 (2013).

56. Kong, H.J., Hsiong, S. & Mooney, D.J. Nanoscale cell adhesion ligand presentation regulates nonviral gene delivery and expression. *Nano Lett* **7**, 161-166 (2007).

57. Shepard, J.A., Huang, A., Shikanov, A. & Shea, L.D. Balancing cell migration with matrix degradation enhances gene delivery to cells cultured three-dimensionally within hydrogels. *J Control Release* **146**, 128-135 (2010).

58. Lei, Y.G. & Segura, T. DNA delivery from matrix metal lop roteinase degradable poly(ethylene glycol) hydrogels to mouse cloned mesenchymal stem cells. *Biomaterials* **30**, 254-265 (2009).

59. Baldwin, S.P. & Saltzman, W.M. Materials for protein delivery in tissue engineering. *Adv Drug Deliver Rev* **33**, 71-86 (1998).

60. Jay, S.M. & Saltzman, W.M. Controlled delivery of VEGF via modulation of alginate microparticle ionic crosslinking. *J Control Release* **134**, 26-34 (2009).

61. Golub, J.S. et al. Sustained VEGF delivery via PLGA nanoparticles promotes vascular growth. *Am J Physiol-Heart C* **298**, H1959-H1965 (2010).

62. Bible, E. et al. Neo-vascularization of the stroke cavity by implantation of human neural stem cells on VEGF-releasing PLGA microparticles. *Biomaterials* **33**, 7435-+ (2012).

63. Peng, Q. et al. Injectable and biodegradable thermosensitive hydrogels loaded with PHBHHx nanoparticles for the sustained and controlled release of insulin. *Acta Biomater* **9**, 5063-5069 (2013).

64. Willems, W.F., Larsen, M., Friedrich, P.F., Shogren, K.L. & Bishop, A.T. Induction of angiogenesis and osteogenesis in surgically revascularized frozen bone allografts by sustained delivery of FGF-2 and VEGF. *J Orthop Res* **30**, 1556-1562 (2012).

65. Richardson, T.P., Peters, M.C., Ennett, A.B. & Mooney, D.J. Polymeric system for dual growth factor delivery. *Nat Biotechnol* **19**, 1029-1034 (2001).

66. Shah, N.J. et al. Tunable dual growth factor delivery from polyelectrolyte multilayer films. *Biomaterials* **32**, 6183-6193 (2011).

67. Silva, A.K.A., Richard, C., Bessodes, M., Scherman, D. & Merten, O.W. Growth Factor Delivery Approaches in Hydrogels. *Biomacromolecules* **10**, 9-18 (2009).

68. Cai, S.S., Liu, Y.C., Shu, X.Z. & Prestwich, G.D. Injectable glycosaminoglycan hydrogels for controlled release of human basic fibroblast growth factor. *Biomaterials* **26**, 6054-6067 (2005).

69. Bishop, J.R., Schuksz, M. & Esko, J.D. Heparan sulphate proteoglycans fine-tune mammalian physiology. *Nature* **446**, 1030-1037 (2007).

70. Gallagher, J.T. Heparan sulfate: growth control with a restricted sequence menu. *J Clin Invest* **108**, 357-361 (2001).

71. Thomas, A.M., Gomez, A.J., Palma, J.L., Yap, W.T. & Shea, L.D. Heparin-chitosan nanoparticle functionalization of porous poly(ethylene glycol) hydrogels for localized lentivirus delivery of angiogenic factors. *Biomaterials* **35**, 8687-8693 (2014).

72. Singh, S., Wu, B.M. & Dunn, J.C.Y. The enhancement of VEGF-mediated angiogenesis by polycaprolactone scaffolds with surface cross-linked heparin. *Biomaterials* **32**, 2059-2069 (2011).

73. Mizuguchi, H. Recent advance of development of viral and non-viral vectors for gene therapy. *Yakugaku Zasshi* **126**, 1011-1011 (2006).

74. Bonadio, J., Smiley, E., Patil, P. & Goldstein, S. Localized, direct plasmid gene delivery in vivo: prolonged therapy results in reproducible tissue regeneration. *Nat Med* **5**, 753-759 (1999).

75. Chun, K.W., Lee, J.B., Kim, S.H. & Park, T.G. Controlled release of plasmid DNA from photo-cross-linked pluronic hydrogels. *Biomaterials* **26**, 3319-3326 (2005).

76. Quick, D.J. & Anseth, K.S. DNA delivery from photocrosslinked PEG hydrogels: encapsulation efficiency, release profiles, and DNA quality. *Journal of Controlled Release* **96**, 341-351 (2004).

77. Kasper, F.K. et al. Characterization of DNA release from composites of oligo(poly(ethylene glycol) fumarate) and cationized gelatin microspheres in vitro. *Journal of Biomedical Materials Research Part A* **78A**, 823-835 (2006).

78. Megeed, Z. et al. In vitro and in vivo evaluation of recombinant silk-elastinlike hydrogels for cancer gene therapy. *J Control Release* **94**, 433-445 (2004).

79. Jang, J.H., Rives, C.B. & Shea, L.D. Plasmid delivery in vivo from porous tissue-engineering scaffolds: transgene expression and cellular transfection. *Mol Ther* **12**, 475-483

(2005).

80. Lei, P., Padmashali, R.M. & Andreadis, S.T. Cell-controlled and spatially arrayed gene delivery from fibrin hydrogels. *Biomaterials* **30**, 3790-3799 (2009).

81. Wieland, J.A., Houchin-Ray, T.L. & Shea, L.D. Non-viral vector delivery from PEG-hyaluronic acid hydrogels. *Journal of Controlled Release* **120**, 233-241 (2007).

82. Saul, J.M., Linnes, M.P., Ratner, B.D., Giachelli, C.M. & Pun, S.H. Delivery of non-viral gene carriers from sphere-templated fibrin scaffolds for sustained transgene expression. *Biomaterials* **28**, 4705-4716 (2007).

83. Trentin, D., Hall, H., Wechsler, S. & Hubbell, J.A. Peptide-matrix-mediated gene transfer of an oxygen-insensitive hypoxia-inducible factor-1 alpha variant for local induction of angiogenesis. *Proceedings of the National Academy of Sciences of the United States of America* **103**, 2506-2511 (2006).

84. Trentin, D., Hubbell, J. & Hall, H. Non-viral gene delivery for local and controlled DNA release. *Journal of Controlled Release* **102**, 263-275 (2005).

85. Lungwitz, U., Breunig, M., Blunk, T. & Gopferich, A. Polyethylenimine-based non-viral gene delivery systems. *European Journal of Pharmaceutics and Biopharmaceutics* **60**, 247-266 (2005).

86. Abdallah, B. et al. A powerful nonviral vector for in vivo gene transfer into the adult mammalian brain: Polyethylenimine. *Human Gene Therapy* **7**, 1947-1954 (1996).

87. Wang, S., Ma, N., Gao, S.J., Yu, H. & Leong, K.W. Transgene expression in the brain stem effected by intramuscular injection of polyethylenimine/DNA complexes. *Molecular Therapy* **3**, 658-664 (2001).

88. Wiseman, J.W., Goddard, C.A., McLelland, D. & Colledge, W.H. A comparison of linear and branched polyethylenimine (PEI) with DCChol/DOPE liposomes for gene delivery to epithelial cells in vitro and in vivo. *Gene Therapy* **10**, 1654-1662 (2003).

89. Kichler, A., Chillon, M., Leborgne, C., Danos, O. & Frisch, B. Intranasal gene delivery with a polyethylenimine-PEG conjugate. *Journal of Controlled Release* **81**, 379-388 (2002).

90. Rudolph, C. et al. Nonviral gene delivery to the lung with copolymer-protected and transferrin-modified polyethylenimine. *Biochimica Et Biophysica Acta-General Subjects* **1573**, 75-83 (2002).

91. Gautam, A., Densmore, C.L., Golunski, E., Xu, B. & Waldrep, J.C. Transgene expression in mouse airway epithelium by aerosol gene therapy with PEI-DNA complexes. *Molecular Therapy* **3**, 551-556 (2001).

92. Segura, T., Schmokel, H. & Hubbell, J.A. RNA interference targeting hypoxia inducible

factor 1alpha reduces post-operative adhesions in rats. *J Surg Res* **141**, 162-170 (2007).

93. Iwai, M. et al. Polyethylenimine-mediated suicide gene transfer induces a therapeutic effect for hepatocellular carcinoma in vivo by using an Epstein-Barr virus-based plasmid vector. *Biochemical and Biophysical Research Communications* **291**, 48-54 (2002).

94. Aoki, K. et al. Polyethylenimine-mediated gene transfer into pancreatic tumor dissemination in the murine peritoneal cavity. *Gene Therapy* **8**, 508-514 (2001).

95. Coll, J.L. et al. In vivo delivery to tumors of DNA complexed with linear polyethylenimine. *Human Gene Therapy* **10**, 1659-1666 (1999).

96. Fukunaka, Y., Iwanaga, K., Morimoto, K., Kakemi, M. & Tabata, Y. Controlled release of plasmid DNA from cationized gelatin hydrogels based on hydrogel degradation. *J Control Release* **80**, 333-343 (2002).

97. Lei, Y.G., Ng, Q.K.T. & Segura, T. Two and Three-Dimensional Gene Transfer from Enzymatically Degradable Hydrogel Scaffolds. *Microsc Res Techniq* **73**, 910-917 (2010).

98. Phelps, E.A. & Garcia, A.J. Engineering more than a cell: vascularization strategies in tissue engineering. *Curr Opin Biotechnol*.

99. Liu, L.Y., Ratner, B.D., Sage, E.H. & Jiang, S.Y. Endothelial cell migration on surface-density gradients of fibronectin, VEGF, or both proteins. *Langmuir* **23**, 11168-11173 (2007).

100. Lee, S., Jilani, S.M., Nikolova, G.V., Carpizo, D. & Iruela-Arispe, M.L. Processing of VEGF-A by matrix metalloproteinases regulates bioavailability and vascular patterning in tumors. *J. Cell Biol.* **169**, 681-691 (2005).

101. Chen, T.T. et al. Anchorage of VEGF to the extracellular matrix conveys differential signaling responses to endothelial cells. *J Cell Biol* **188**, 595-609.

102. Fairbrother, W.J., Champe, M.A., Christinger, H.W., Keyt, B.A. & Starovasnik, M.A. Solution structure of the heparin-binding domain of vascular endothelial growth factor. *Structure* **6**, 637-648 (1998).

103. Ruhrberg, C. et al. Spatially restricted patterning cues provided by heparin-binding VEGF-A control blood vessel branching morphogenesis. *Gene Dev* **16**, 2684-2698 (2002).

104. Lee, S., Jilani, S.M., Nikolova, G.V., Carpizo, D. & Iruela-Arispe, M.L. Processing of VEGF-A by matrix metalloproteinases regulates bioavailability and vascular patterning in tumors. *J Cell Biol* **169**, 681-691 (2005).

105. Holmes, K., Roberts, O.L., Thomas, A.M. & Cross, M.J. Vascular endothelial growth factor receptor-2: Structure, function, intracellular signalling and therapeutic inhibition. *Cell Signal* **19**, 2003-2012 (2007).

106. Roskoski, R. Vascular endothelial growth factor (VEGF) signaling in tumor progression. *Crit Rev Oncol Hemat* **62**, 179-213 (2007).

107. Olsson, A.K., Dimberg, A., Kreuger, J. & Claesson-Welsh, L. VEGF receptor signalling - in control of vascular function. *Nat Rev Mol Cell Bio* **7**, 359-371 (2006).

108. Ferrara, N., Gerber, H.P. & LeCouter, J. The biology of VEGF and its receptors. *Nat Med* **9**, 669-676 (2003).

109. Giacca, M. & Zacchigna, S. VEGF gene therapy: therapeutic angiogenesis in the clinic and beyond. *Gene Ther* **19**, 622-629 (2012).

110. Rini, B.I. & Small, E.J. Biology and clinical development of vascular endothelial growth factor-targeted therapy in renal cell carcinoma. *J Clin Oncol* **23**, 1028-1043 (2005).

111. De Smet, F., Segura, I., De Bock, K., Hohensinner, P.J. & Carmeliet, P. Mechanisms of Vessel Branching Filopodia on Endothelial Tip Cells Lead the Way. *Arterioscl Throm Vas* **29**, 639-649 (2009).

112. Gerhardt, H. VEGF and endothelial guidance in angiogenic sprouting. *Organogenesis* **4**, 241-246 (2008).

113. Horowitz, A. & Simons, M. Branching morphogenesis. *Circ Res* **103**, 784-795 (2008).

114. Kume, T. Novel insights into the differential functions of Notch ligands in vascular formation. *J Angiogenes Res* **1**, 8 (2009).

115. Mahabeleshwar, G.H., Feng, W.Y., Phillips, D.R. & Byzova, T.V. Integrin signaling is critical for pathological angiogenesis. *J Exp Med* **203**, 2495-2507 (2006).

116. Kolodziej, C.M. et al. Combination of Integrin-Binding Peptide and Growth Factor Promotes Cell Adhesion on Electron-Beam-Fabricated Patterns. *J Am Chem Soc* **134**, 247-255 (2012).

117. Martino, M.M. et al. Controlling integrin specificity and stem cell differentiation in 2D and 3D environments through regulation of fibronectin domain stability. *Biomaterials* **30**, 1089-1097 (2009).

118. Carmeliet, P. Angiogenesis in health and disease. *Nat Med* **9**, 653-660 (2003).

119. Morgan, M.R., Byron, A., Humphries, M.J. & Bass, M.D. Giving off Mixed Signals-Distinct Functions of alpha(5)beta(1) and alpha(V)beta(3) Integrins in Regulating Cell Behaviour. *Iubmb Life* **61**, 731-738 (2009).

120. Ravelli, C., Mitola, S., Corsini, M. & Presta, M. Involvement of alpha(v)beta(3) integrin in gremlin-induced angiogenesis. *Angiogenesis* **16**, 235-243 (2013).

121. Yang, J.T., Rayburn, H. & Hynes, R.O. Embryonic mesodermal defects in alpha 5 integrin-deficient mice. *Development* **119**, 1093-1105 (1993).

122. Shalaby, F. et al. Failure of blood-island formation and vasculogenesis in Flk-1-deficient mice. *Nature* **376**, 62-66 (1995).

123. Traub, S. et al. The promotion of endothelial cell attachment and spreading using FNIII10 fused to VEGF-A(165). *Biomaterials* **34**, 5958-5968 (2013).

124. Martino, M.M. et al. Engineering the Growth Factor Microenvironment with Fibronectin Domains to Promote Wound and Bone Tissue Healing. *Sci Transl Med* **3** (2011).

125. Yu, M. et al. Preparation and characterization of a VEGF-Fc fusion protein matrix for enhancing HUVEC growth. *Biotechnol Lett* **34**, 1765-1771 (2012).

126. Wijelath, E.S. et al. Heparin-II domain of fibronectin is a vascular endothelial growth factor-binding domain - Enhancement of VEGF biological activity by a singular growth factor/matrix protein synergism. *Circ Res* **99**, 853-860 (2006).

127. Dvorak, H.F. Angiogenesis: update 2005. *J Thromb Haemost* **3**, 1835-1842 (2005).

128. Rupp, P.A. & Little, C.D. Integrins in vascular development. *Circ Res* **89**, 566-572 (2001).

129. Saha, K. et al. Substrate modulus directs neural stem cell behavior. *Biophys J* **95**, 4426-4438 (2008).

130. Engler, A.J., Sen, S., Sweeney, H.L. & Discher, D.E. Matrix elasticity directs stem cell lineage specification. *Cell* **126**, 677-689 (2006).

131. Huebsch, N. et al. Harnessing traction-mediated manipulation of the cell/matrix interface to control stem-cell fate. *Nat Mater* **9**, 518-526 (2010).

132. Zhang, J. et al. Protein-polymer nanoparticles for nonviral gene delivery. *Biomacromolecules* **12**, 1006-1014 (2011).

133. Godbey, W.T., Wu, K.K. & Mikos, A.G. Poly(ethylenimine) and its role in gene delivery. *Journal of Controlled Release* **60**, 149-160 (1999).

134. Dhaliwal, A., Maldonado, M., Han, Z. & Segura, T. Differential uptake of DNA-poly(ethylenimine) polyplexes in cells cultured on collagen and fibronectin surfaces. *Acta Biomater* **6**, 3436-3447 (2010).

135. Hsiong, S.X., Huebsch, N., Fischbach, C., Kong, H.J. & Mooney, D.J. Integrin-adhesion ligand bond formation of preosteoblasts and stem cells in three-dimensional RGD presenting matrices. *Biomacromolecules* **9**, 1843-1851 (2008).

136. Petrie, T.A. et al. Multivalent integrin-specific ligands enhance tissue healing and

biomaterial integration. *Sci Transl Med* **2**, 45ra60 (2010).

137. Ng, Q.K. et al. Clustered arg-gly-asp peptides enhances tumor targeting of nonviral vectors. *ChemMedChem* **6**, 623-627 (2011).

138. Ng, Q.K. et al. Engineering clustered ligand binding into nonviral vectors: alphavbeta3 targeting as an example. *Mol Ther* **17**, 828-836 (2009).

139. Carmeliet, P. Angiogenesis in health and disease. *Nat Med* **9**, 653-660 (2003).

140. Winkler, E.A., Bell, R.D. & Zlokovic, B.V. Central nervous system pericytes in health and disease. *Nat Neurosci* **14**, 1398-1405 (2011).

141. Lee, K., Silva, E.A. & Mooney, D.J. Growth factor delivery-based tissue engineering: general approaches and a review of recent developments. *J R Soc Interface* **8**, 153-170 (2011).

142. Roskoski, R., Jr. Vascular endothelial growth factor (VEGF) signaling in tumor progression. *Crit Rev Oncol Hematol* **62**, 179-213 (2007).

143. Tung, J.J., Tattersall, I.W. & Kitajewski, J. Tips, Stalks, Tubes: Notch-Mediated Cell Fate Determination and Mechanisms of Tubulogenesis during Angiogenesis. *Cold Spring Harb Perspect Med* **2**, a006601 (2012).

144. del Toro, R. et al. Identification and functional analysis of endothelial tip cell-enriched genes. *Blood* **116**, 4025-4033 (2010).

145. Suchting, S. et al. The Notch ligand Delta-like 4 negatively regulates endothelial tip cell formation and vessel branching. *Proc Natl Acad Sci U S A* **104**, 3225-3230 (2007).

146. Hellstrom, M. et al. Dll4 signalling through Notch1 regulates formation of tip cells during angiogenesis. *Nature* **445**, 776-780 (2007).

147. Jakobsson, L. et al. Endothelial cells dynamically compete for the tip cell position during angiogenic sprouting. *Nat Cell Biol* **12**, 943-953 (2010).

148. Tammela, T. et al. VEGFR-3 controls tip to stalk conversion at vessel fusion sites by reinforcing Notch signalling. *Nat Cell Biol* **13**, 1202-1213 (2011).

149. Garrison, K.R. et al. Clinical effectiveness and cost-effectiveness of bone morphogenetic proteins in the non-healing of fractures and spinal fusion: a systematic review. *Health Technol Asses* **11**, 1-+ (2007).

150. Gautschi, O.P., Frey, S.P. & Zellweger, R. Bone morphogenetic proteins in clinical applications. *ANZ J Surg* **77**, 626-631 (2007).

151. Ehrbar, M. et al. The role of actively released fibrin-conjugated VEGF for VEGF receptor 2

gene activation and the enhancement of angiogenesis. *Biomaterials* **29**, 1720-1729 (2008).

152. Tibbitt, M.W. & Anseth, K.S. Hydrogels as Extracellular Matrix Mimics for 3D Cell Culture. *Biotechnol Bioeng* **103**, 655-663 (2009).

153. Zisch, A.H. et al. Cell-demanded release of VEGF from synthetic, biointeractive cell ingrowth matrices for vascularized tissue growth. *FASEB J* **17**, 2260-2262 (2003).

154. Zisch, A.H., Lutolf, M.P. & Hubbell, J.A. Biopolymeric delivery matrices for angiogenic growth factors. *Cardiovasc Pathol* **12**, 295-310 (2003).

155. Phelps, E.A. & Garcia, A.J. Update on therapeutic vascularization strategies. *Regen Med* **4**, 65-80 (2009).

156. Langer, R. & Tirrell, D.A. Designing materials for biology and medicine. *Nature* **428**, 487-492 (2004).

157. Lutolf, M.P. & Hubbell, J.A. Synthetic biomaterials as instructive extracellular microenvironments for morphogenesis in tissue engineering. *Nat Biotechnol* **23**, 47-55 (2005).

158. Zhu, J.M. & Marchant, R.E. Design properties of hydrogel tissue-engineering scaffolds. *Expert Rev Med Devic* **8**, 607-626 (2011).

159. Gao, F. et al. Hyaluronan oligosaccharides promote excisional wound healing through enhanced angiogenesis. *Matrix Biol* **29**, 107-116 (2010).

160. Carmichael, S.T. Rodent models of focal stroke: size, mechanism, and purpose. *NeuroRx* **2**, 396-409 (2005).

161. Salhia, B. et al. Expression of vascular endothelial growth factor by reactive astrocytes and associated neoangiogenesis. *Brain Res* **883**, 87-97 (2000).

162. Tsai, P.T. et al. A critical role of erythropoietin receptor in neurogenesis and post-stroke recovery. *J Neurosci* **26**, 1269-1274 (2006).

163. Hicklin, D.J. & Ellis, L.M. Role of the vascular endothelial growth factor pathway in tumor growth and angiogenesis. *J Clin Oncol* **23**, 1011-1027 (2005).

164. Nakatsu, M.N. et al. VEGF(121) and VEGF(165) regulate blood vessel diameter through vascular endothelial growth factor receptor 2 in an in vitro angiogenesis model. *Lab Invest* **83**, 1873-1885 (2003).

165. Blanco, R. & Gerhardt, H. VEGF and Notch in Tip and Stalk Cell Selection. *Csh Perspect Med* **3** (2013).

166. Hofmann, J.J. & Iruela-Arispe, M.L. Notch signaling in blood vessels - Who is talking to whom about what? *Circ Res* **100**, 1556-1568 (2007).

167. Benedito, R. et al. The Notch Ligands Dll4 and Jagged1 Have Opposing Effects on Angiogenesis. *Cell* **137**, 1124-1135 (2009).

168. Radtke, F., Koch, U., Lehal, R., Junker, F. & Poisson, C. Notch Signaling in Normal and Malignant T-Cells. *Exp Hematol* **40**, S21-S21 (2012).

169. Takahashi, T., Yamaguchi, S., Chida, K. & Shibuya, M. A single autophosphorylation site on KDR/Flk-1 is essential for VEGF-A-dependent activation of PLC-gamma and DNA synthesis in vascular endothelial cells. *Embo J* **20**, 2768-2778 (2001).

170. Dayanir, V., Meyer, R.D., Lashkari, K. & Rahimi, N. Identification of Tyrosine Residues in Vascular Endothelial Growth Factor Receptor-2/FLK-1 Involved in Activation of Phosphatidylinositol 3-Kinase and Cell Proliferation. *J. Biol. Chem.* **276**, 17686-17692 (2001).

171. Fujio, Y. & Walsh, K. Akt Mediates Cytoprotection of Endothelial Cells by Vascular Endothelial Growth Factor in an Anchorage-dependent Manner. *J. Biol. Chem.* **274**, 16349-16354 (1999).

172. Lamalice, L., Houle, F., Jourdan, G. & Huot, J. Phosphorylation of tyrosine 1214 on VEGFR2 is required for VEGF-induced activation of Cdc42 upstream of SAPK2/p38. *Oncogene* **23**, 434-445 (2004).

173. Rousseau, S., Houle, F., Landry, J. & Huot, J. p38 MAP kinase activation by vascular endothelial growth factor mediates actin reorganization and cell migration in human endothelial cells. *Oncogene* **15**, 2169-2177 (1997).

174. Giancotti, F.G. & Tarone, G. Positional control of cell fate through joint integrin/receptor protein kinase signaling. *Annu Rev Cell Dev Bi* **19**, 173-206 (2003).

175. Guo, W.J. & Giancotti, F.G. Integrin signalling during tumour progression. *Nat Rev Mol Cell Bio* **5**, 816-826 (2004).

176. Yamada, K.M. & Even-Ram, S. Integrin regulation of growth factor receptors. *Nat Cell Biol* **4**, E75-E76 (2002).

177. Wijelath, E.S. et al. Novel vascular endothelial growth factor binding domains of fibronectin enhance vascular endothelial growth factor biological activity. *Circ Res* **91**, 25-31 (2002).

178. Risau, W. & Lemmon, V. Changes in the Vascular Extracellular-Matrix during Embryonic Vasculogenesis and Angiogenesis. *Dev Biol* **125**, 441-450 (1988).

179. Larsen, M., Artym, V.V., Green, J.A. & Yamada, K.M. The matrix reorganized: extracellular matrix remodeling and integrin signaling. *Curr Opin Cell Biol* **18**, 463-471 (2006).

180. Taverna, D. & Hynes, R.O. Reduced blood vessel formation and tumor growth in alpha 5-integrin-negative teratocarcinomas and embryoid bodies. *Cancer Res* **61**, 5255-5261 (2001).

181. Yang, J.T., Rayburn, H. & Hynes, R.O. Embryonic Mesodermal Defects in Alpha(5) Integrin-Deficient Mice. *Development* **119**, 1093-1105 (1993).

182. Danen, E.H.J. et al. Requirement for the Synergy Site for Cell-Adhesion to Fibronectin Depends on the Activation State of Integrin Alpha-5-Beta-1. *J Biol Chem* **270**, 21612-21618 (1995).

183. Baron, M. et al. H-1-Nmr Assignment and Secondary Structure of the Cell-Adhesion Type-Iii Module of Fibronectin. *Biochemistry-Us* **31**, 2068-2073 (1992).

184. Krammer, A., Craig, D., Thomas, W.E., Schulten, K. & Vogel, V. A structural model for force regulated integrin binding to fibronectin's RGD-synergy site. *Matrix Biol* **21**, 139-147 (2002).

185. Grant, R.P., Spitzfaden, C., Altroff, H., Campbell, I.D. & Mardon, H.J. Structural requirements for biological activity of the ninth and tenth FIII domains of human fibronectin. *J Biol Chem* **272**, 6159-6166 (1997).

186. Altroff, H. et al. Interdomain tilt angle determines integrin-dependent function of the ninth and tenth FIII domains of human fibronectin. *J Biol Chem* **279**, 55995-56003 (2004).

187. van der Walle, C.F., Altroff, H. & Mardon, H.J. Novel mutant human fibronectin FIII9-10 domain pair with increased conformational stability and biological activity. *Protein Eng* **15**, 1021-1024 (2002).